E-CADHERIN REGULATES EPITHELIAL TISSUE STRUCTURE AND FUNCTION BY CONTROLLING β-ACTIN MONOMER SYNTHESIS SITES

By

LISSETTE A. CRUZ

A dissertation submitted to the

School of Graduate Studies

Rutgers, The State University of New Jersey

In partial fulfillment of the requirements

For the degree of

Doctor of Philosophy

Graduate Program in Biological Sciences

Written under the direction of

Alexis J. Rodriguez

and approved by

_____

_____

_____

_____

Newark, New Jersey

October 2018

ABSTRACT OF THE DISSERTATION

E-cadherin regulates epithelial tissue structure and function by controlling β-actin monomer synthesis sites

By LISSETTE A. CRUZ

Dissertation Director:

Dr. Alexis J. Rodriguez

Adherens junctions support strong cell-cell adhesions to create tissues. The core of the adherens junction protein complex consists of three parts: 1) an adhesion transmembrane receptor called E-cadherin, 2) the plaque proteins: p120-catenin, β-catenin and α-catenin, 3) and actin, to anchor these adhesive components (e.g. E-cadherin and plaque proteins). The E-cadherin ectodomain binds to an identical molecule on the surface of an adjacent cell. The E-cadherin cytoplasmic domain is required for the plaque proteins to bind, which in turn bind the adhesion complex to the actin cytoskeleton. The events induced by E-cadherin binding leads to the development of tissue with well-defined apical, lateral and basal cell zones. Previously, it was demonstrated E-cadherin overexpression rescues permeability barrier in tissues assembled from MDCK cells where β-actin monomer synthesis is partially delocalized. β-actin mRNA contains a nucleotide

sequence in its 3'UTR region called the zipcode; and the translational regulator zipcode binding protein-1, ZBP1, recognizes this sequence. Both the zipcode sequence and ZBP1 are essential for targeting and translational regulation of the β-actin transcript. Additionally, a wide range of tyrosine kinases are present at cell-cell contact zones. E-cadherin homophilic binding leads to Src activation, a non-receptor tyrosine kinase, at cell-cell contact zones. Active Src is known to phosphorylate ZBP1 which is bound to the β-actin mRNA zipcode nucleotide sequence, initiating β-actin monomer synthesis. In this investigation using Madin-Darby Canine Kidney (MDCK) cells, I demonstrate E-cadherin overexpression in cells partially delocalizing β-actin monomer synthesis rescues adherens junction assembly. I also show E-cadherin homophilic binding and protein expression regulates the spatial localization of β-actin monomer synthesis at cell-cell contact zones during *de novo* adherens junction formation. Furthermore, inhibiting E-cadherin function or protein expression decreases cell-cell contact localized active Src. Interestingly, inhibiting E-cadherin endocytosis in MDCK cells with partial β-actin monomer synthesis delocalization during *de novo* cell-cell contact rescues tissue permeability barrier and adherens junction assembly; both of these rescues are prevented when the β-actin mRNA zipcode is masked using antisense oligonucleotides. Taken together, these data reveal the relationship between E-cadherin, active Src and β-actin monomer synthesis at cell-cell contact during *de novo* adherens junction assembly. Also, these data support a model where E-cadherin mediates spatially regulated β-actin protein expression during *de novo* adherens junction assembly through the mRNA zipcode/ZBP1 pathway.

ACKNOWLEDGMENTS

“Walking in a straight line one can not get very far” ~Antoine de Saint-Exupéry

I would like to gratefully acknowledge various people who have helped me from the beginning. First, I am thankful to my advisor Dr. Alexis J. Rodriguez, for his guidance and encouragement through rough times and for giving me the freedom to choose my research topic.

Next, I am extremely thankful to Dr. Edward M. Bonder, Dr. Gregory Weber and Dr. Ryan Petrie for being part of my dissertation committee. Dr. Edward M. Bonder, whose expertise, generous guidance and support had a huge impact on my personal and professional career. Dr. Gregory Weber for his time and input in helping me with the E-cadherin function blocking studies. Dr. Ryan Petrie for accepting to be my outside thesis committee member and for his support during my ASCB poster presentations.

Dr. Pavan Vedula, we co-authored two manuscripts, we had interesting scientific discussions when we were preparing these manuscripts. Dr. Natasha Gutierrez, I admire your strong and sincere character. I would like to thank you both for all your helpful advice during laboratory meetings. Itua Eromobor, thank you for your words of encouragement during these last years. Brian Ayee, Justin Davis, Huri Mucahit and Prutha Bhavsar, I learned a lot from all of you, from science to life experiences. Thank you for all your helpful recommendations during laboratory meetings. I huge thanks to all the undergraduates that form/formed part of this laboratory. A special thanks to Clarisse Jose, Maria Aguirre and Neel Shah whose contribution helped in the completion of my thesis.

I appreciate the time and effort Dr. Barry Komisaruk and Wendy Birbano put in the Minority Biomedical Research Support (MBRS) Program. Thank you to the NIH for the funding of this program. Within this program, I was able to participate in scientific conferences and received valuable input from Barry and my MBRS peers.

Thank you for the support and guidance to all in the Biology Department. I would like to extend special thanks to Rucha Shah, Chaitali Saqcena and Ming-shuo Chen for your words of encouragement. To my friends Yaritsa Villegas and Cristina Rosado for your support during this time.

I would like to thank my parents. They have given up many things, among them their professional careers so that my brothers and I can have a better future in this country. To my brother Jorge Cruz, he helped me to recover all my thesis data when it was accidentally erased from both back-up external hard drives… I don't know what I would have done without you. And I need to thank the rest of my family members in Spanish now…

¡MUCHAS GRACIAS a toda la familia! A mis hermanos Alberto y Alfredo por soportarme siempre. A mi abuela Julia Vargas y a mis tíos Teresa y Marcelino, por brindarnos la ayuda para poder venir a este país. A toda mi familia peruana, chilena y venezolana por recargarnos de energía a mis papás, hermanos y a mí para trabajar con más ganas. A Eduardo Guzmán por hacer de este periodo de mi vida más fácil de llevar, no pensé encontrar en este país a un hermano más.

I would like to dedicate my thesis to my cousin Angel Moya (1976-2016).

TABLE OF CONTENTS

LIST OF ILLUSTRATIONS

CHAPTER 1: Introduction

Cell-cell adhesion is tightly regulated by numerous cell surface receptors and is essential for multicellular life (Chu et al., 2006). Cell-cell adhesive interactions have to be dynamic to allow for tissue remodeling and strong to maintain tissue integrity. Many research studies have addressed intercellular junction composition and formation. However, a full understanding of all the molecular pathways regulating intercellular junction formation and maintenance is still lacking. Interestingly, recent work demonstrates localized protein synthesis is required for formation of intercellular junctions and establishment of cell polarity (Gu et al., 2012). Localized protein synthesis involves a subset of mRNAs regulated by their zipcode sequences interacting with the translational regulator Zipcode Binding Protein 1 (ZBP1) (Ben-Ari et al., 2010).

E-cadherin is required for epithelial adherens junction assembly

One of the prominent cell surface receptors participating in cell adhesive interactions are the transmembrane calcium-dependent scaffold proteins known as cadherins. The principal roles of cadherin proteins are regulating cell-cell adhesion, cell sorting, epithelial tissue assembly and maintenance, and establishing cell and tissue polarity. Importantly, cadherin protein adhesive function is critical for maintaining the structural integrity and function of many multicellular tissues (Leckband and de Rooij, 2014). Cadherin proteins are divided into six families: classical cadherins, fat, dachsous, fat-like, CELSR/flamingo and protocadherins (Nichols et al., 2012). Classical cadherins are further subdivided into type I and

type II characterized by five extracellular cadherin repeats (ECs), a single segment transmembrane domain and a cytoplasmic catenin binding domain critical for actin cytoskeleton anchoring (Gooding et al., 2004; Halbleib and Nelson, 2006). Type I classical cadherins include epithelial (E), neuronal (N) and placental (P) cadherins, among others.

In cells, cadherin expression and function is regulated in several ways. For instance, cadherin activity is regulated through proteolytic processing. A pro-domain is present at the N-terminus of E-cadherin and N-cadherin (Koch et al., 2004; Niessen et al., 2011; Ozawa, 2002). The E-cadherin pro-domain is cleaved in the ER or Golgi compartment activating E-cadherin for adhesion (Curtis et al., 2008). In addition, E-cadherin function is modulated through proteolytic cleavage of E-cadherin ectodomain by disintegrin and ADAMs metalloproteases (Maretzky et al., 2005). Furthermore, E-cadherin function is regulated by glycosylation (Pinho et al., 2011). Also, epigenetic regulation of E-cadherin expression has been well studied and characterized. For example, methylation of the E-cadherin promoter regulates epithelial to mesenchymal transition (Blanco et al., 2002; Lombaerts et al., 2006). Last, E-cadherin down-regulation by transcriptional repression has also been shown (Korpal et al., 2008). All of these regulatory mechanisms controlling E-cadherin expression and function have an impact on junction architecture, which is important for morphogenetic movements during development. Additionally, regulating E-cadherin expression and function is essential for postnatal life, in breaking and reforming cell-cell contacts. It has been a challenge to determine how cadherins assemble their intercellular junctions due to the fact that their function and expression are regulated in several ways. Since most cancers are derived

from epithelial tissues (Cairns, 1975), researchers began to investigate E-cadherin cellular distribution as well to understand further how this molecule can regulate tissue morphogenesis and maintenance.

Adherens junctions are mechanosensitive signaling complexes regulating actin cytoskeleton contractility

Cadherin proteins were previously regarded as passive structural elements of adherens junction complexes. Recent findings demonstrate cadherin complexes sense fluctuations in tension and direct cell and tissue behavior accordingly (Le Duc et al., 2010). This specific function is called mechanotransduction (Leckband and de Rooij, 2014). Cadherin adherens junction complexes remodel in response to both endogenous and exogenous forces. In endothelial cells, endogenous tugging forces on adherens junctions between cell doublets increase tension and the size (width) of the VE-cadherin based cell-cell contact. Interestingly, this increase in junctional tension and size is produced by actomyosin contractility (Liu et al., 2010). In a mouse teratocarcinoma cell line (F9), the force-induced stiffening of Fc-E-cadherin-coated beads attached to F9 cells increases with time during continuous shear conditions. Importantly, stiffness decreases in the presence of E-cadherin function blocking antibodies, when actin filaments are perturbed with cytochalasin D or latrunculin D, or when myosin contractility is inhibited with blebbistatin (Le Duc et al., 2010). Also, local mechanical stimulation of cadherin bonds triggers actin recruitment to stressed cadherin complexes (Barry et al., 2014). Another study demonstrated E-cadherin transmits mechanical tension between MDCK cells via homophilic binding and through α-catenin and β-catenin

to the actin cytoskeleton. Once again, the observed tension decreases when the cells are treated with cytochalasin B or ML-7, which inhibit actin polymerization and myosin II activity (Borghi et al., 2012). These data demonstrate there is a positive feedback loop involving E-cadherin, myosin activity, and F-actin. Thus, through an undefined sensory and positive feedback loop, endogenous E-cadherin based contractile forces increase demonstrating the E-cadherin-catenin complex is an active mechanosensor.

E-cadherin regulates signal pathways required to localize protein synthesis

Adherens junctions function as signaling centers that respond to biochemical and mechanical stimuli from the environment (Wu et al., 2015). Two signaling pathways active at adherens junction sites are RhoA and Src (McLachlan et al., 2007; Rodriguez et al., 2008; Rodriguez et al., 2006; Gutierrez et al. 2014). Src participates in cell differentiation, growth, division and survival signaling pathways (Fincham and Frame, 1998; Roskoski, 2004). Also, Src plays a role in cell adhesion, cell morphology, and motility. Src consists of four SH domains. From the N- to C- terminus, Src contains an N-terminal with myristoyl group (SH4 domain), a unique segment, an SH3 domain, an SH2 domain, a protein tyrosine kinase domain and a C terminal regulatory domain (tail). There are two main phosphorylation sites on Src. At the C-terminus, autophosphorylation of tyrosine 416 (Y416) results in Src activation while phosphorylation at tyrosine 527 (Y527) results in Src inhibition (Roskoski, 2004). When the Y527 of Src is phosphorylated by C-terminal Src kinase (CSK), Src adopts a closed inactive conformation (Xu et al., 1997). Dephosphorylation of the Y527-Src site by protein-tyrosine

phosphatases leads to Src activation. For Src to achieve full activation, the Y416 site is autophosphorylated (Yeatman, 2004).

Activation of Src has been observed in liver, lung, breast and pancreatic cancers. In all of these cancers, Src activity has been found to increase (Roskoski, 2015). For example in breast cancer, EGFR and Src enhance the effects of one another (Biscardi et al., 1998). Interestingly, Src also participates in cell-cell interactions. In fact, cadherin-mediated adhesion can stimulate Src signaling at *de novo* intercellular contacts in the human breast adenocarcinoma (MCF7) cell line (McLachlan et al., 2007). To confirm this, cells seeded on coated substrata containing recombinant cadherin ligands (hE/Fc) stimulated Src signaling. This finding demonstrates E-cadherin adhesion targets Src signaling to cell-cell contacts independently of other juxtacrine signals (McLachlan et al., 2011; Le Duc et al., 2010). Also, Src signal strength affects cadherin based cell spreading in a bimodal manner in hE-CHO cells (McLachlan et al., 2007). RPTPα, a receptor protein-tyrosine phosphatase, is enriched at cadherin-based adherens junction in MCF7 cells and it participates in Src activation upon E-cadherin engagement at cell-cell contacts (Truffi et al., 2014). The same study proposed a model in which E-cadherin transmits a conformational signal to the RPTPα ectodomain which will result in Src activation.

RhoA, Rac1 and Cdc42 are GTPases that form part of Ras superfamily. These molecules participate in the formation of distinct actin cytoskeletal structures: stress fibers, lamellipodia and filopodia, respectively (Marjoram et al., 2014). In one study, a chimeric Rho protein insensitive to Rho inhibition restored E-

cadherin based intercellular junctions during calcium switch assays in keratinocytes (Braga et al., 1997). In another study, an activated RhoA mutant construct resulted in a significant increase in β-actin mRNA localization to the cell periphery in sparse plated chicken embryo fibroblast cells (Latham et al., 2001). In contrast, when cells were transfected with dominant-negative RhoA mutant, β-actin mRNA localization at the cell periphery decreased (Latham et al., 2001). Activated Rac1 and Cdc24 did not demonstrate a highly significant difference in β-actin localization in the same study (Latham et al., 2001). Based on the studies performed by Latham et al. (2001), a model for β-actin mRNA transport was postulated. Near the nucleus, outside-in signaling activates Rho-kinase, which in turn activates myosin IIB and stress fiber assembly increasing myosin IIB and its associated mRNA complex motility towards the cell leading edge. Protein kinase C at the cell periphery phosphorylates myosin IIB heavy chains rendering them inactive, promoting the disassembly of myosin IIB and its associated mRNA complex at the leading edge unloading the β-actin mRNA. This demonstrates the ability of the RhoA signaling pathway to modulate β-actin mRNA distribution in single cells (Latham et al., 2001). In a recent study, E-cadherin knockdown in MCF7 cells failed to generate a RhoA zone at cell-cell contacts. Importantly, this study also found knockdown of myosin IIA or myosin inhibition by blebbistatin failed to generate a RhoA zone at cell-cell contacts (Priya et al., 2015). We demonstrated β-actin monomer synthesis delocalization resulted in a decrease of active RhoA at the plasma membrane. Likewise, inhibiting Src activity decreased the number of β-actin monomers being synthesized during calcium switch assays (Gutierrez et al., 2014). Primarily, the studies mentioned before showed decreased

β-actin mRNA at the cell periphery or decreased E-cadherin at cell-cell contacts when RhoA signaling pathway is perturbed. However, the exact mechanism used by E-cadherin to integrate the signaling pathways mentioned before to cause local changes in the actin cytoskeleton organization remains poorly understood.

Local distribution of β-actin mRNA

Cytoplasmic factors in the egg are selectively distributed to a specific cell compartment to direct specific developmental programs (Davidson, 1971; Jeffery et al., 1983). Actin RNA was found in the ectoplasm and myoplasm of unfertilized eggs (Jeffery et al., 1983). One developmental role has been suggested for localized mRNAs: localized protein synthesis generates asymmetries in developmental determinants specifying embryonic cell fate. These phenomena of mRNA asymmetric distribution also happen in somatic cells. For example, in fibroblasts, actin mRNA concentrations are higher at the cell periphery and vimentin mRNA concentrations are highest near the nucleus (Lawrence and Singer, 1986). One possible explanation for the utility of these processes is that the actin protein is involved in the formation of lamellipodia; and vimentin, which is a type of intermediate filament component, is needed around the nucleus (Lawrence and Singer, 1986). In fibroblasts, β-actin mRNA is transported as granules on actin filaments (Sundell and Singer, 1991). The localization signal of the β-actin mRNA is contained within its 3'UTR sequence, which is a 54 nt cis-acting element called the mRNA zipcode (Kislauskis et al., 1994). The trans-actin factor, zipcode binding protein 1 (ZBP1) binds directly to the zipcode of β-actin mRNA and is essential for both granule formation and association with the cytoskeleton (Farina et al., 2003;

Oleynikov and Singer, 2003; Ross et al., 1997). Treatment with β-actin mRNA zipcode antisense oligos, which are phosphorothioate-modified oligonucleotides to inhibit zipcode function, results in a nonlocalized distribution of β-actin protein (Shestakova et al., 2001). Also, MDCK cells treated with β-actin mRNA zipcode antisense oligos during calcium switch experiments disrupts epithelial adherens junction assembly (Gutierrez et al., 2014).

E-cadherin is anchored to linear actin filaments

The adherens junctions have two crucial roles: sensors of extracellular stimuli and regulators of epithelial sheets dynamics. They form at the most apical part of the lateral membrane (Nagafuchi, 2001). The core of adherens junction complex includes a single pass transmembrane glycoprotein, E-cadherin, and catenin family members (**Figure 1**) that in turn anchor to the actin cytoskeleton (Serres et al., 2000; Drees et al., 2005; Hartsock and Nelson, 2008). E-cadherin extracellular binding domain is weak, but lateral clustering of cadherins strengthens cell-cell adhesion. These interactions stabilize the weak extracellular interactions between cadherin molecules on opposing cells (Serres et al., 2000; Yamada et al., 2005). Also, the stability of cell-cell adhesions increases with their association with actin (Serres et al., 2000; Nagafuchi, 2001; Yamada et al., 2005). Nascent cell-cell contacts occur due to E-cadherin based lamellar overlap, mediated by Rac1 (Drees et al., 2005; Kovacs et al., 2002). Since actin dynamics are important for the generation of cell-cell contacts, Dress et al., 2005, examined α-catenin's role in actin filament bundling. They found α-catenin concentration has to be significantly higher at nascent cell-cell contacts to form homodimers and

suppress Arp2/3-mediated actin polymerization. This will result in the transition from active lamellipodia characterized by branched arrays to their inhibition and bundling of actin filaments at cell-cell contacts. Also, formins, actin filament polymerase, participate in nucleation of unbranched actin cables. α-Catenin knockdown in mouse epidermis decreases formin-1 (mDia) at cell-cell contacts. In addition, formin-1 was found to be in complex with α-catenin in the same study (Kobielak et al., 2004). Furthermore, another study suggested α-catenin has a role in reinforcing adherens junctions by recruiting vinculin molecules to cell-cell contacts resulting in an increased association with actin filaments (Yonemura et al., 2010). It is still unclear how these processes are regulated precisely in space and time during *de novo* adherens junction assembly, from E-cadherin homophilic binding, the positioning of the actomyosin contractile apparatus resulting in adherens junction anchoring to actin.

Based on previous studies mentioned before, I hypothesize E-cadherin adhesion activates signaling pathways to localize and translate β-actin mRNA at cell-cell contacts. The two signaling pathways are Src and RhoA. Sorting of the β-actin mRNA to the cell periphery requires RhoA (Latham et al., 2001). Translation occurs when ZBP1-β-actin mRNA complex reach cell periphery where active Src is located (Hüttelmaier et al., 2005; McLachlan et al., 2007). For translation to occur ZBP1 has to be released from the β-actin mRNA, and this is accomplished by Src (Hüttelmaier et al., 2005). Src phosphorylates ZBP1, resulting β-actin mRNA translation at the cell periphery (Hüttelmaier et al., 2005). The localized translation of β-actin monomers results in an increased above its critical concentration

(Bonder et al., 1986; Gutierrez et al., 2014) resulting in F-actin filament growth. These processes result in adherens junction formation, stability and maturation.

Significance of localized protein synthesis on health and disease

IMP1 is orthologous to the chicken zipcode binding protein 1 (ZBP1) and it is involved in mRNA localization, translational control and turnover (Hansen et al., 2004; Wang et al., 2016). Local translation of β-actin and E-cadherin mRNAs mediated by ZBP1 influences actin dynamics and the formation of cell-cell adhesions (Wang et al., 2016). This could explain why similar effects are observed when E-cadherin expression is perturbed. For instance, in one study intestinal E-cadherin knockout mice present a severe body weight loss due to compromised intestinal epithelial architecture (Schneider et al., 2010) similar to when ZBP1 protein expression is reduced in mice pups (Hansen et al., 2004). Also this study revealed E-cadherin's indirect defense role against enteropathogenic bacteria (Schneider et al., 2010). In homozygous mice pups (ZBP1−/−), intestinal necrotic patches were observed with significant adherences indicating their early death is associated with a dysfunctional intestine (Hansen et al., 2004). Moreover, another study showed loss of ZBP1 in mice intestinal mesenchymal stem cells increased tumor number and size upon AOM/DSS treatment, which recapitulates tumor initiation and progression (Hamilton et al., 2015). Interestingly, a breast cancer mouse model with conditional IMP1 expression showed few or no lung metastases in comparison to the non-induced control. Intriguingly, it was observed that with or without induction these mice developed mammary gland masses (Nwokafor et al.,

2016) indicating a metastatic suppression role for ZBP1, which also characterizes E-cadherin.

From studies mentioned before, similar effects are seen when E-cadherin and ZBP1 protein expression are reduced in tissues or cell monolayers. These similar effects indicate these two molecules are in the same mechanotransduction pathway involved in adherens junction assembly. How E-cadherin regulates this mechanotransduction pathway that ultimately leads to the formation of a functional tissue and adherens junction assembly remains elusive. Several studies highlight the importance of protein localization and localized signaling required for proper adherens junction assembly. For instance, E-cadherin modulates RhoA and Src signal at cell-cell contact zones (Weber et al., 2011; Latham et al., 2001; McLachlan et al., 2007). This is required for local β-actin protein synthesis during adherens junction assembly (Gutierrez et al., 2014). The biological consequences when this pathway is perturbed encompass defects seen in a plethora of diseases such as IBS (Inflammatory Bowel Syndrome), cancer and inflammation. I want to address the extent to which E-cadherin regulates Src activity and β-actin protein synthesis during adherens junction assembly.

In this thesis, I investigated the role of E-cadherin in localized β-actin monomer synthesis during *de novo* adherens junction assembly in MDCK cells. First, I demonstrate E-cadherin homophilic binding and protein expression is required to stimulate β-actin monomer synthesis during *de novo* adherens junction assembly at cell-cell contacts. Second, I show E-cadherin homophilic binding and expression is required to localize active Src for adherens junction assembly at cell-

cell contacts. Third, I demonstrate that increasing cadherin clustering at the cell surface rescues adherens junction assembly and tissue barrier integrity in MDCK cells with partial β-actin monomer synthesis delocalization.

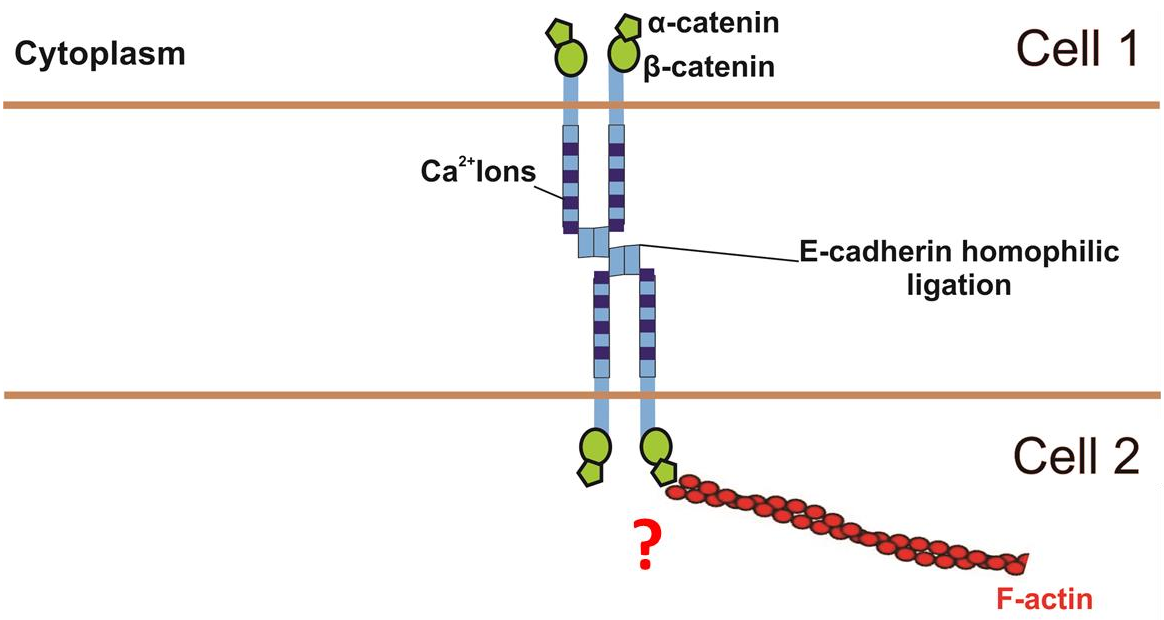
Cytoplasm
α-catenin
β-catenin
Cell 1
Ca2+Ions
E-cadherin homophilic ligation
Cell 2
?
F-actin

Figure 1: The cadherin-catenin complex anchored to actin filaments.

E-cadherin *cis* and *trans* interactions are shown. The extracellular region of E-cadherin consists of five extracellular (EC) domains. Blue dots indicate Ca^{2+} ions that are inserted into the linker regions between neighboring cadherin extracellular domains to rigidify E-cadherin's extracellular region. β-catenin (green circle) binds to the distal region of E-cadherin, which in turns binds to α-catenin (green pentagon). In a less well-understood way, the cadherin-catenin complex can influence how actin filaments remodel at cell-cell contacts. Also, cadherins have also been found to control signaling protein activity at cell-cell contacts to control actin filament remodeling.

Specific Aims:

1. To determine the extent to which E-cadherin expression and functionality regulates cell-cell contact localized β-actin monomer synthesis following *de novo* cell-cell contact.

1.1. Determine the effects of E-cadherin overexpression in MDCK cells with partially delocalized β-actin monomers synthesis during *de novo* adherens junction assembly (**Chapter 2**).

1.2. Quantify E-cadherin and F-actin using Fluorescence Covariance Index analyses when E-cadherin function is blocked during adherens junction assembly (**Chapter 2**).

1.3. Determine the spatial localization of β-actin monomer synthesis sites during adherens junction assembly when E-cadherin function is blocked (**Chapter 2**).

1.4. Determine the spatial localization of β-actin monomer synthesis sites during adherens junction assembly when E-cadherin protein expression is downregulated (**Chapter 2**).

2. To determine the extent to which E-cadherin expression and functionality regulates active Src localization following *de novo* cell-cell contact.

2.1. Quantify active Src and E-cadherin complex assembly when E-cadherin function is blocked during *de novo* adherens junction formation.

2.1.1. Determine relative protein densities for active Src and total Src in tissues assembled from MDCK cells during adherens junction assembly (**Chapter 3**).

2.2. Quantify active Src and F-actin when E-cadherin protein expression is reduced during *de novo* adherens junction assembly

2.2.1. Determine relative protein densities for total Src in tissues assembled from MDCK cells during *de novo* adherens junction assembly (**Chapter 3**).

3. To determine the extent to which positive and negative pathways regulate E-cadherin surface expression to control epithelial tissue structure and function

3.1. Quantify E-cadherin and F-actin complex assembly when endocytosis is inhibited in tissues assembled from cells with partial delocalization of β-actin monomer synthesis during *de novo* adherens junction formation (**Chapter 4**).

3.2. Quantify E-cadherin and F-actin complex assembly when endocytosis and actin/ZBP1 interaction are inhibited in tissues assembled from cells with partial delocalization of β-actin monomer synthesis during *de novo* adherens junction formation (**Chapter 4**).

3.3. Characterize *de novo* adherens junction assembly in tissues assembled from cells with a partial delocalization of β-actin monomer synthesis when endocytosis and E-cadherin function are inhibited (**Chapter 4**).

3.4. Measure tissue permeability using TRITC-dextran when endocytosis and β-actin/ZBP1 interaction are inhibited in tissues assembled from MDCK cells with partial delocalization of β-actin monomer synthesis (**Chapter 4**).

CHAPTER 2: E-cadherin expression and binding function modulates β-actin monomer synthesis following *de novo* cell-cell contact to control adherens junction assembly

INTRODUCTION

Epithelial cells exhibit two major types of actin structures associated with intercellular adhesions, branched actin networks and linear actin cables. Early during adherens junction assembly, Rho GTPases stimulate both lamellipodial (branched F-actin) and filopodial (F-actin cable) extensions (Vasioukhin et al., 2000). Once nascent adherens junction puncta have assembled, they are stabilized and anchored to radial linear actin cables at the tip of each puncta (Vasioukhin et al., 2000). Consequently, actin polymerization is initiated at F-actin anchored adherens junction sites. At later stages of adherens junction formation, the actin cytoskeleton adopts a circumferential ring morphology at the apical zone generating contractility that seals opposing cell membranes into an epithelial sheet (Adams et al., 1998; Vasioukhin et al., 2000). Importantly, an mRNA zipcode sequence present in β-actin 3' untranslated region is required to localize monomer synthesis to cell-cell contact sites and regulate adherens junction assembly (Rodriguez et al., 2006; Gutierrez et al., 2014). In fact, delocalizing β-actin monomer synthesis by deleting the mRNA zipcode caused C2C12 and MDCK cells to delocalize N-cadherin and E-cadherin, respectively, from cell-cell contact sites (Rodriguez et al., 2006; Gutierrez et al., 2014). Additionally, increasing the concentration of translation regulator ZBP1 decreased β-actin protein synthesis (Hüttelmaier et al., 2005). These data demonstrate ZBP1 controls β-actin

monomer synthesis through mRNA zipcode binding. Consequently, perturbing β-actin/ZBP1 interactions causes adherens junctions and tissue permeability defects during *de novo* adherens junction assembly (**Figure 2**; Cruz et al., 2015; Gutierrez et al., 2014). Therefore, assembling a functional epithelial tissue requires spatially regulated β-actin monomer synthesis (**Figure 3**). In fact, MDCK steady state tissue assembled from cells that properly localize β-actin monomer synthesis form functional epithelial barriers (**Figure 3: β-actin$_{(Unmasked)}$**). However, these functional epithelial barrier are perturbed when β-actin monomer synthesis is delocalized by β-actin zipcode masking with antisense oligonucleotides which blocks ZBP1 binding to β-actin mRNA (**Figure 3: β-actin$_{(Zipcode\ Masked)}$**). A functional epithelial barrier is observed in tissues assembled from cells with unmasked β-actin zipcodes in which scrambled antisense oligonucleotides are used during calcium switch assay (**Figure 3: β-actin$_{(Unmasked\text{-}scrambled)}$**). RhoA and Src signaling participate in local β-actin translation by localizing the transcript and initiating monomer synthesis respectively (Rodriguez et al., 2008). Also, E-cadherin had been shown to modulate RhoA and Src signaling at cell-cell contacts (Shewan et al., 2005; McLachlan et al., 2007; Gutierrez et al., 2014). We also observed tissue permeability defects when Rho and Src signals are inhibited during *de novo* adherens junction assembly (**Figure 3: Rho$_{(Inh)}$**; **Src$_{(Inh)}$**). When E-cadherin was overexpressed, we observed a (**Figure 4A: Δ3'UTR β-actin + 1.5X E-cadherin; Figure 4B**) rescue in barrier permeability in tissues assembled from cells that have a dominant negative adherens junction assembly phenotype caused by partial delocalization of β-actin monomer synthesis (**Figure 4A: Δ3'UTR β-actin**). Taken together these studies demonstrate spatial localization of β-actin

translation is necessary to assemble a *de novo* adherens junction and consequently assemble a functional epithelial tissue barrier. Since E-cadherin overexpression rescues tissue permeability in cells with partially delocalized β-actin monomer synthesis, I investigated E-cadherin's role in spatially regulating β-actin monomer synthesis. First, I investigated the extent to which E-cadherin overexpression rescues a dominant negative adherens junction assembly phenotype in cells with partially delocalized β-actin monomer synthesis (**Δ3'UTR β-actin**). Second, I investigated the role of E-cadherin expression or homophilic binding in spatially regulating β-actin monomer synthesis during *de novo* adherens junction formation.

RESULTS

Overexpressing E-cadherin rescues adherens junction assembly defects caused by mRNA zipcode mediated β-actin monomer synthesis delocalization

Previously, it was demonstrated *de novo* epithelial cell-cell contact induces spatially localized β-actin monomer synthesis throughout the contact zone which is required for adherens junction assembly (Gutierrez et al., 2014). Moreover, it was shown deleting the β-actin 3'UTR which contains the mRNA zipcode sequence in ~20% of β-actin transcripts, is sufficient to generate a dominant negative phenotype caused by β-actin monomer synthesis delocalization (Cruz et al., 2015; Gutierrez et al., 2014). This tissue assembled from cells that partially delocalized β-actin is characterized by ectopic E-cadherin and F-actin colocalization throughout the cytoplasm as well as a decreased cell-cell contact colocalization (Cruz et al., 2015; Gutierrez et al., 2014). To investigate the function of E-cadherin mediated β-actin monomer synthesis, fluorescence microscopy of adherens junction complex assembly in MDCK tissue assembled from cells partially perturbed in their ability to target β-actin monomer synthesis was performed. First, I imaged MDCK steady state tissue assembled from cells that properly localize β-actin monomer synthesis (FL-β-actin) and observed significant colocalization of E-cadherin and β-actin fluorescence at cell-cell contacts (**Figure 5A, white arrows**) with little to no colocalization observed throughout the cytoplasm (**Figure 5A, blue arrowheads**). By contrast, MDCK steady state tissue assembled from cells that partially delocalize β-actin monomer synthesis (Δ3'UTR β-actin), show ectopic E-cadherin and β-actin colocalization throughout the cytoplasm (**Figure 5B, blue**

arrowheads), as well as at cell-cell contacts colocalization (**Figure 5B, white arrows**). Interestingly, overexpressing E-cadherin in MDCK cells with partially delocalized β-actin monomer synthesis (**Δ3'UTR β-actin + E-cadherin 1.5X**) shifts E-cadherin and β-actin colocalization from the mixed cytoplasmic and intercellular contact distribution back to a predominately cell-cell contact localization (**Figure 5C, white arrows**). To quantify the extent of E-cadherin/β-actin complex assembly a Pearson's correlation coefficient based method was developed to measure E-cadherin and β-actin fluorescence covariance. This method is a useful proxy for adherens junction assembly (Barlow et al., 2010; Costes et al., 2004; Vedula et al., 2016). Briefly, freehand regions of interest of the cell-cell contact and cytoplasmic zones for each cell were drawn, and Pearson's correlation coefficient values in each region were measured using Volocity® 6.0.1 Software, PerkinElmer. Because a Pearson's correlation coefficient value of 0.1 represents a very weak correlation, we set a lower bound on all Pearson's correlation coefficient values to 0.1 (Zinchuk et al., 2013). Then, for every cell, the Pearson's correlation coefficient value at the cell-cell contact zone was divided by the Pearson's correlation coefficient value in the cytoplasm (**Figure 6A, 6B**). Then, the ratio was logarithm transformed, and this measure was termed Fluorescence Covariance Index (**Figure 6C**; Vedula et al., 2016). Consequently, Fluorescence Covariance Index values between -1 and 0 indicate a higher correlation between E-cadherin and actin fluorescence in the cytoplasm of the cell. By contrast, Fluorescence Covariance Index values between 0 and +1 indicate a higher correlation between E-cadherin and actin fluorescence at cell-cell contact zones. Fluorescence Covariance Analyses indicates there is no significant difference in the localization

of E-cadherin/β-actin complexes in MDCK cells that properly localize β-actin monomer synthesis to cell-cell contact sites compared to MDCK cells overexpressing E-cadherin in a background of partially delocalized β-actin monomer synthesis (**Figure 7: FL β-actin 1X E-cadherin versus Δ3'UTR β-actin 1.5X E-cadherin**). In fact, Fluorescence Covariance Analysis demonstrates overexpressing E-cadherin ~1.5 fold increases steady state adherens junction ~4-fold in comparison to MDCK cells partially delocalizing β-actin monomer synthesis (**Figure 7: Δ3'UTR β-actin 1.5X E-cadherin versus Δ3'UTR β-actin**). Of note, the ~4-fold increase in steady state adherens junctions inversely correlates with the observed ~4-fold decrease in steady state dextran permeability (**Figure 4: compare Δ3'UTR β-actin versus Δ3'UTR β-actin 1.5X E-cadherin, blue bars**) demonstrating E-cadherin and β-actin mRNA transcripts function synergistically to regulate epithelial adherens junction and tissue permeability barrier assembly. To assess adherens junction assembly after Ca^{2+} switch assays, I used Fluorescence Covariance Index analyses to study the extent to which E-cadherin and β-actin fluorescence signals co-vary in E-cadherin overexpression MDCK cell line when β-actin monomer synthesis is partially delocalized (**Figure 8: 1.5X E-cadherin/Δ3'UTR β-actin**). These cells were fixed during different times of the Ca^{2+} switch assay: steady state (SS), low calcium (LC), 1 hour, 2 hours and 3 hours calcium repletion (for details see Materials and Methods). At steady state when E-cadherin is overexpressed in the MDCK cell line where β-actin monomer synthesis is partially delocalized (**Figure 8: 1.5X E-cadherin/Δ3'UTR β-actin**) adherens junction assembly is rescued characterized by immunofluorescent labeled E-cadherin and fluorescent labeled β-actin complexes at the cell-cell

contact zones (**Figure 8 and Figure 9: SS**). Addition of low calcium culture medium (4 mM EGTA; see Materials and Methods) to these cells for 1 hour resulted in the progressive breakdown of intercellular junctions and cell rounding (**Figure 8: LC**) characterized by a combination of E-cadherin and β-actin diffuse and punctate staining in the cytoplasm. In addition, compared to steady state tissues, fewer cells had high Fluorescence Covariance Index values following EGTA-induced junction disassembly (**Figure 9: Low Ca^{2+}**), indicating that this quantitative method is a useful measure of adherens junction assembly/disassembly. After returning the cells to Ca^{2+} recovery media (Ca^{2+} repletion; see Materials and Methods), the formation of new adherens junctions was examined and quantified at different times. Within 1 hour post-contact spreading of the cells occurred concomitantly with the appearance of E-cadherin and β-actin immunofluorescence staining at some cell-cell contact zones (**Figure 8: 1hr**). 2 and 3 hours post-contact, E-cadherin and β-actin continue to accumulate at cell-cell contacts (**Figure 8: 2 hr, 3 hr**). Importantly, Fluorescence Covariance Index analyses demonstrates cells overexpressing E-cadherin in a background of partially delocalized β-actin monomer synthesis rescues *de novo* adherens junction assembly (**Figure 9**). In support of this concept, Ca^{2+} switch experiments confirm the inverse correlation between adherens junctions assembly (**Figure 9**; measured by Fluorescence Covariance Index) and tissue permeability (**Figure 4A: Δ3'UTR β-actin 1.5X E-cadherin**; measured by TransWell) in cells with partial delocalization of β-actin monomer synthesis when E-cadherin is overexpressed. Taken together, these data demonstrate E-cadherin and the β-actin mRNA transcript function synergistically to control *de novo* adherens junction

assembly and epithelial tissue self-assembly. It is well known adherens junction complex stabilization and maturation requires F-actin anchoring (Harris et al., 2014; Hong et al., 2013). Therefore to further investigate E-cadherin and actin colocalization in tissues assembled from cells overexpressing E-cadherin in a background of partially delocalized β-actin monomer synthesis (**Δ3'UTR β-actin 1.5X E-cadherin**), Ca^{2+} switch assays were performed and F-actin was stained with phalloidin (**Figure 10**; see Materials and Methods). Fluorescence microscopy of E-cadherin and F-actin show both the adhesion receptor and actin filaments are enriched at the cell-cell contacts in steady state tissue (**Figure 10: SS**), similar to the results obtained when E-cadherin and β-actin were visualized using fluorescence microscopy (**Figure 8: SS**). Addition of low calcium media (4 mM EGTA) resulted in junction disassembly characterized by a decrease of E-cadherin and F-actin at cell-cell contacts and an increase of E-cadherin and F-actin staining in the cytoplasm (**Figure 10: LC**). After returning the cells to Ca^{2+} recovery media (Ca^{2+} repletion; for details see Materials and Methods) the formation of new adherens junctions was examined and quantified. During *de novo* cell-cell contact, E-cadherin/F-actin colocalization increases at cell-cell contact zones along with a decrease of cytoplasmic E-cadherin/F-actin colocalization (**Figure 10: 1 hr, 2 hr and 3 hr calcium repletion**). Importantly, during calcium switch assays I observed adherens junction complexes anchored to the F-actin cytoskeleton at cell-cell contacts. This was confirmed by increasing Fluorescence Covariance Index values for E-cadherin and F-actin during *de novo* cell-cell contact formation (**Figure 11; Vedula et al., 2016**). These results demonstrate E-cadherin organizes F-actin at intercellular contacts. Additionally, these data demonstrate F-actin is assembled

from β-actin monomers synthesized at cell-cell contact zones during *de novo* adherens junction assembly.

E-cadherin homophilic binding is required for adherens junction assembly

Using the calcium switch method I quantified E-cadherin and F-actin colocalization at cell-cell contacts and in the cytoplasm during tissue monolayer assembly. At steady state, wild type MDCK cells assemble a tissue with immunofluorescent labeled E-cadherin and fluorescently labeled F-actin localizing to cell-cell contact zones (**Figure 12A: SS, blue arrows**). Thus, I observed E-cadherin and F-actin have higher colocalization at cell-cell contact zones in comparison to the cytoplasm at steady state. Quantitatively, E-cadherin and F-actin peripheral Pearson's correlation coefficient (0.77) is ~2.5 times higher that their cytoplasmic Pearson's correlation coefficient values (0.29) (**Figure 12B: SS**). Then, adherens junctions were disassembled by the addition of low calcium medium containing 4 mM EGTA (for details see Materials and Methods and **Figure 2A**) for 1 hour. Low Ca^{2+} media treatment caused an increase in adherens junction disassembly and cell rounding (**Figure 12A: LC**). Quantitatively, E-cadherin and F-actin Pearson's correlation coefficient values at intercellular contacts (**periphery**) decrease, while Pearson's correlation coefficient value throughout the cytoplasm increases (**Figure 12B: LC**). Then, I induced MDCK tissues to synchronously undergo *de novo* cell-cell contact by incubating Ca^{2+}-containing culture media (Ca^{2+} repletion). Cell spreading was observed within 1 hour post-contact (**Figure 12A: 1 hr**) concomitant with the appearance of E-cadherin and F-actin immunofluorescence staining at some cell-cell contact zones (**Figure 12A: 1 hr, blue arrows**). 2 and 3 hours post-contact E-cadherin and F-actin continue to

localize to cell-cell contact zones (**Figure 12A: 2 hr, 3 hr; blue arrows**). Note 3 hours post-contact the re-formation of tissue was complete characterized by cells exhibiting a classic cobblestone pattern (**Figure 12A: 3 hr**) similar to that observed at steady state (**Figure 12A: SS**). E-cadherin and F-actin colocalization at 1, 2 and 3 hours post-contact preferentially begin to occur at cell-cell contact zones in MDCK tissues. This is demonstrated by an increase in peripheral Pearson's correlation coefficient values between E-cadherin and F-actin (**periphery**) 1, 2 and 3 hours post-contact (**Figure 12B: 1 hour, 2 hours, 3 hours**) and a decrease in cytoplasmic Pearson's correlation coefficient values following *de novo* cell-cell contact (**Figure 12B: 1 hour, 2 hours, 3 hours**). As a consequence, I measured increases in adherens junction complex assembly 1, 2 and 3 hours post-contact as shown by Fluorescence Covariance Index values for E-cadherin and F-actin (**Figure 15**). Also, note adherens junction complex formation is complete at ~3 hours post-contact since Fluorescence Covariance Index value 3 hours post-contact recover their steady state Fluorescence Covariance Index values (**Figure 15: 3 hour control versus Steady State control**).

To study the extent to which E-cadherin regulates adherens junction anchoring to F-actin at cell-cell contacts, tissues composed of wild type MDCK cells were subjected to calcium switch assays in the presence of E-cadherin function blocking antibodies (Vedula et al., 2016; Vestweber and Kemler, 1985; Volberg et al., 1986). E-cadherin function blocking antibody, DECMA-1, has been used extensively in epithelial cell lines to disrupt intercellular contacts (Fingleton et al., 2010; Vedula et al., 2016; Vestweber and Kemler, 1985). Briefly, DECMA-1 targets E-cadherin's EC5 ectodomain preventing homophilic interactions from

opposing contacting epithelial cells (Brouxhon et al., 2013; C.-L.Chen and Chen, 2009; Ozawa et al.,1990). This E-cadherin function blocking antibody, DECMA-1, was added to tissues composed of MDCK cells during synchronized cell-cell contact stimulation. Then, these tissues were fixed at 1, 2 and 3 hours post-contact and immunostained for E-cadherin and F-actin to investigate adherens junction complex assembly (**Figure 13**). Similar to untreated control cells, Cell spreading was observed within 1 hour post-contact in the presence of the function blocking antibody (**Figure 13A: 1 hr**). In addition, E-cadherin and F-actin were present in a few cell-cell contacts (**Figure 13A: 1hr, blue arrows**). Interestingly, same spatial distribution of adhesive complexes was observed at 1 hour post-contact when E-cadherin function is blocked in comparison to the control cells at 1 hour post-contact (**Figure 13B and Figure 12B: 1 hr**). 2 hours post-contact, cell spreading continued along with an increase of E-cadherin and F-actin immunofluorescence staining at cell-cell contacts (**Figure 13A: 2 hr, blue arrows**). Surprisingly, 3 hours post-contact, E-cadherin and F-actin accumulation at intercellular contacts decreases when E-cadherin binding is inhibited (**Figure 13A: 3hr, blue arrows**) in comparison to the control cells 3 hours post-contact (**Figure 12A: 3hr, blue arrows**). Quantitatively, this is shown by peripheral Pearson's correlation coefficient values of 0.51, 0.63 and 0.54 at 1, 2 and 3 hours post-contact respectively (**Figure 13B**). As a result, adherens junction complex assembly dynamics following *de novo* cell-cell contact when E-cadherin function is inhibited increases but to a lesser extent in comparison to control cells, as shown by the significantly lower Fluorescence Covariance Index values 3 hours post-contact (**Figure 15: Control versus DECMA-1 100 µg/ml**). In addition, when E-cadherin

function is inhibited during *de novo* adherens junction assembly the progressive increase in adherens junction complex assembly dynamics is perturbed in comparison to control cells. This is shown by Fluorescence Covariance Index values for E-cadherin and F-actin during *de novo* adherens junction assembly when E-cadherin function is blocked (**Figure 15: DECMA-1 (100 µg/ml)**). Interestingly, live cell imaging of tissues composed of MDCK cells with E-cadherin-RFP and eGFP-FL-β-actin was performed for 12 hours post-contact in the presence of DECMA-1. Treatment with the E-cadherin binding inhibitor perturbed E-cadherin and β-actin localization to cell-cell contacts during the 3 hours post-contact in comparison to the control. However, 12 hours post-contact, the accumulation of E-cadherin and β-actin at the cell-cell contacts was similar to the control (Vedula et al., 2016) demonstrating a temporal delay in E-cadherin/β-actin complex formation. To further investigate the role of E-cadherin homophilic binding during adherens junction complex assembly a higher concentration of E-cadherin function blocking antibodies was utilized (**Figure 14A**). The increase in E-cadherin function blocking antibody to 200 µg/mL has a stronger effect in blocking E-cadherin and F-actin localization to cell-cell contacts (**Figure 14A: blue arrows**). As a consequence, a further decrease in the amount of *de novo* adherens junction complex assembly was observed. This is demonstrated by low peripheral Pearson's correlation coefficient values of 0.48, 0.52 and 0.47 1, 2 and 3 hours post-contact respectively (**Figure 14B: periphery**), while cytoplasmic Pearson's correlation coefficient values remained low at all times (**Figures 14B: cytoplasm**). In fact, after effectively blocking E-cadherin homophilic binding function, adherens junction complex assembly at cell-cell contacts further

decreased. This was demonstrated by the decrease of Fluorescence Covariance Index values at the cell-cell contact zones (**Figure 15: DECMA-1 200 µg/ml**). Moreover, the cells optimally inhibited with DECMA-1 failed to undergo adherens junction maturation 3 hours post-contact in comparison to control cells. This is shown by the Fluorescence Covariance Index value at 3 hours in 200 µg/ml DECMA-1 treated cells, which goes down by a ~half in comparison to the 3 hour post-contact control (**Figure 15: 3 hours; Control versus DECMA-1 200 µg/ml**). Together these data confirm blocking E-cadherin homophilic binding with DECMA-1 antibody decreases adherens junction complex assembly.

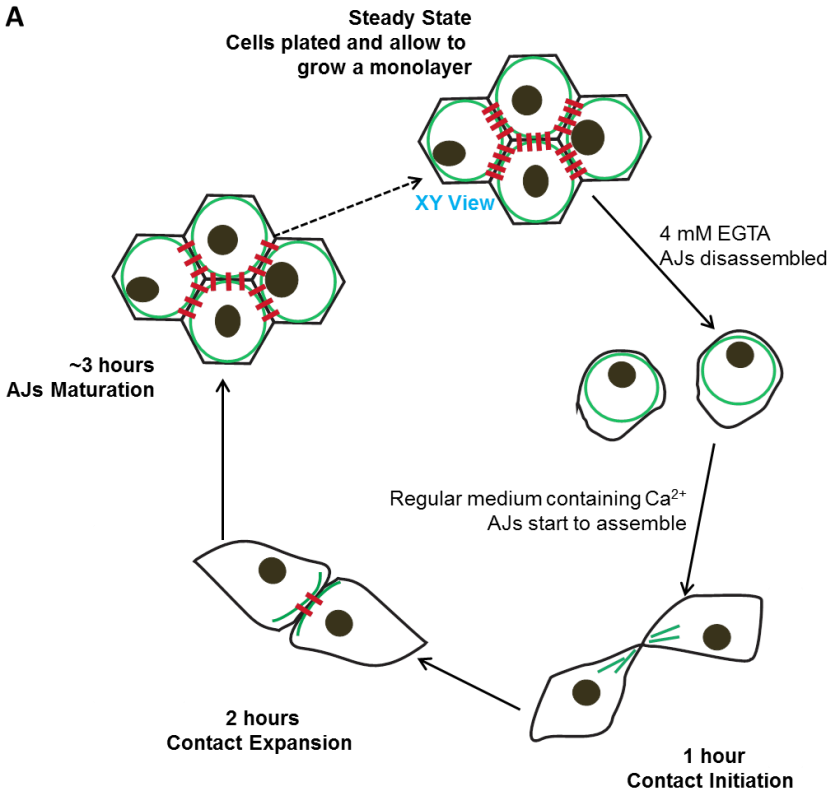
A
Steady State
Cells plated and allow to
grow a monolayer
XY View
4 mM EGTA
AJs disassembled
Regular medium containing Ca^{2+}
AJs start to assemble
1 hour
Contact Initiation
2 hours
Contact Expansion
~3 hours
AJs Maturation

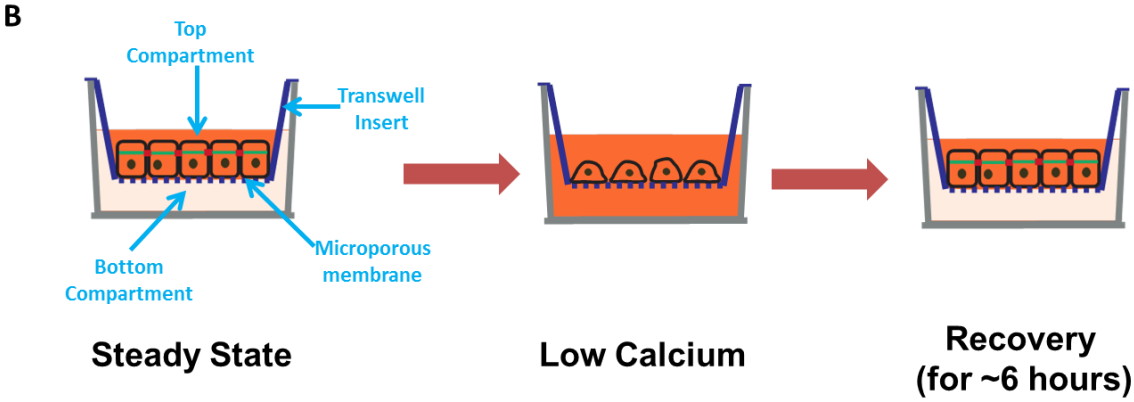
B
Top
Compartment
Transwell
Insert
Microporous
membrane
Bottom
Compartment
Steady State
Low Calcium
Recovery
(for ~6 hours)

Figure 2: Calcium Switch Assay Schematic.

(A) MDCK cells were plated on coverslips for 48 hours until ~90% confluent (Steady state-SS). Addition of low Ca^{2+} media for an hour results in the breakdown of intercellular junctions and cell rounding. Then MDCK cells were induced to synchronously undergo *de novo* cell-cell contact by incubating them in Ca^{2+} containing media. 1, 2 and 3 hours following *de novo* cell-cell contact (post-contact or recovery), cells were fixed in 4% paraformaldehyde and immunostained for adherens junctional proteins to study their intracellular distribution.

(B) Cells were seeded on a permeable membrane to measure their epithelial permeability barrier using 10 µg/mL TRITC-dextran. TRITC-dextran was applied to the top compartment in steady state MDCK cells. Also at 3, 4, 5 and 6 hours following *de novo* cell-cell contact fluorescence intensity from the top and bottom compartment were obtained to determine the % of dextran in the bottom compartment. Red lines spanning cell-cell contacts represent E-cadherin adhesions. Green lines spanning single cells represent F-actin.

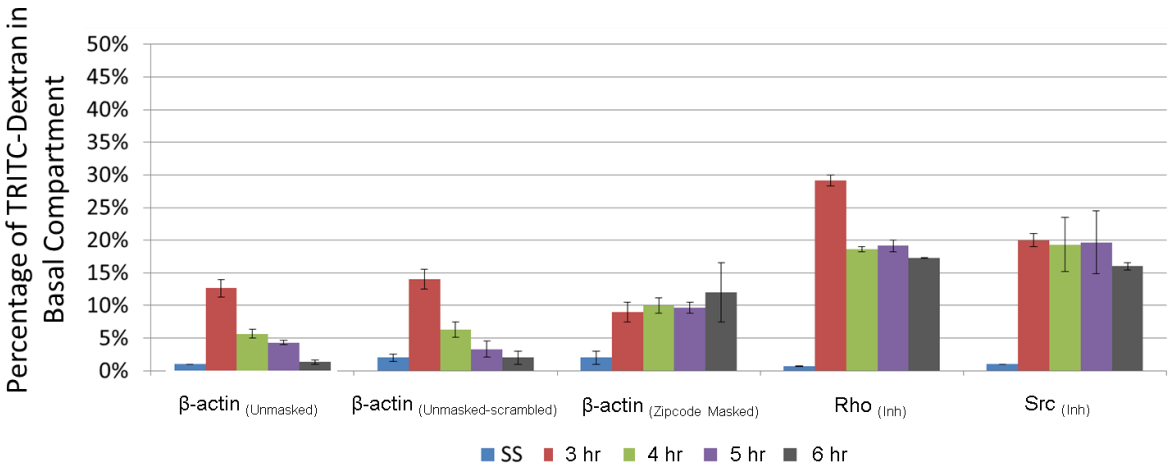
Percentage of TRITC-Dextran in Basal Compartment
50%
45%
40%
35%
30%
25%
20%
15%
10%
5%
0%
β-actin (Unmasked)
β-actin (Unmasked-scrambled)
β-actin (Zipcode Masked)
Rho (Inh)
Src (Inh)
SS
3 hr
4 hr
5 hr
6 hr

Figure 3: Spatially regulated β-actin monomer synthesis is required to assemble a functional epithelial tissue.

Graph illustrating the percent of TRITC-dextran in the bottom compartment measured in an *in vitro* permeability assay for MDCK cells with proper localization of β-actin monomer synthesis (β-actin $_{(Unmasked)}$) during calcium switch assay (left). The same cell line was used for calcium switch experiments in which scrambled oligonucleotides (β-actin $_{(Unmasked\text{-}scrambled)}$), β-actin zipcode antisense oligonucleotides (β-actin $_{(Zipcode\ Masked)}$), C3 transferase ($Rho_{(Inh)}$) or Src Inhibitor-1 ($Src_{(Inh)}$) were used. Error bars show mean ± SEM based on three independent experiments. The graph in this figure is adapted from "*Contact localized β-actin translation drives epithelial adherens junction assembly*" by Natasha C. Gutierrez. Ph.D. Thesis. Rutgers University. Newark, 2014.

A

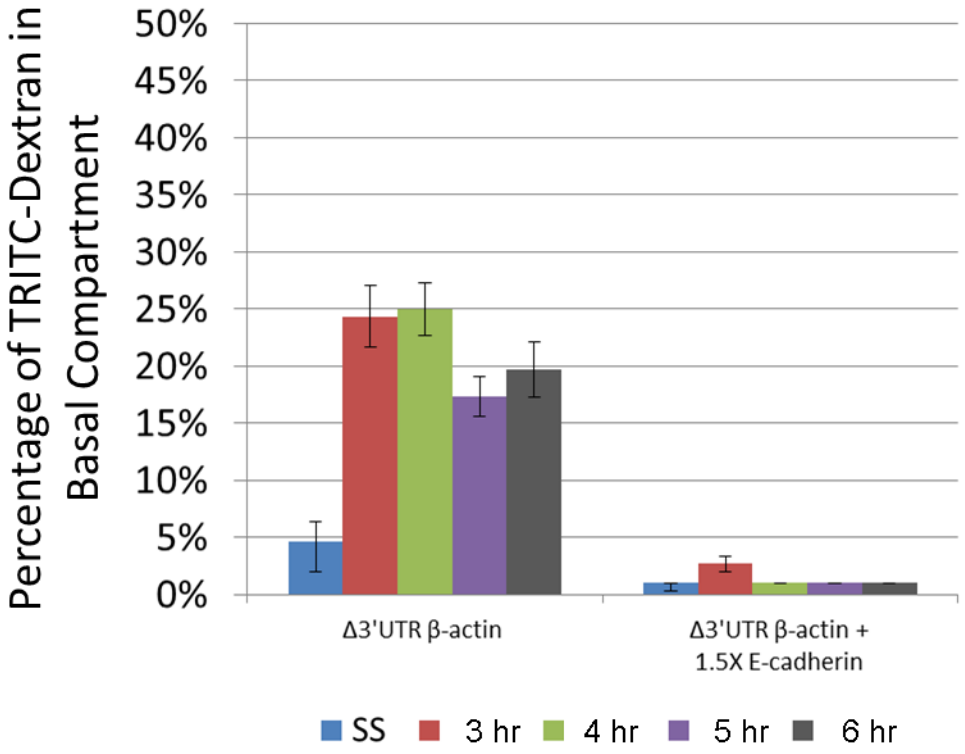

B

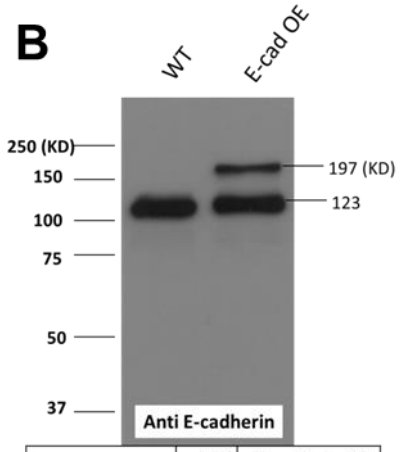

	WT	E-cadherin OE
Relative Density	1.00	1.498148

Figure 4: E-cadherin overexpression rescues tissue permeability barrier in MDCK cells with partial β-actin monomer synthesis delocalization.

(A) Graph illustrating the percent of TRITC-dextran in the bottom compartment measured in an *in vitro* permeability assay for MDCK cells with partial delocalization of β-actin monomer synthesis (Δ3'UTR β-actin MDCK) and in cells with partial delocalization of β-actin monomer synthesis with E-cadherin overexpression (Δ3'UTR β-actin + 1.5X E-cadherin) during calcium switch assay. Error bars in both graphs show Mean ± SEM based on three independent experiments. The graph in this figure is from "*Contact localized β-actin translation drives epithelial adherens junction assembly*" by Natasha C. Gutierrez. Ph.D. Thesis. Rutgers University. Newark, 2014.

(B) Wild type MDCK cell lysates were analyzed using Western blot, staining for E-cadherin in wild type MDCK cells and MDCK cells expressing E-cadherin – RFP under transcriptional control of CMV promoter (E-cad OE). E-cadherin band of the appropriate molecular weight was identified in both cell lysates. Also, a higher E-cadherin molecular weight band corresponding to E-cadherin - RFP (E-cad OE) was observed. The graph in this figure is adapted from "*Contact localized β-actin translation drives epithelial adherens junction assembly*" by Natasha C. Gutierrez. Ph.D. Thesis. Rutgers University. Newark, 2014.

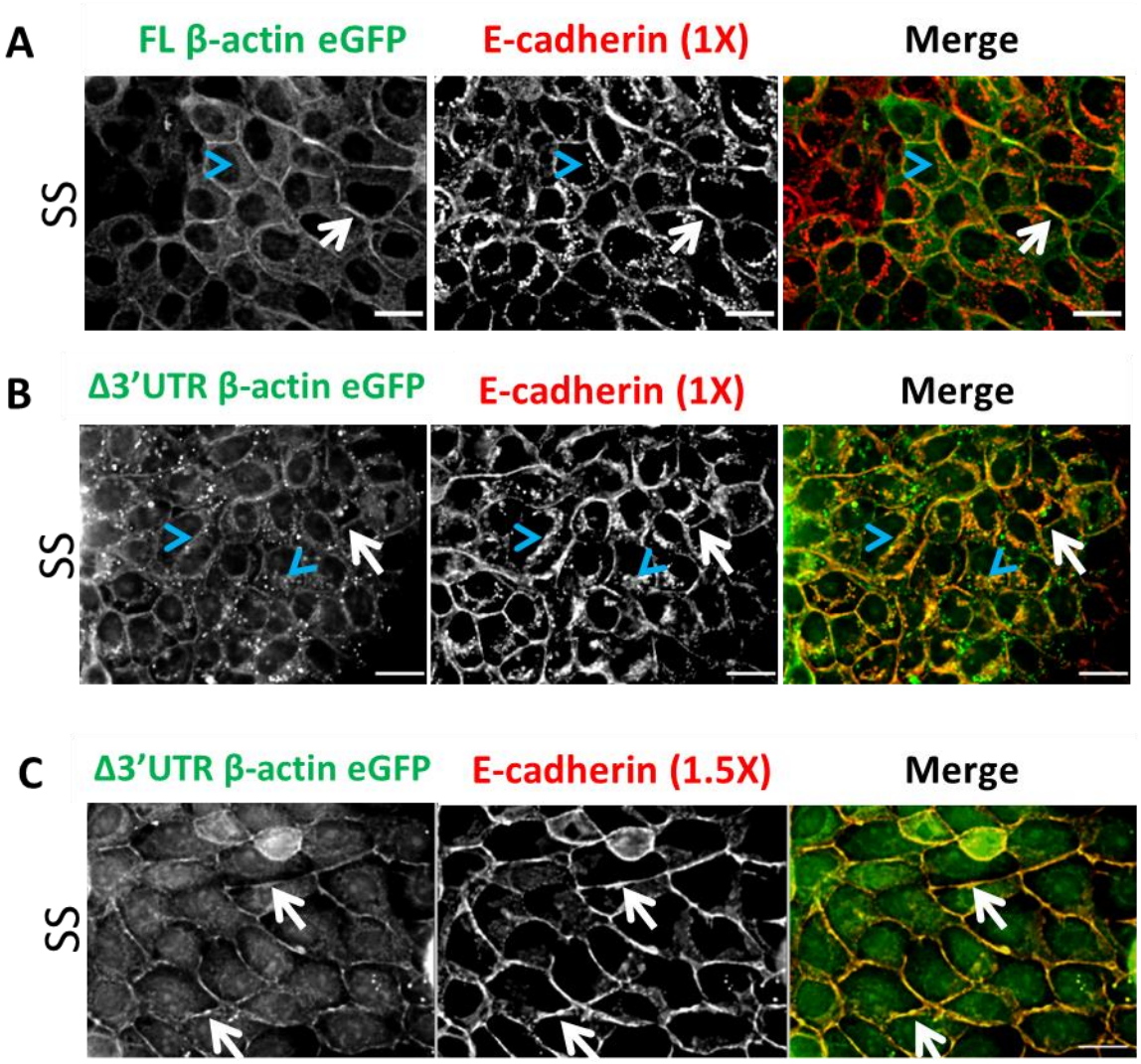
A
FL β-actin eGFP
E-cadherin (1X)
Merge
SS
B
Δ3'UTR β-actin eGFP
E-cadherin (1X)
Merge
SS
C
Δ3'UTR β-actin eGFP
E-cadherin (1.5X)
Merge
SS

Figure 5: E-cadherin overexpression in MDCK cells with partial delocalization of β-actin monomer synthesis rescues adherens junction assembly defects.

E-cadherin and β-actin deconvoluted epifluorescence images of a single plane of MDCK cells at steady state for:

(A) cells that properly localized β-actin monomer synthesis (FL β-actin eGFP),

(B) cells with partial delocalization of β-actin monomer synthesis (Δ3'UTR β-actin) and

(C) cells that overexpress E-cadherin in a partial β-actin monomer synthesis delocalization background (Δ3'UTR β-actin 1.5X E-cadherin).

Note E-cadherin and β-actin colocalization at cell-cell contacts is higher when E-cadherin is overexpressed (white arrows). Cytoplasmic colocalization of E-cadherin with β-actin is only observed in cells with partial delocalization of β-actin monomer synthesis (blue arrowheads).

A

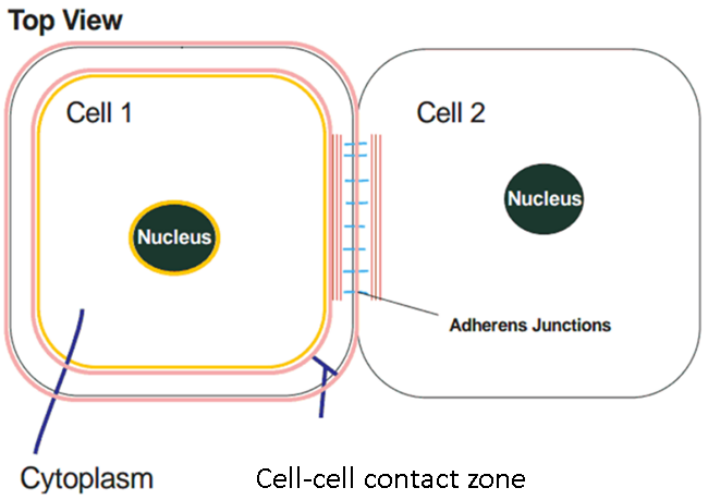

B $$\text{Ratio of Correlations} = \frac{Pearson's\ correlation\ in\ the\ periphery}{Pearson's\ correlation\ in\ the\ cytoplasm}$$

C $$\text{Fluorescence Covariance Index} = \log_{10}(\text{Ratio of Correlations})$$

Figure 6: Fluorescence Covariance Index (FCI) derivation.

(A) Schematic of two cells where the regions of interest are drawn and utilized to calculate the Pearson's Correlation Coefficient in the cytoplasm excluding the nucleus and periphery for two proteins of interest (in our case adherens junctional proteins).

(B) Calculation of the ratio of Pearson's correlations. Pearson's correlation values lower than 0.1 were reassigned to 0.1 since Pearson's correlation values between 0.1 and 0 carry little biological significance (Zinchuk et al., 2013).

(C) Calculation of the Fluorescence Covariance Index (FCI) value. FCI values given by the equation in C. FCI measures relative asymmetry in Pearson's correlation between two cellular compartments: cell-cell contacts and cytoplasm. If ratio is between -1 and 0, then higher Pearson's correlation are present in the cytoplasm. If ratio is between 0 and +1, then higher Pearson's correlations are present at cell-cell contacts.

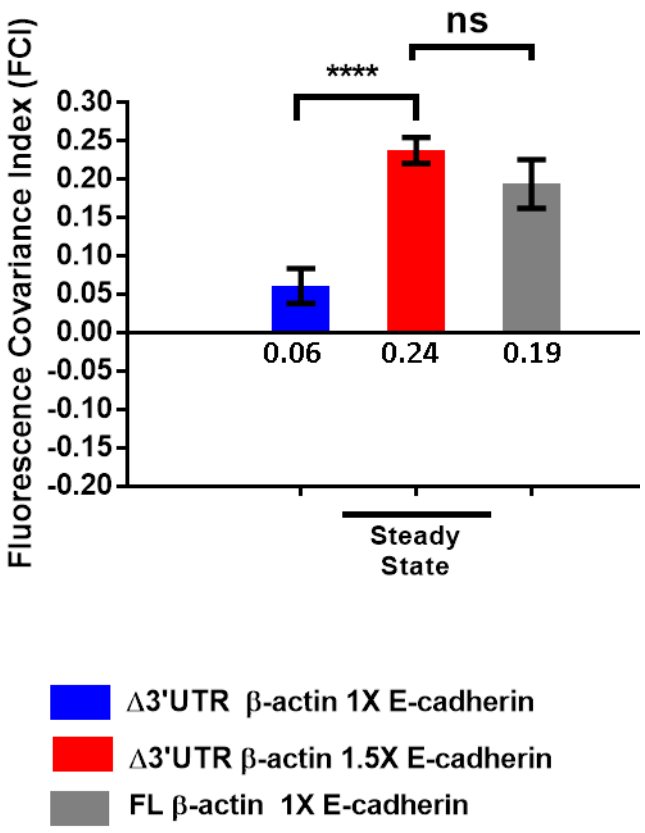
ns
****
Fluorescence Covariance Index (FCI)
0.30
0.25
0.20
0.15
0.10
0.05
0.00
-0.05
-0.10
-0.15
-0.20
0.06
0.24
0.19
Steady State
Δ3'UTR β-actin 1X E-cadherin
Δ3'UTR β-actin 1.5X E-cadherin
FL β-actin 1X E-cadherin

Figure 7: **Fluorescence Covariance Index analysis for E-cadherin and β-actin.** Mean Fluorescence Covariance Index values of MDCK cells with partial delocalization of β-actin monomer synthesis (Δ3'UTR-β-actin 1X E-cadherin - blue bar), cells with E-cadherin overexpression in a partial delocalization β-actin monomer synthesis background (Δ3'UTR-β-actin 1.5X E-cadherin - red bar) and cells that properly localize β-actin monomer synthesis (FL β-actin1X E-cadherin – grey bar) at steady state. Error bars show Mean ± SEM based on three independent experiments for Δ3'UTR-β-actin MDCK cells (blue bar, n=64), Δ3'UTR-β-actin MDCK cells with E-cadherin overexpression (red bar, n=242) and two independent experiments for FL β-actin MDCK cells (grey bar, n=20). The symbol n represents the total number of cells quantified. Kruskal-Wallis test yielded a *p*-value < 0.0001. Dunn's post-hoc multiple comparison test results are **** $p < 0.0001$ and *ns*: not significant.

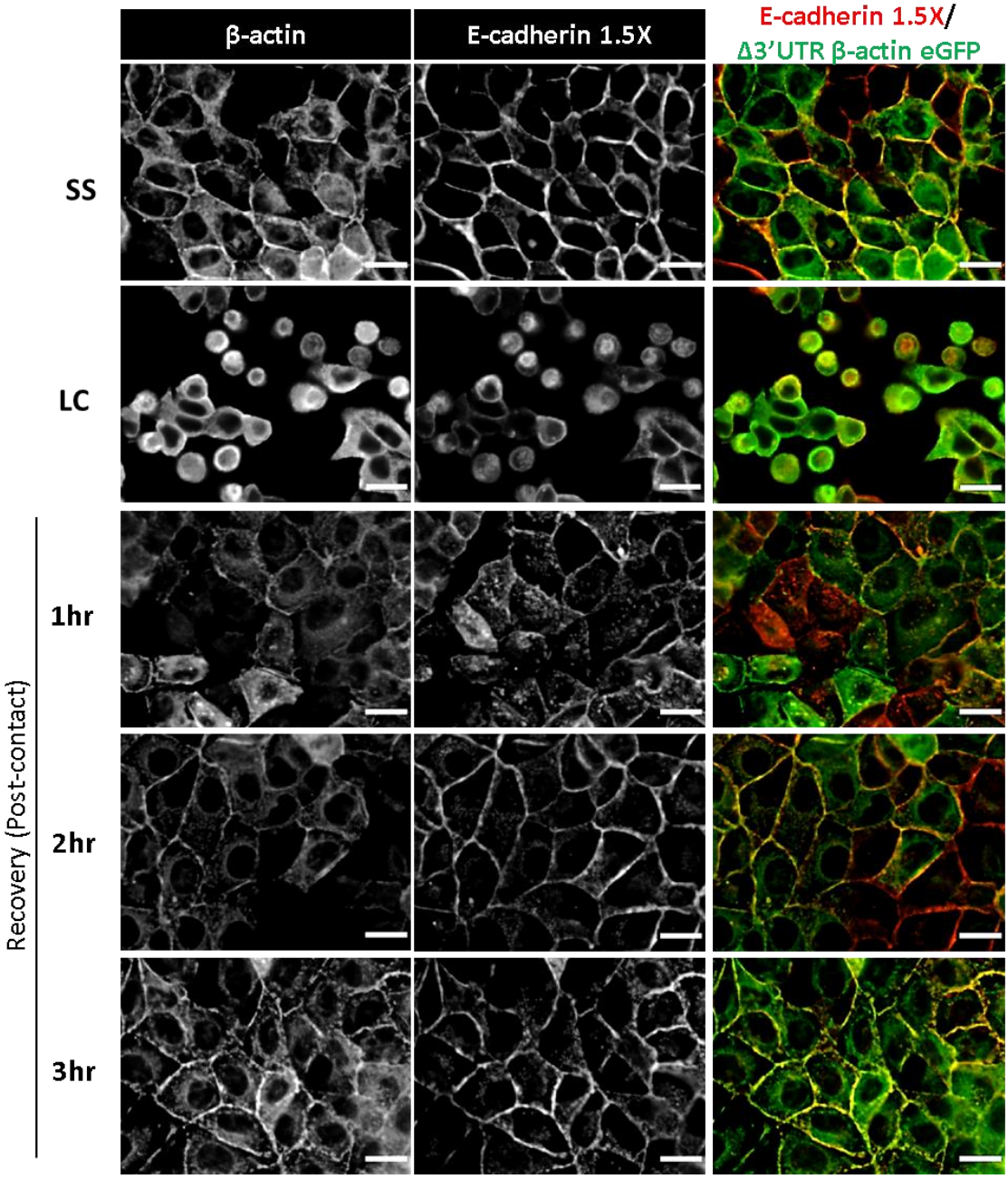
β-actin
E-cadherin 1.5X
E-cadherin 1.5X/
Δ3'UTR β-actin eGFP
SS
LC
Recovery (Post-contact)
1hr
2hr
3hr

Figure 8: E-cadherin overexpression rescues adherens junction assembly defects in MDCK cells partially delocalizing β-actin monomer synthesis characterized by E-cadherin localization with β-actin at cell-cell contacts.

Deconvoluted epifluorescence images of MDCK cells overexpressing E-cadherin (red) in a background of partially delocalized β-actin monomer synthesis (green). Cells were grown until ~90% confluency (SS), treated with low Ca^{2+} media for an hour (LC) to induce the breakdown of intercellular junctions. Then, cells were incubated in Ca^{2+} containing media for 3 hours to examine and quantitate the formation of new adherens junctions (Recovery). Scale bars represent 20μm.

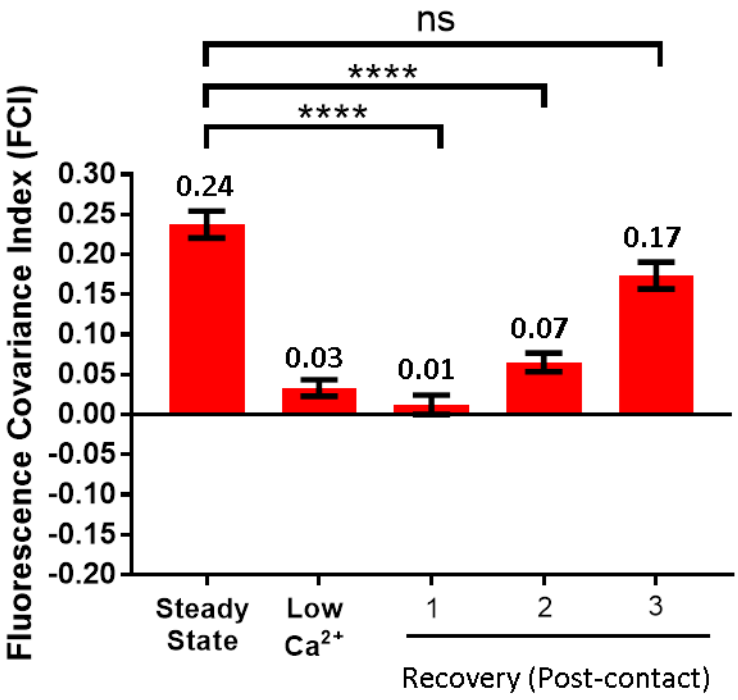
ns
****
****
Fluorescence Covariance Index (FCI)
0.30
0.25
0.20
0.15
0.10
0.05
0.00
-0.05
-0.10
-0.15
-0.20
0.24
0.03
0.01
0.07
0.17
Steady State
Low Ca2+
1
2
3
Recovery (Post-contact)

Figure 9: FCI analysis of E-cadherin and β-actin.

Mean FCI values for images presented in **Figure 8**. Error bars show Mean ± SEM based on three independent experiments. A Kruskal-Wallis test excluding low calcium data yielded a *p*-value < 0.0001. Dunn's post-hoc multiple comparison test results are **** $p < 0.0001$ and *ns*: not significant (SS, n=242; LC, n=105; 1 hour, n=178; 2 hours, n=215; 3 hours, n=204). The symbol n represents the total number of cells quantified. I would like to acknowledge Bryan Ayee and Justin Davis for obtaining FCI values for this graph.

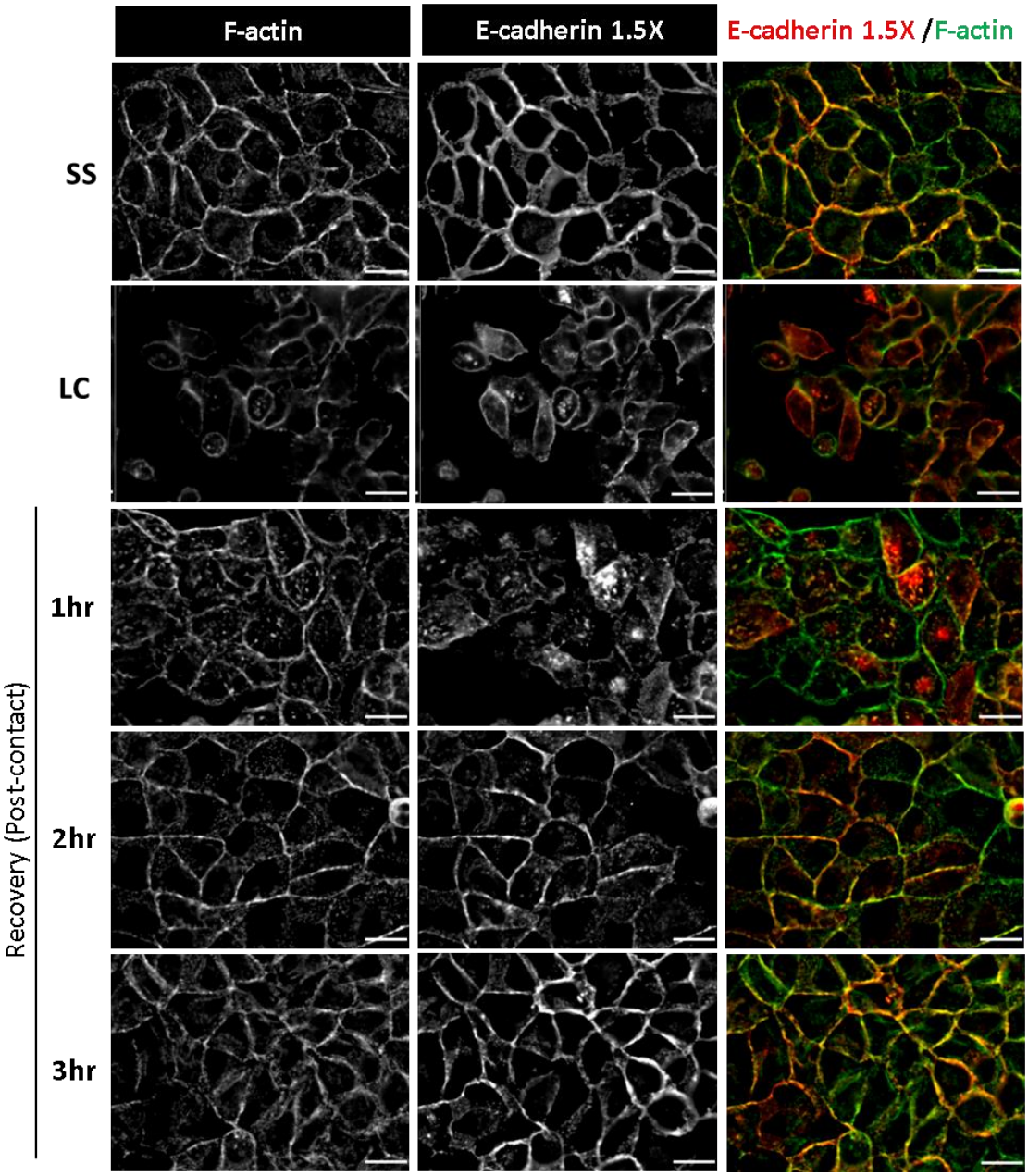
F-actin
E-cadherin 1.5X
E-cadherin 1.5X /F-actin
SS
LC
1hr
2hr
3hr
Recovery (Post-contact)

Figure 10: E-cadherin overexpression rescues adherens junction assembly defects in MDCK cells partially delocalizing β-actin monomer synthesis characterized by E-cadherin localization with F-actin at cell-cell contacts.

Deconvoluted epifluorescence images of MDCK cells overexpressing E-cadherin (red) in a background of partially delocalized β-actin monomer synthesis. Cells were grown until ~90% confluency (SS), treated with low Ca^{2+} media for an hour (LC) to induce the breakdown of intercellular junctions. Then, cells were incubated in Ca^{2+} containing media for 3 hours to examine and quantitate the formation of new adherens junctions (Recovery). E-cadherin = red; F-actin = green. Scale bars represent 20μm.

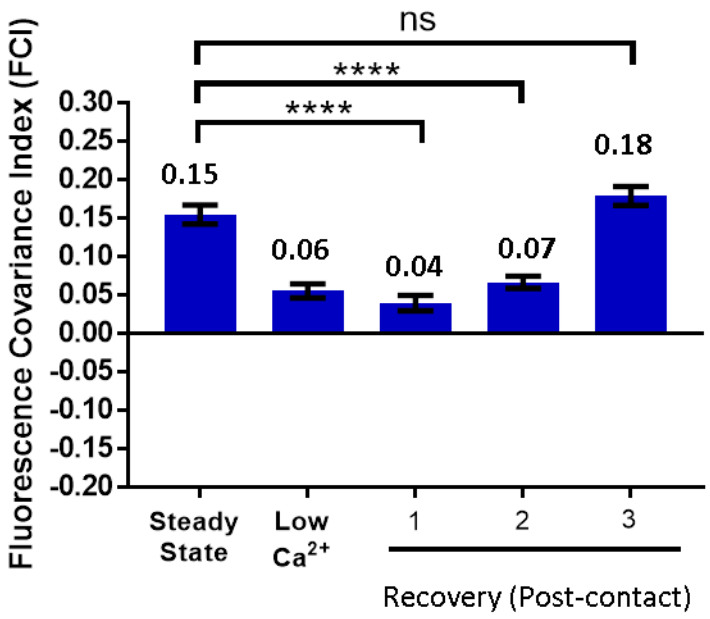
ns
****
****
Fluorescence Covariance Index (FCI)
0.30
0.25
0.20
0.15
0.10
0.05
0.00
-0.05
-0.10
-0.15
-0.20
0.15
0.06
0.04
0.07
0.18
Steady State
Low Ca2+
1
2
3
Recovery (Post-contact)

Figure 11: FCI analysis of E-cadherin and F-actin.

Mean FCI values for images shown in **Figure 10**. Error bars show Mean ± SEM based on three independent experiments. A Kruskal-Wallis test (excluding low calcium data) yielded a *p*-value < 0.0001. Dunn's post-hoc multiple comparison test results are **** $p < 0.0001$ and *ns*: not significant (SS, n=242; LC, n=105; 1 hour, n=178; 2 hours, n=215; 3 hours, n=204). The symbol n represents the total number of cells quantified. I would like to acknowledge Bryan Ayee and Justin Davis for obtaining FCI values for this graph.

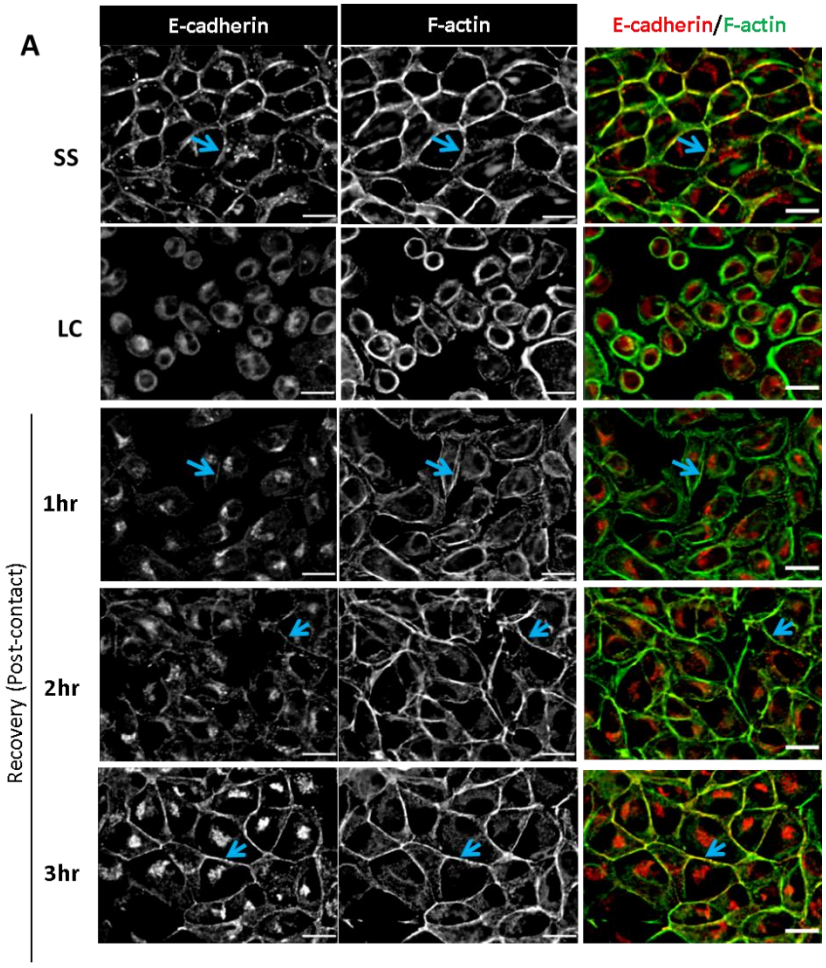
A
E-cadherin
F-actin
E-cadherin/F-actin
SS
LC
1hr
2hr
3hr
Recovery (Post-contact)

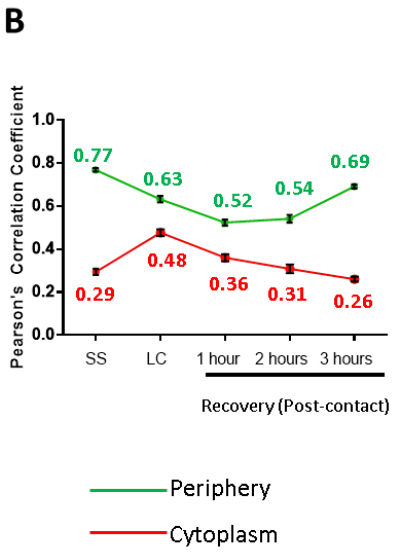
B
Pearson's Correlation Coefficient
1.0
0.8
0.6
0.4
0.2
0.0
0.77
0.63
0.52
0.54
0.69
0.29
0.48
0.36
0.31
0.26
SS
LC
1 hour
2 hours
3 hours
Recovery (Post-contact)
Periphery
Cytoplasm

Figure 12: **E-cadherin localization with F-actin increase at epithelial cell-cell contact zones following *de novo* adherens junction assembly in wild type MDCK cells.**

(A) Deconvoluted single plane images for wild type MDCK cells at steady state (SS), low calcium (LC) and 1, 2 and 3 hours post-contact. Blue arrows indicate cell-cell contacts. Notice E-cadherin (red) and F-actin (green) co-stain at cell-cell contacts in steady state (SS). Following *de novo* cell-cell contact 1, 2 and 3 hours F-actin and E-cadherin gradually accumulate at cell-cell contacts. Scale bar in all images = 20μm.

(B) Change in Pearson's correlation coefficient values for E-cadherin and F-actin in the periphery and the cytoplasm measured for wild type MDCK cells shown in panel **A**. Points represent mean ± SEM. Note that 3 hours post-contact mean Pearson's correlation coefficient value in the periphery increases.

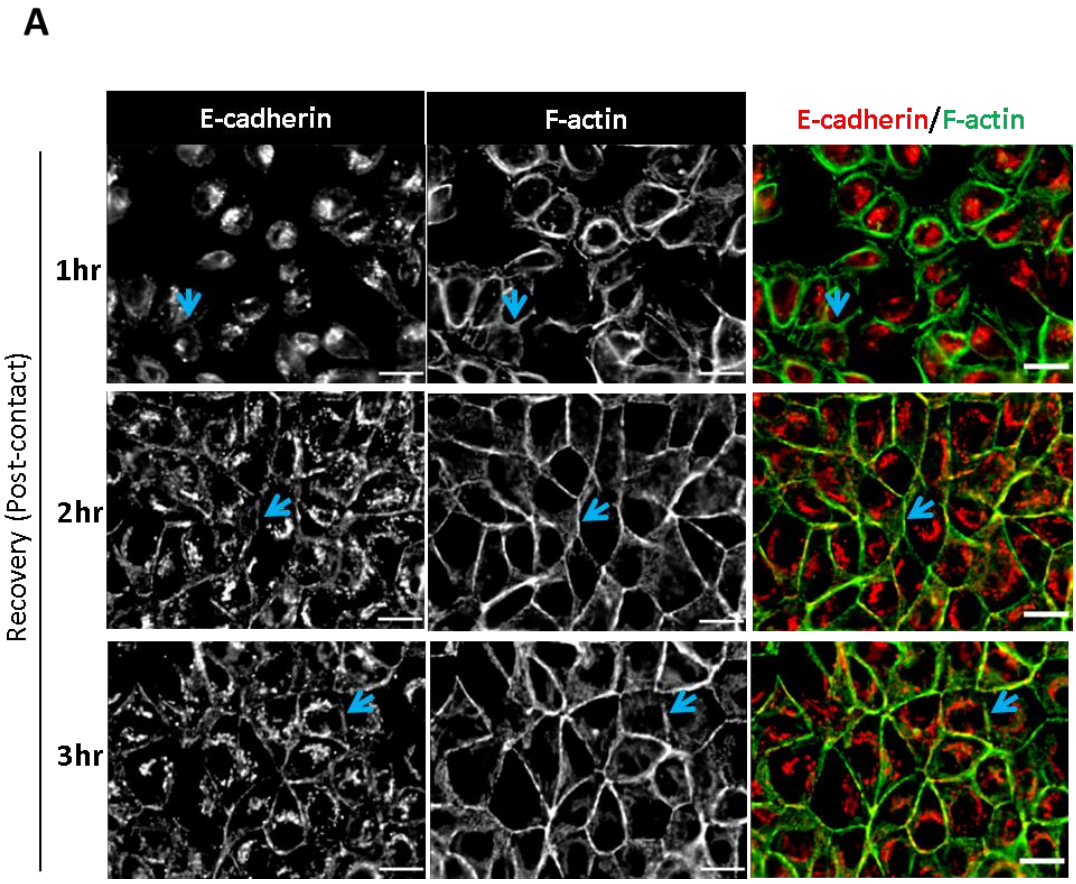
A
E-cadherin
F-actin
E-cadherin/F-actin
Recovery (Post-contact)
1hr
2hr
3hr
B
Pearson's Correlation Coefficient
1.0
0.8
0.6
0.4
0.2
0.0
0.51
0.63
0.54
0.38
0.30
0.23
1 hour
2 hours
3 hours
Recovery (Post-contact)
+DECMA-1 = 100 µg/ml
Periphery
Cytoplasm

Figure 13: Adherens junction formation is perturbed when E-cadherin function is inhibited in wild type MDCK cells.

(A) Representative images for MDCK cells treated with 100 µg/mL of E-cadherin function blocking antibodies (DECMA-1) at 1, 2 and 3 hours post-contact. Blue arrows indicate cell-cell contacts. Notice F-actin (green) and E-cadherin (red) accumulation at cell-cell contacts decreases in comparison to the controls (compare **Figure 13** and **Figure 12**: 3hrs, blue arrows). Scale bar in all images = 20µm.

(B) Change in Pearson's correlation coefficient values for E-cadherin and F-actin in the periphery and the cytoplasm measured for MDCK cells treated with DECMA-1 (100 µg/ml) during *de novo* cell-cell contact. Points represent Mean ± SEM. Note 3 hours post-contact mean Pearson's correlation coefficient value in the periphery decreases.

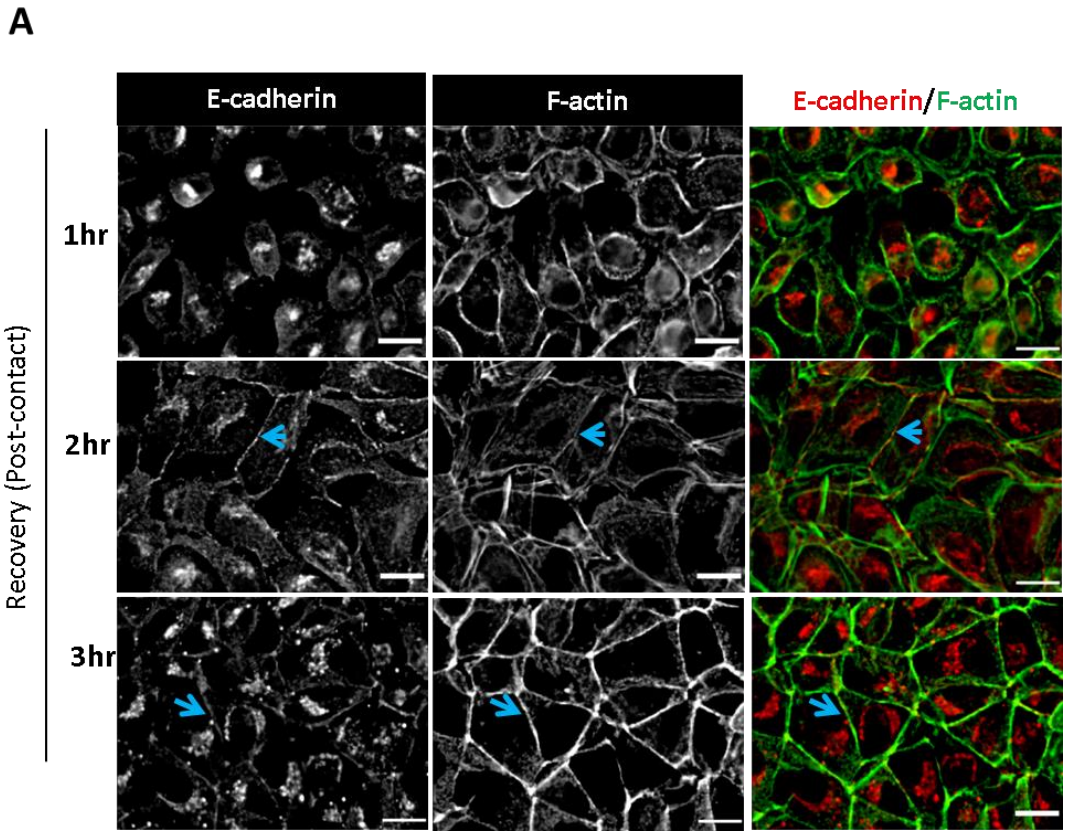
A
E-cadherin
F-actin
E-cadherin/F-actin
Recovery (Post-contact)
1hr
2hr
3hr

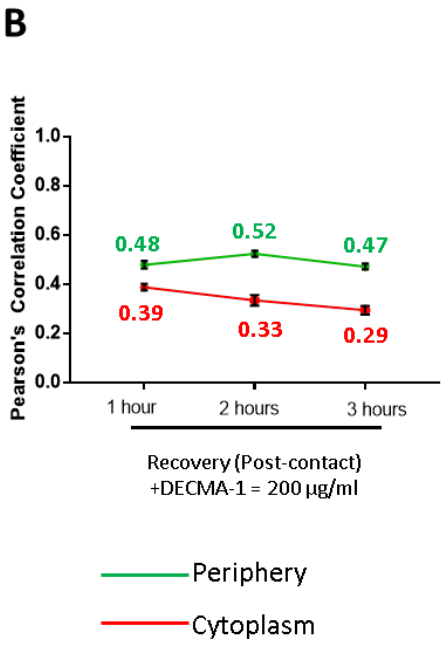
B
Pearson's Correlation Coefficient
1.0
0.8
0.6
0.4
0.2
0.0
0.48
0.52
0.47
0.39
0.33
0.29
1 hour
2 hours
3 hours
Recovery (Post-contact)
+DECMA-1 = 200 µg/ml
Periphery
Cytoplasm

Figure 14: **Adherens junction formation is effectively perturbed when higher concentration of E-cadherin function inhibition antibody is used in wild type MDCK cells**.

(A) Representative images of cells treated with 200 µg/mL of E-cadherin function blocking antibodies (DECMA-1) at 1, 2 and 3 hours post-contact. Blue arrows indicate cell-cell contacts. Notice F-actin (green) and E-cadherin (red) accumulation at cell-cell contacts is further decreased in comparison to the controls **(Figure12)** and MDCK cells treated with a lower concentration of E-cadherin function blocking antibodies **(Figure 13).** Scale bar in all images = 20µm.

(B) Change in Pearson's correlation coefficient values for E-cadherin and F-actin in the periphery and the cytoplasm measured for MDCK cells treated with DECMA-1 (200 µg/ml) 1, 2 and 3 hours post-contact. Points represent Mean ± SEM. Note that at 3 hours post-contact mean Pearson's correlation coefficient value in the periphery remains low.

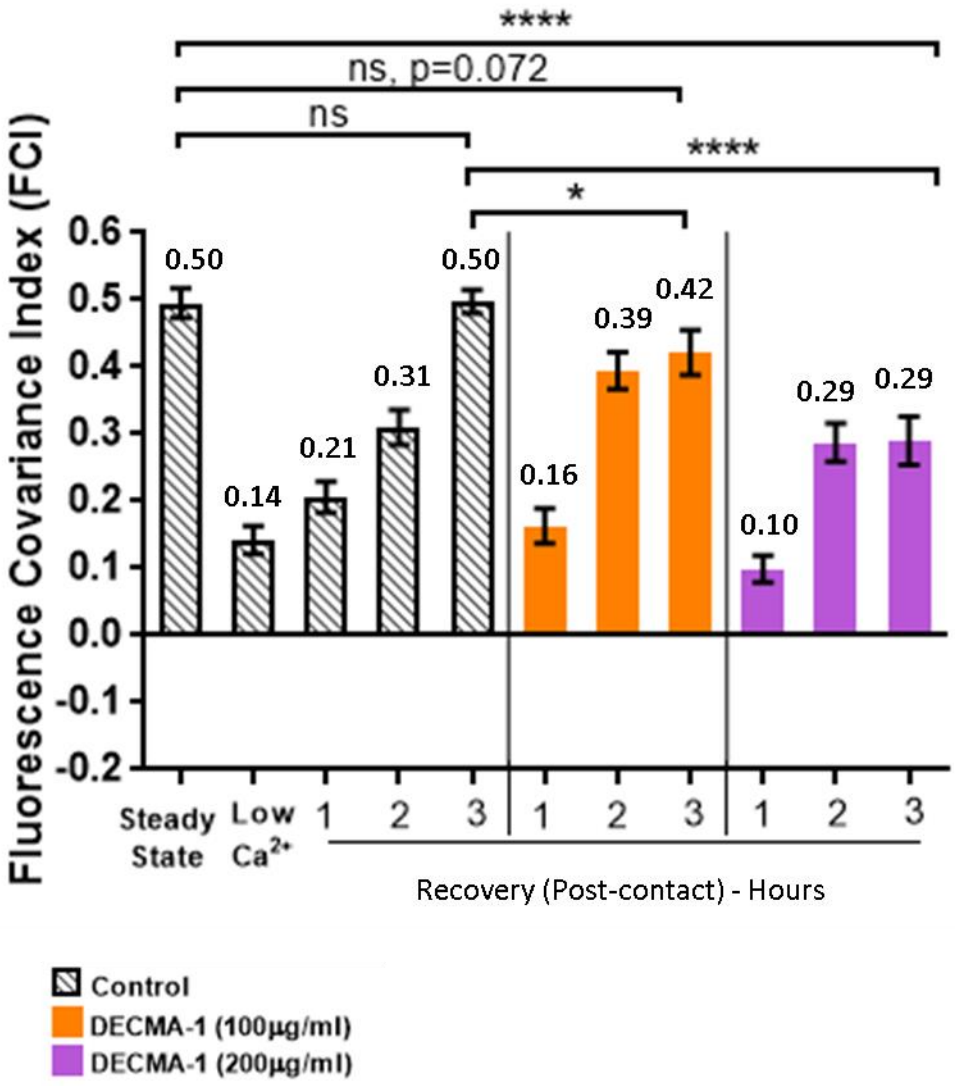
****
ns, p=0.072
ns
****
*
Fluorescence Covariance Index (FCI)
0.6
0.5
0.4
0.3
0.2
0.1
0.0
-0.1
-0.2
0.50
0.14
0.21
0.31
0.50
0.16
0.39
0.42
0.10
0.29
0.29
Steady State
Low Ca2+
1
2
3
1
2
3
1
2
3
Recovery (Post-contact) - Hours
Control
DECMA-1 (100µg/ml)
DECMA-1 (200µg/ml)

Figure 15: **Fluorescence Covariance Index analyses of E-cadherin and F-actin during *de novo* adherens junction assembly.**

Mean FCI measurements for E-cadherin and F-actin with (orange and magenta bars) and without (black bars) DECMA-1 treatment following *de novo* cell-cell contact for **Figures 12, 13 and 14**. Error bars show Mean ± SEM based on three independent experiments. Unpaired t-test with Welch's correction result: * P<0.05; ** P<0.005; **** P<0.0001. Note as increasing concentrations of E-cadherin function blocking antibody is used during calcium switch assays, adherens junction assembly decreases depicted by the decrease in mean FCI values. Controls black bars (SS, n=140; LC, n=105; 1 hour, n=141; 2 hours, n=99; 3 hours, n=196). Orange bars 100 µg/mL of DECMA-1 (1 hour, n=83; 2 hours, n=82; 3 hours, n=76). Magenta bars 200 µg/mL of DECMA-1 (1 hour, n=126; 2 hours, n=100; 3 hours, n=110). The symbol n represents the total number of cells quantified.

E-cadherin knockdown delocalizes β-actin monomer synthesis from *de novo* cell-cell contact

Previous research using a β-actin translation site imaging reporter MDCK cell line demonstrated *de novo* cell-cell contact induces spatially localized β-actin monomer synthesis (Gutierrez et al., 2014). Spatially localized β-actin monomer synthesis is required for epithelial adherens junction assembly and subsequent formation of a functional epithelial tissue barrier (Gutierrez et al., 2014; Cruz et al., 2015). Mechanistically, *de novo* cell-cell contact localized β-actin monomer synthesis is regulated by reversible binding between the β-actin mRNA zipcode and the translational regulator Zipcode Binding Protein-1 (ZBP1) (Gutierrez et al., 2014; Hüttelmaier et al., 2005). The β-actin and ZBP1 interaction is mediated by Src kinase. Specifically, Src phosphorylates the translational repressor zipcode binding protein-1 (ZBP-1) when is bound to the β-actin mRNA, resulting in ZBP-1/β-actin complex disassembly leading to β-actin monomer synthesis (Hüttelmaier et al., 2005). It is well known that E-cadherin localizes the regulators of β-actin mRNA localization, RhoA and Src, at cell-cell contacts (McLachlan et al., 2007; Rodriguez et al., 2008; Rodriguez et al., 2006; Gutierrez et al. 2014). However, E-cadherin's role in regulating downstream β-actin monomer synthesis during *de novo* adherens junction assembly has not been studied.

I quantified β-actin monomer synthesis at *de novo* cell-cell contact sites when E-cadherin protein expression is reduced (for details see Materials and Methods). An MDCK stable cell line was generated using the construct full-length TC-eGFP-β-actin translation site reporter (FL-β-actin; Gutierrez et al., 2014; Rodriguez et al., 2006) (**Figure 16B**). MDCK cells expressing the β-actin

translation site reporter were stained with the biarsenical dyes FlAsH (fluorescein arsenical harpain binder) and ReAsH (resorufin arsenical hairpin binder) (**Figure 16A;** Adams et al., 2002; Gutierrez et al., 2014; Rodriguez et al., 2006). Both biarsenical dyes bind to a cysteine tetrad that is generated by the TC-eGFP-β-actin construct expressed in MDCK cells (**Figure 16B;** Adams et al., 2002; Madani et al., 2009). Adherens junctional complexes were disassembled and existing β-actin monomers were labelled using low calcium media containing FlAsH for one hour. *De novo* cell-cell contacts were initiated by incubating the reporter cell lines in Ca^{2+}-containing recovery media for 2.5 hours. After 2.5 hours in recovery media, β-actin translation sites were chase-stained with ReAsH staining solution containing cycloheximide for 30 minutes labeling every β-actin nascent polypeptide chain at polysomes red. Consequently, β-actin monomers synthesized prior to *de novo* cell-cell contact are green while β-actin synthesized following *de novo* contacts are red. In the β-actin translation site imaging reporter MDCK cells expressing endogenous E-cadherin levels, *de novo* cell-cell contact robustly induces β-actin monomer synthesis throughout both the cytoplasm and cell-cell contact zone (**Figure 17A: Endogenous E-cadherin**; Gutierrez et al., 2014).

To assess the relationship between E-cadherin expression and β-actin monomer synthesis, we made a set of E-cadherin knockdowns in MDCK cells expressing the β-actin translation site reporter (for details see Material and Methods). Knocking down E-cadherin had no effect in endogenous total actin and β-catenin protein levels (**Figure 18**). A “mock” control was used to confirm the lipid based transfection reagent is not altering total protein expression levels (**Figure 18: Mock**). β-actin monomer synthesis sites were imaged during Ca^{2+}

switch experiments in each of the E-cadherin knockdown β-actin translation site reporter MDCK cell lines (**Figure 17A**). Similar to MDCK cells expressing endogenous E-cadherin, MDCK cells expressing 0.70X E-cadherin in the β-actin translation site imaging reporter cell line, also robustly induces β-actin monomer synthesis throughout both the cytoplasm and contact zone (**Figure 17A: ~70 Remaining E-cadherin protein expression**). Quantitatively, although *de novo* cell-cell contact robustly induces β-actin monomer synthesis throughout the cytoplasm in the 70%-E-cadherin cells, there was a modest reduction in the number of cell-cell contacts localized β-actin translation sites (**Figure 17B: compare control versus ~70% remaining E-cadherin**). By contrast, in the 50%-E-cadherin β-actin translation site imaging reporter cells, *de novo* cell-cell contact robustly induces β-actin monomer synthesis throughout the cytoplasm but not at the contact zone where there are only ~0.27x the number of β-actin translation sites relative to endogenous E-cadherin cells (**Figure 17A and 17B: ~50% remaining E-cadherin).** Similarly, in the 30%-E-cadherin β-actin translation site imaging reporter cells, *de novo* cell-cell contact also robustly induces β-actin monomer synthesis throughout the cytoplasm but not at the contact zone where there are only ~0.37x the number of β-actin translation sites relative to endogenous E-cadherin cells (**Figure 17A and 17B: ~30% remaining E-cadherin**). Together, these data demonstrate cell-cell contact localized β-actin monomer synthesis correlates with E-cadherin protein expression levels. Consequently, cells with reduced E-cadherin protein expression are expected to have defects in polymerizing cell-cell contact localized linear actin filaments required for E-cadherin anchoring and formation of a functional tissue barrier.

E-cadherin homophilic binding is required for localized β-actin monomer synthesis at *de novo* cell-cell contact sites

Since E-cadherin knockdown induces and shuts off numerous transcription factors regulating both compensatory and antagonistic pathways, I determined the extent to which inhibiting E-cadherin homophilic binding with function blocking antibodies in MDCK cells expressing the β-actin translation site reporter perturbed *de novo* cell-cell contact localized β-actin monomer synthesis. Adherens junction complexes were disassembled using low calcium media containing FlAsH for one hour. FlAsH labels all existing β-actin monomers synthesize prior to and during the disassembly of adherens junction complexes. *De novo* cell-cell contact was initiated by incubating with Ca^{2+} recovery media containing the E-cadherin homophilic binding inhibitor, DECMA-1, for 2.5 (for details see Materials and Methods). After, 2.5 hours in recovery media with the binding inhibitor, MDCK cells were chase-stained with ReAsH for 30 minutes. As a result, β-actin monomers synthesized before *de novo* cell-cell contacts are green and those synthesized post-contact are red. In MDCK cells treated with recovery media without binding inhibitor, β-actin monomer synthesis sites were present throughout the cell-cell contact zones as well as in the cytoplasm (**Figure 19A: Control**). Interestingly, at suboptimal concentrations of binding inhibitor (50 and 100 µg/ml DECMA-1 antibody; for details see Material and Methods), there were modest but reproducible reductions in the number of cell-cell contact localized β-actin monomer synthesis sites 3-hours post-contact (**Figure 19A: DECMA-1 50 µg/ml and DECMA-1 100 µg/ml**). By contrast, at the optimal concentration of the binding inhibitor, approximately 1/3 of β-actin monomer synthesis sites were

observed at cell-cell contacts **(Figures 19A and 19B: DECMA-1 200 µg/ml**). Taken together these data demonstrate the number of cell-cell contact localized β-actin monomer synthesis sites is inversely proportional to the concentration of binding inhibitor (**Figure 19B**). These data demonstrate E-cadherin homophilic binding activity is required to localize β-actin monomer synthesis to *de novo* cell-cell contact sites. Furthermore, quantifying adherens junction complex assembly during calcium switch assays in the presence of binding inhibitor demonstrated decreases in E-cadherin and F-actin anchoring, which correlated with the observed decreases in cell-cell contact localized β-actin monomer synthesis **(Figure 15; Figure 19B**). Remarkably, Western blots from tissues assembled from wild type MDCK cells where E-cadherin function is inhibited (200 µg/ml DECMA-1) during Ca^{2+} switch assay showed no significant changes in total β-actin protein expression (**Figure 20A and 20B**); demonstrating spatial regulation of local translation is important during adherens junction assembly. Taken together, these results demonstrate E-cadherin homophilic binding is required to localize β-actin monomer synthesis to cell-cell contact sites to facilitate *de novo* adherens junction assembly.

A

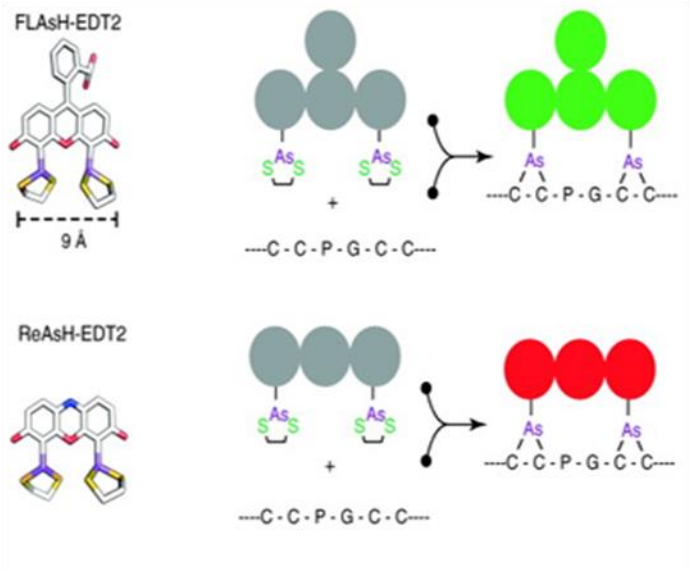
FLAsH-EDT2
9 Å
ReAsH-EDT2
----C - C - P - G - C - C----
----C - C - P - G - C - C----

B

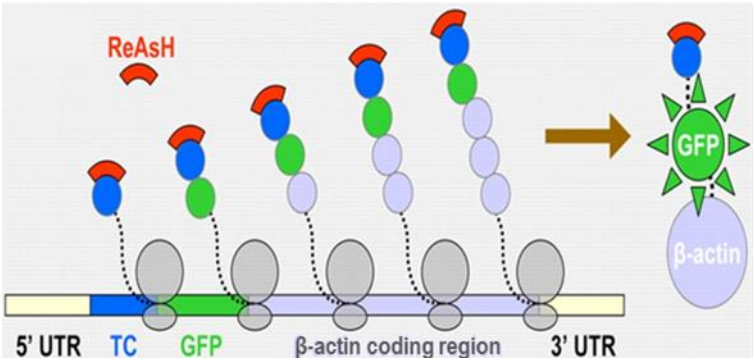
ReAsH
GFP
β-actin
5' UTR
TC
GFP
β-actin coding region
3' UTR

Figure 16: Translation Site Imaging Method to detect β-actin monomer synthesis at cell-cell contact zones.

(A) Structure of the biarsenicel dyes FLAsH-EDT_2 and ReAshH-EDT_2 from Crivat, G., and Taraska, W. Trends in Biotechnol. (2012 Jan). These biarsenical dyes become fluorescent when they bind to recombinant proteins containing the tetracysteine motif (-C-C-P-G-C-C-).

(B) Schematic representation of the translation site detection scheme from Rodriguez, A.J., Shenoy, S.M., Singer, R.H., and Condeelis J. in JCB. (2006 Oct). ReAsH labels cells containing the tetracysteine motif of nascent chains of β-actin.

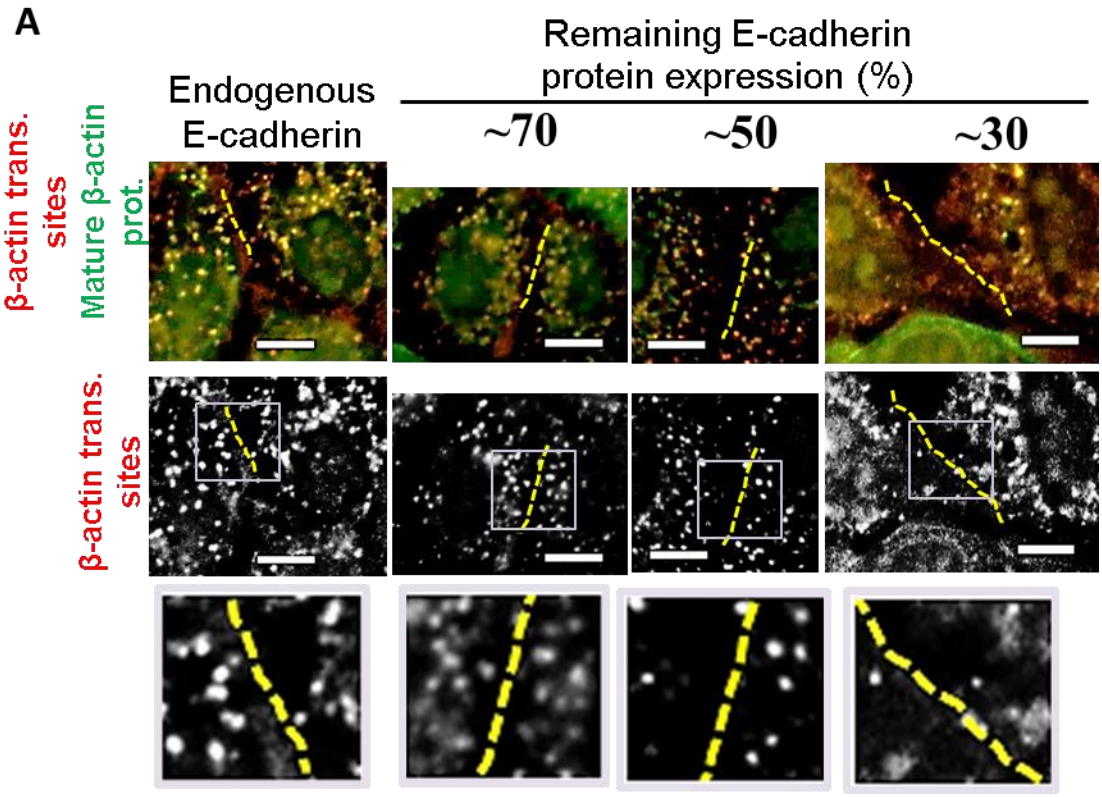
A
Remaining E-cadherin protein expression (%)
Endogenous E-cadherin
~70
~50
~30
β-actin trans. sites
Mature β-actin prot.
β-actin trans. sites

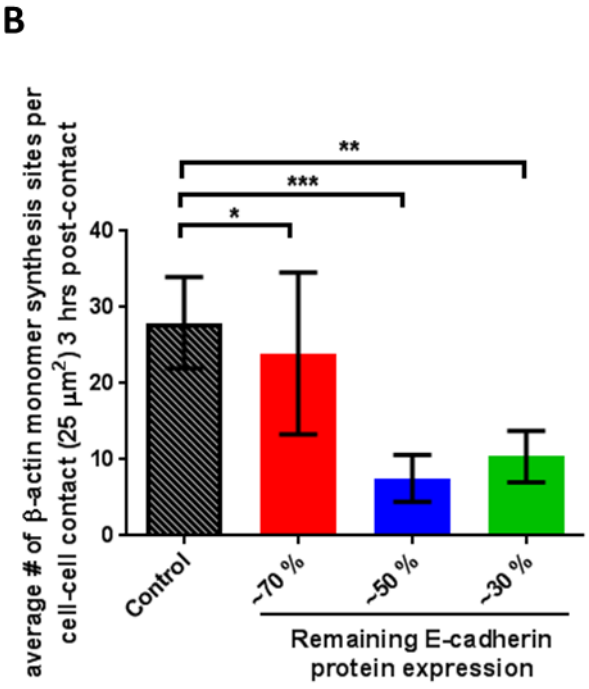
B
average # of β-actin monomer synthesis sites per cell-cell contact (25 μm²) 3 hrs post-contact
0
10
20
30
40
*
***
**
Control
~70 %
~50 %
~30 %
Remaining E-cadherin protein expression

Figure 17: E-cadherin expression regulates β-actin monomer synthesis sites at epithelial cell-cell contacts.

(A) Deconvoluted epifluorescence images of MDCK cells properly localizing β-actin monomer synthesis (FL β-actin mRNA) fixed at 3 hrs post-contact when E-cadherin protein expression is decreased. These cells were stained for *de novo* β-actin monomer synthesis (red). Mature β-actin is green. Dotted yellow lines indicate cell-cell contacts (determined by DIC). Scale bars 10 μm

(B) Mean average number of β-actin monomer synthesis sites per cell-cell contacts for images shown in **A**. Single plane image was used to quantify translation sites at cell-cell contact zone (Area back from the cell edge: 5 um^2). Mann-Whitney test was applied. * $p < 0.05$; **, $p < 0.01$; ***,$p < 0.001$ and error bars indicate mean ± SEM. n=20, where n is the number of cells quantified from a single experiment.

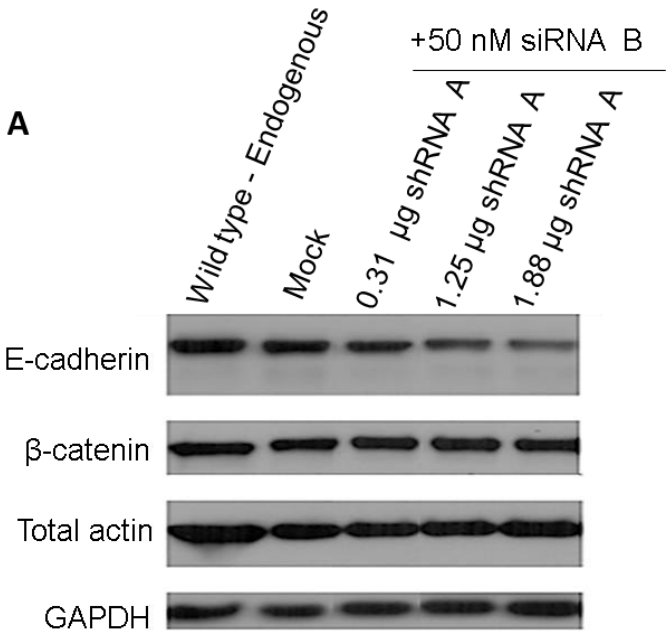
A
+50 nM siRNA B
Wild type - Endogenous
Mock
0.31 µg shRNA A
1.25 µg shRNA A
1.88 µg shRNA A
E-cadherin
β-catenin
Total actin
GAPDH

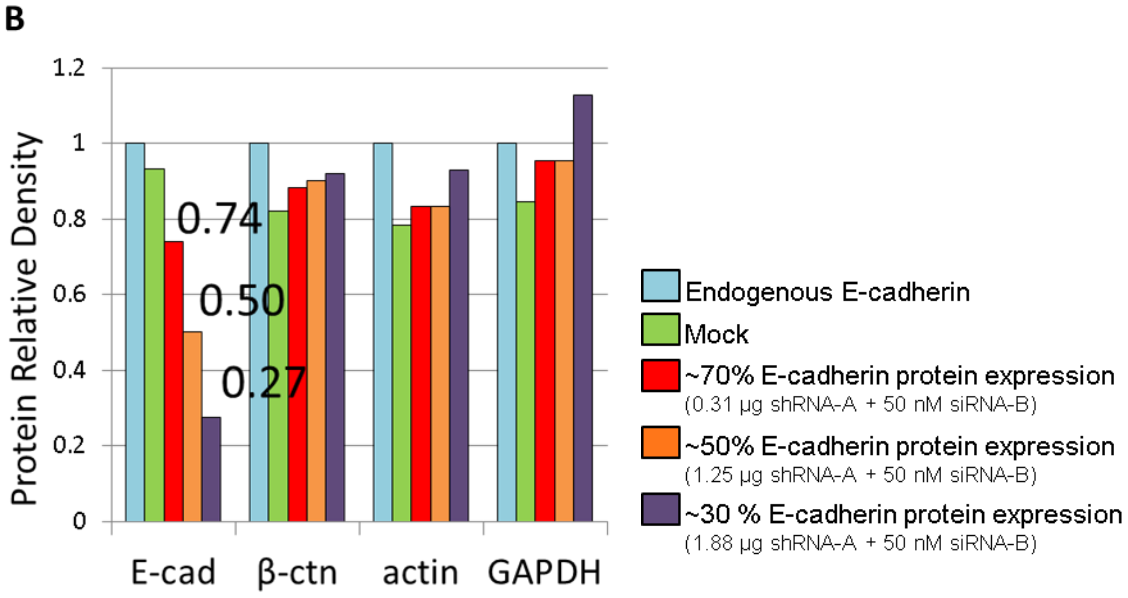
B
Protein Relative Density
1.2
1
0.8
0.6
0.4
0.2
0
0.74
0.50
0.27
E-cad
β-ctn
actin
GAPDH
Endogenous E-cadherin
Mock
~70% E-cadherin protein expression
(0.31 µg shRNA-A + 50 nM siRNA-B)
~50% E-cadherin protein expression
(1.25 µg shRNA-A + 50 nM siRNA-B)
~30 % E-cadherin protein expression
(1.88 µg shRNA-A + 50 nM siRNA-B)

Figure 18: FL β-actin MDCK cell lysates at steady state treated with a combination of E-cadherin shRNA and E-cadherin siRNA.

(A) Immunoblot for E-cadherin, β-catenin, total actin and loading control GAPDH. Note that loading control GAPDH do not change when E-cadherin protein expression is reduced.

(B) Graph illustrating the relative protein levels for the immunoblots in panel **A**.

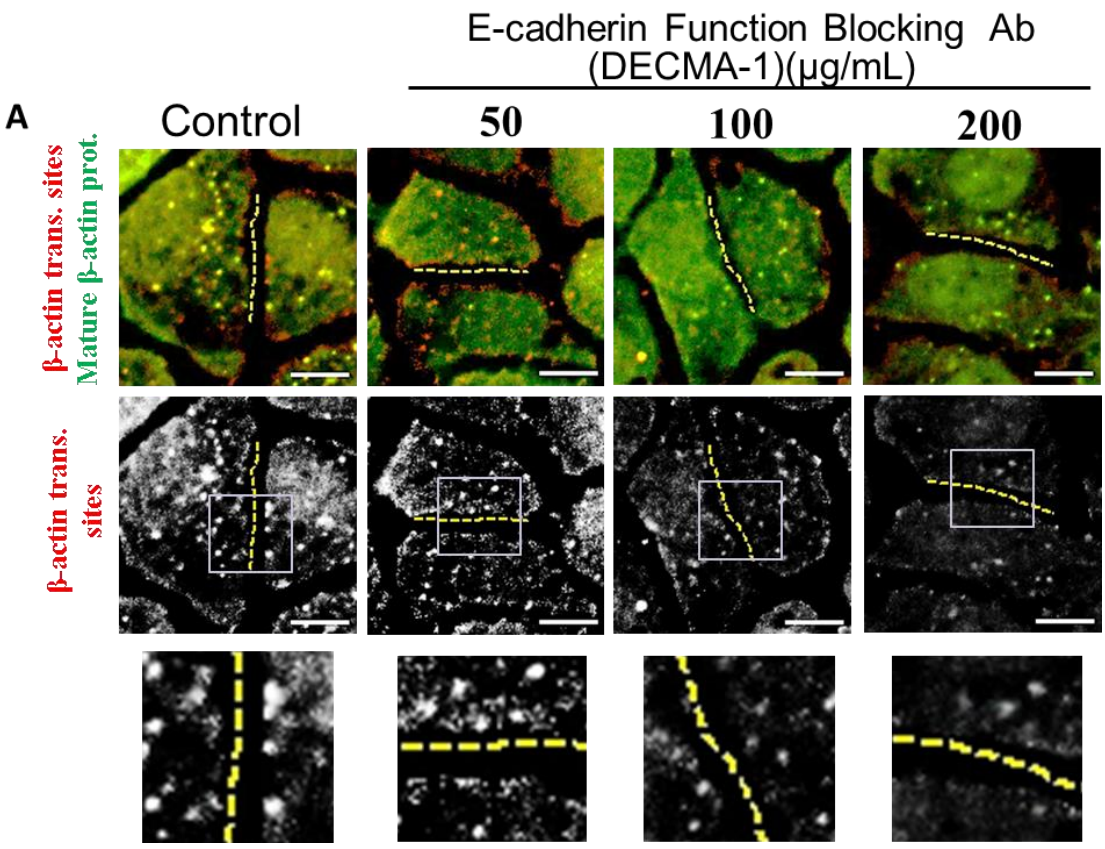
A
E-cadherin Function Blocking Ab
(DECMA-1)(μg/mL)
Control
50
100
200
β-actin trans. sites
Mature β-actin prot.
β-actin trans. sites

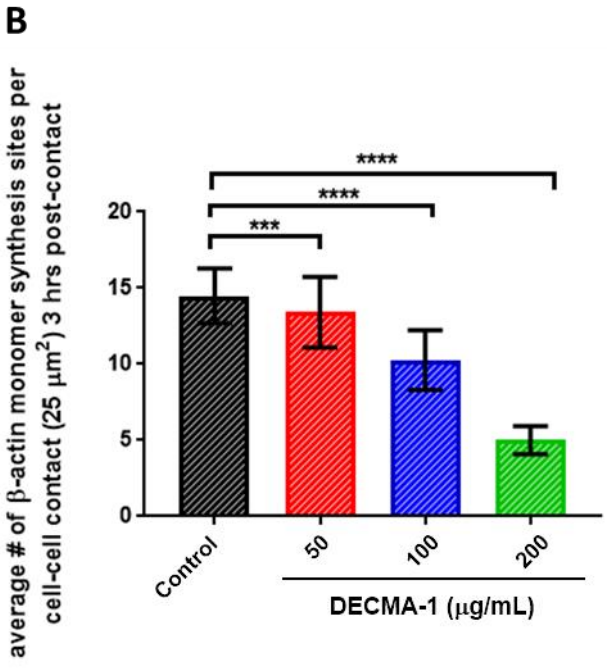
B
average # of β-actin monomer synthesis sites per cell-cell contact (25 μm²) 3 hrs post-contact
****
****
***
20
15
10
5
0
Control
50
100
200
DECMA-1 (μg/mL)

Figure 19: E-cadherin function regulates β-actin monomer synthesis sites at *de novo* epithelial cell-cell contacts.

(A) Deconvoluted epifluorescence images of MDCK cells properly localizing β-actin monomer synthesis (FL β-actin mRNA) fixed 3 hrs post-contact when E-cadherin function is inhibited. These cells were stained for *de novo* β-actin monomer synthesis (red). Mature β-actin is green. Dotted yellow lines indicate cell-cell contacts (determined by differential interference contrast microscopy). Scale bars 10 μm

(B) Mean average number of β-actin monomer synthesis sites per cell-cell contacts for images shown in **A**. Single plane image was used to quantify translation sites at cell-cell contact zone (Area back from the cell edge: 5 um^2). Mann-Whitney test was applied. ***,$p < 0.001$; ****, $p < 0.0001$ and error bars indicate Mean ± SEM. n=130, where n indicates the number of cells analyzed per treatment from 3 independent experiments.

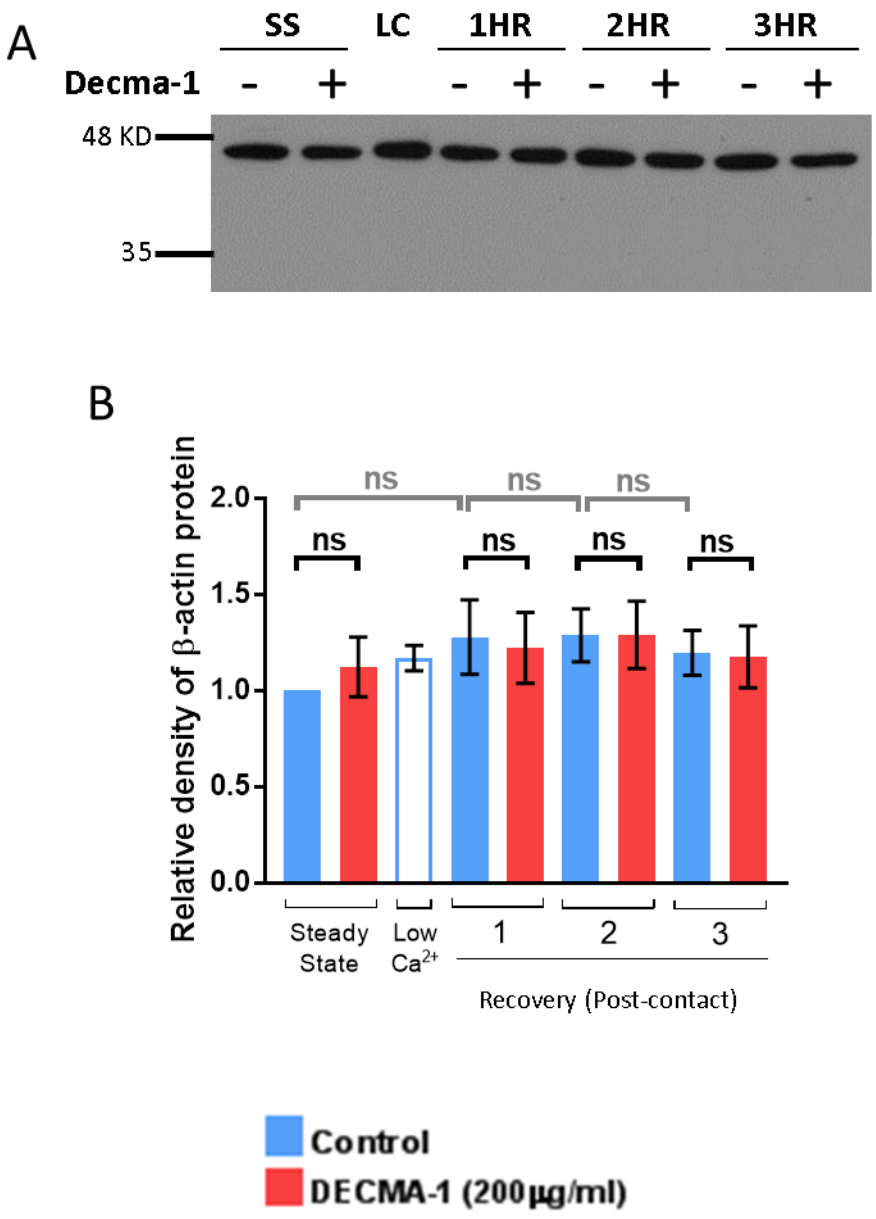
A
SS
LC
1HR
2HR
3HR
Decma-1
- + - + - + - +
48 KD
35
B
Relative density of β-actin protein
2.0
1.5
1.0
0.5
0.0
ns
Steady State
Low Ca2+
1
2
3
Recovery (Post-contact)
Control
DECMA-1 (200µg/ml)

Figure 20: E-cadherin loss of function does not affect total β-actin monomer synthesis during *de novo* adherens junction assembly.

(A) Immunoblot for β-actin of wild type MDCK whole cell lysates: steady state (SS), low calcium (LC) and 1(1H) , 2 and (2H), 3 hours (3H) post-contact and DECMA-1 treated cells at steady state (SS), 1 (1H), 2 (2H) and 3 hours (3H) post-contact.

(B) Protein relative density analysis of β-actin from the same lysates showed in panel **A** demonstrated that there is no change in β-actin protein expression in DECMA-1 treated cells (200 µg/ml) in comparison to the wild type MDCK cells (Control). Relative protein levels analyses were performed using ImageJ. Error bars represent Mean ± SEM based on 3 experimental replicates. Unpaired T-test (black brackets) and One-Way Anova (grey brackets) results ns: not significant.

DISCUSSION

E-cadherin overexpression is sufficient to rescue the dominant negative epithelial adherens junction assembly defects and tissue barrier permeability cause by delocalizing β-actin monomer synthesis.

De novo MDCK cell-cell contact induces β-actin monomer synthesis throughout the cytoplasm out to cell-cell contact sites (Gutierrez et al., 2014). Initiation of β-actin monomer synthesis in the peripheral cytoplasm and cell-cell contact sites requires reversible binding between a 3'UTR localized zipcode sequence in the β-actin mRNA transcript and the translational inhibitor Zipcode Binding Protein-1 (ZBP1) (Gutierrez et al., 2014; Hüttelmaier et al., 2005). Consequently, delocalizing β-actin monomer synthesis away from *de novo* cell-cell contacts by β-actin mRNA 3'UTR deletion or β-actin mRNA zipcode antisense oligonucleotide masking results in perturbed E-cadherin anchoring to linear actin filament and adherens junction maturation (Gutierrez et al., 2014). In fact, a stable MDCK cell line partially defective in localizing β-actin monomer synthesis due to expressing ~20% of its β-actin mRNA with a 3' UTR deletion (Δ3'β-actin) exhibits a dominant negative phenotype during adherens junction assembly (Gutierrez et al., 2014). Intriguingly, overexpressing E-cadherin is sufficient to rescue the epithelial tissue barrier permeability defect caused by partially delocalizing β-actin monomer synthesis in the Δ3'UTR β-actin MDCK cells (**Figure 4A**). In addition to recovering the classic epithelial cobblestone phenotype, overexpressing E-cadherin by 1.5-fold significantly increased the number of steady state adherens junctions (**Figures 5 and 7**) and *de novo* adherens junction complexes 3-hours post-contact (**Figure 9: 3 hr Ca^{2+} repletion**). Moreover, previous laboratory studies showed delocalizing

β-actin monomer synthesis by antisense oligonucleotide masking, RhoA inhibition, or Src inhibition perturbed adherens junction assembly and epithelial tissue permeability (Figure 3; Gutierrez et al., 2014). Importantly, Ca^{2+} switch studies confirm the extent of adherens junction assembly calculated using fluorescence covariance analysis (Vedula et al., 2016) inversely correlates with the degree of tissue permeability. Together, these data demonstrate E-cadherin overexpression is sufficient to rescue the dominant negative adherens junction assembly, cell-cell adhesion, and epithelial tissue barrier formation defects caused by partially delocalized β-actin monomer synthesis in Δ3'UTR-β-actin MDCK cells.

E-cadherin expression is required to localize β-actin monomer synthesis to *de novo* cell-cell contact sites.

After demonstrating overexpressing E-cadherin 1.5-fold was sufficient to rescue the Δ3' UTR-β-actin dominant negative adherens junction assembly, cell-cell contact, and epithelial tissue permeability defects, I hypothesized E-cadherin specifies β-actin monomer synthesis at *de novo* cell-cell contact sites. I directly tested this hypothesis by quantifying the number of cell-cell contact localized β-actin monomer synthesis sites 3 hours post contact during Ca^{2+} switch experiment in the β-actin translation site imaging reporter cell line when E-cadherin expression is knockdown using RNA interference (Brummelkamp et al., 2002; Capaldo and Macara, 2007). Importantly, reducing E-cadherin expression reduced the number of *de novo* cell-cell contact localized β-actin monomer synthesis sites. In fact, when E-cadherin expression is knockdown by 50% or more, I observed greater than a 60% reduction in the number of *de novo* cell-cell contact localized β-actin monomer synthesis sites (**Figure 17**). This indicates that the newly synthesized β-

actin monomers will be incorporated into actin filaments leading to adherens junction stabilization and maturation (Ballestrem et al., 1998). Furthermore, these data demonstrate E-cadherin expression and the number of *de novo* cell-cell contact localized β-actin monomer synthesis sites positively correlate.

E-cadherin homophilic binding activity is required to localize β-actin monomer synthesis to *de novo* cell-cell contact sites.

It was previously shown the number of *de novo* cell-cell contact localized β-actin monomer synthesis sites correlate with E-cadherin expression. However, many well-characterized molecular and cellular changes caused by reduced E-cadherin expression can affect our measurements. To exclude the contributions from these changes, E-cadherin adhesive function was acutely blocked using DECMA-1 function blocking antibodies on a β-actin translation site imaging reporter cell line. These reporter cells express E-cadherin at endogenous levels and only have E-cadherin function blocked during the 3-hour recovery period of the Ca^{2+} switch experiment. Predictably, the number of *de novo* cell-cell contact localized β-actin monomer synthesis sites is inversely proportional to the concentration of function blocking antibodies (**Figure 19**). Both knockdown and function blocking antibody data confirm the number of *de novo* cell-cell contact localized β-actin monomer synthesis sites correlates with E-cadherin expression or adhesive function. A previous study found actin depolymerization is not the major contributing factor for incorporation of actin monomers into junctional actin filaments (Zhang et al., 2005). Based on the accumulated data, I propose a model in which E-cadherin homophilic binding has an important yet unappreciated

function in specifying β-actin monomer synthesis at adherens junction assembly sites to control cytoskeletal remodeling (**Figure 21**).

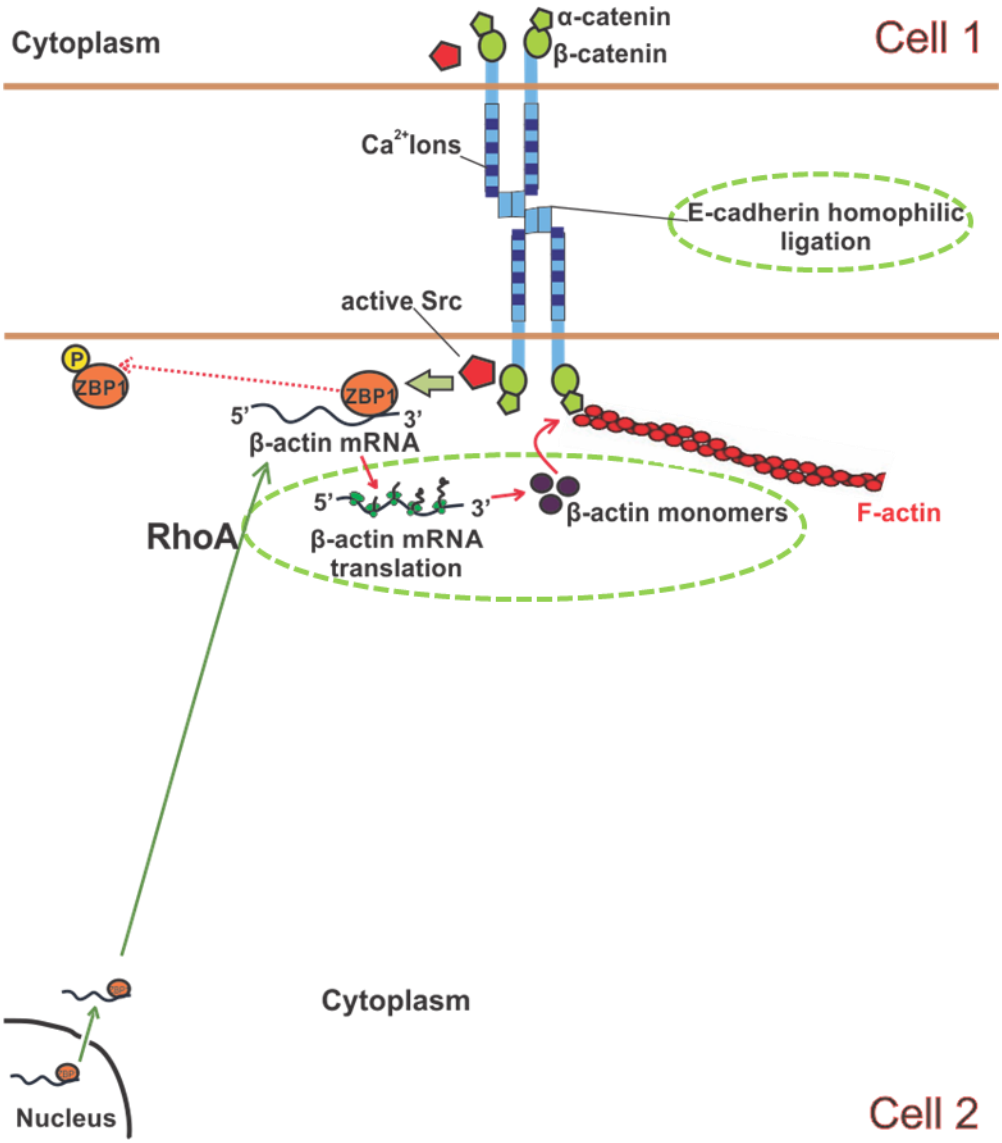
Cytoplasm
α-catenin
β-catenin
Cell 1
Ca2+Ions
E-cadherin homophilic ligation
active Src
P
ZBP1
ZBP1
5'
3'
β-actin mRNA
5'
3'
β-actin mRNA translation
β-actin monomers
F-actin
RhoA
Cytoplasm
Nucleus
Cell 2

Figure 21: (Summary of proposed working model and findings) E-cadherin function is important for local β-actin monomer synthesis during de *novo* adherens junction assembly.

I have found that E-cadherin function regulates β-actin monomer synthesis at cell-cell contact zones which drives *de novo* adherens junction assembly (dotted green circles). Previous studies showed RhoA triggers the targeting of the β-actin mRNA/ZBP1 complex to cell-cell contact zones. In addition, active Src phosphorylates ZBP1, which is bound to the β-actin mRNA. This releases the translational repression of ZBP1 on the β-actin transcript, resulting in β-actin monomer synthesis. Briefly, I proposed a working model in which E-cadherin homophilic binding initiates cell-cell contact localized β-actin monomer synthesis; leading to adherens junction complex anchoring to F-actin.

MATERIALS AND METHODS

Cell Culture

MDCK-NBL-2 (Madin-Darby Canine Kidney-NBL-2 from ATCC®CCL - 34™) is a parental epithelial cell line that will form a polarized monolayer (Dukes, Whitley, and Chalmers, 2011). MDCK epithelial cells were cultured in regular growth media (13.37 g/L of DMEM (Corning cellgro®), 1% penicillin/streptomycin (Corning cellgro®), 10% FBS (Corning cellgro®) and 2 grams/L of sodium bicarbonate) in a 100 x 20 mm cell culture dish. For cell passage, when the cells were ~80-90% confluent, regular growth media was removed, and cells washed twice with 1X PBS pH 7.4. Then, 2 mL of 0.25% Trypsin EDTA pH 8.0 was added to the plate and incubated at room temperature for ~20-30 minutes. When the cells fully lifted from the plate, 8 mL (150 x 25mm dish) of regular growth media was applied and the cells transferred to a 15 mL Falcon tube. The cells were centrifuged for 2 minutes at 1200 rpm, producing a white pellet. The supernatant was discarded, and the cell pellet was re-suspended in 1 mL of regular growth media. 10 µl of the resuspended pellet was pipetted into the hemocytometer and counted. For cell passage one million cells were seeded onto 100 x 20 mm cell culture dish and grown for 2-3 days at 37°C, 5% CO_2, and 95% humidity atmosphere until they were ~80-90% confluent.

Generation of stable cell lines

MDCK cells were transfected with the reporter plasmids TC-eGFP-β-actin full length (Addgene, plasmid #27123) and TC-eGFP-β-actin Δ3'UTR (Addgene, plasmid #27124) using Lipofectamine™ 2000 (Invitrogen) according to

manufacturer's guidelines (Gutierrez et al., 2014). MDCK cells expressing E-cadherin-RFP are a kind gift from Dr. James Nelson, Stanford. These cells were transfected with the TC-eGFP-β-actin Δ3'UTR plasmid using Lipofectamine™ 2000 (Invitrogen) according to manufacturer's guidelines. All the stable cell lines were sorted using FACS and the high β-actin expressing cells were used for the E-cadherin overexpression studies (**Figures 5 and 8**). Cell culture and passage was done as described previously. With the exception that these cells were cultured in regular growth media with G418 at a final concentration of 500 µg/mL, to select transfected clones in all stable MDCK cell lines.

Calcium Switch Assays

For partially delocalized β-actin MDCK cell lines with E-cadherin overexpression:

For calcium switch experiments, 250,000 Δ3'UTR MDCK cells and Δ3'UTR MDCK with E-cadherin overexpression were seeded in a 6-well plate containing glass coverslips (No 1, Fisher Scientific). Cells were grown in regular growth media for 2 days at 37°C, 5% CO_2, and 95% humidity to form a monolayer ~90% confluent. Cells were quickly washed with 1X PBS pH 7.4 and medium containing 4 mM EGTA (low calcium media : 13.37g/L of DMEM, 2g/L of sodium bicarbonate and a final concentration of 4 mM EGTA was added for 1 hour. Then, cells were washed quickly once again with 1X PBS pH 7.4. Next, regular growth medium was added to initiate *de novo* adherens junction assembly (recovery).

For function blocking studies:

For calcium switch experiments, 75,000 wild type MDCK cells were seeded in a 24-well plate containing glass coverslips (No 1, Fisher Scientific). Cells were grown in regular growth media for 2 days at 37°C, 5% CO_2, and 95% humidity to form a monolayer ~90% confluent. Calcium switch procedure was done as described previously. For function blocking studies, an E-cadherin function blocking antibody, DECMA-1, (Sigma-Aldrich, product # U3254) was diluted in regular growth media without antibiotics to three final concentrations: 50 µg/ml (suboptimal concentration), 100 µg/ml (suboptimal concentration) and 200 µg/ml (optimal concentration). These diluted E-cadherin function blocking antibodies were added to the cells during *de novo* junction assembly. For control cells, wild type MDCK cells were used.

Translation Site Assay during calcium switch

75,000 TC-eGFP-β-actin full length MDCK cells (FL β-actin) were seeded in a 24-well plate containing glass coverslips (No 1, Fisher Scientific). Cells were maintained in regular growth media until ~90% confluent. The cells underwent Ca^{2+} switch by incubating them in low calcium media solution containing the biarsenical dye, FlAsH for 1 hour (2 mM EGTA, 0.9 µM FlAsH, 12.5 µM stain stock, in OptiMEM media). Staining stock is 11.9 mM EDT_2 in DMSO. After an hour in low Ca^{2+} media with FlAsH, the cells were washed once with 1X PBS pH 7.4 and returned to regular growth media for 2.5 hours with or without E-cadherin function blocking antibodies. Recovery was followed by treatment in a chase solution (1 µM ReAsH, 12.5 µM stain stock, 100 µg/ml cycloheximide, and DMEM) for 30 minutes with or without E-cadherin function blocking antibodies. Cells were then destained

for 5-10 minutes at 37ºC with destaining solution (600 µM destain stock and OptiMEM media). Destain stock is 9.9 µM of BAL (2,3-60 dimercaptopropanol) in DMSO. Cells were quickly washed thrice with 1X PBS pH 7.4 and fixed with paraformaldehyde in 1X PBS pH 7.4 for 20 minutes. Finally, coverslips were mounted using Prolong® Gold (Life Technologies) and kept on a flat surface in the dark at 4ºC until image acquisition. For E-cadherin knockdown studies the addition of E-cadherin function blocking antibodies were omitted.

Transient inhibition of E-cadherin protein expression

E-cadherin short hairpin RNA (**shRNA-A**) was a kind gift from Dr. Christopher T. Capaldo and Dr. Ian G. Macara from University of Virginia School of Medicine (Capaldo and Macara, 2007; Brummelkamp et al., 2002), and is as follows:

sense strand, 5-
gatccccGGACGTGGAAGATGTGAATttcaagagaATTCACATCTTCCACGTCCtttttggaaa-3';

and antisense, 5-
agcttttccaaaaaGGACGTGGAAGATGTGAATtctcttgaaATTCACATCTTCCACGTCCggg-3'.

Small interfering RNA targeting E-cadherin (**siRNA-B)** were generated by ThermoFisher Scientific (*Silencer*® Select siRNA):

sense strand, 5’-GUCUAACAGGGACAAAGAATT-3’;

and an antisense strand, 5’-UUCUUUGUCCCUGUUAGACTT-3’.

A sequence targeting human ARF4a was used as a negative control (Addgene, plasmid #67497), 5’-TCTGGTAGATGAATTGAGA-3’.

A scramble negative control sequence, *Silencer*™ Select Negative Control # 1 siRNA, was purchased from ThermoFisher Scientific.

For E-cadherin knockdown studies, 25,000 TC-eGFP-β-actin full length MDCK cells were seeded in a 24-well plate containing glass coverslips (#1, Fisher Scientific), and cultured in regular growth media. Next day, cells were serum starved at ~20-30% confluency with Opti-MEM®I media (serum free media-ThermoFisher Scientific) for one hour. For each well to be transfected, 250 µl serum free media containing 1.7 µl of Lipofectamine® RNAiMAX (ThermoFisher Scientific) was prepared and incubated for ~10 min at room temperature. Next, for each well to be transfected, 250 µl serum free media containing E-cad shRNA-A plasmid and E-cad siRNA-B was prepared. Then, the diluted siRNA + shRNA was mixed with the diluted transfection reagent (transfection complexes) and incubated for ~20 min at room temperature. 500 µl was added directly to the cells and mixed. The final concentration of E-cad siRNA-B after addition to the cells was 50 nM in serum free media. E-cad shRNA-A plasmid was used in increasing amounts: 0.31 µg, 1.25 µg, and 1.88 µg to obtain different amounts of E-cadherin protein

reduction (Capaldo and Macara, 2007). Transfection complexes were removed 6 hours after their addition to the cells. Cells were kept in regular growth media for two days when they were ~90% confluent for translation site assay (see Translation Site Assay during calcium switch, pages 80-81) during calcium switch experiments.

Indirect Immunofluorescence

Cells were fixed at room temperature in 4% paraformaldehyde in 1XPBS pH 7.4 for 20 min. A final concentration of 0.5% Triton-X was used to permeabilize cells for 2 min at room temperature, followed by blocking with 1% BSA diluted in 1X PBS pH 7.4 for 1 hour at room temperature. Then, cells were incubated in mouse monoclonal anti-E-cadherin primary antibody (1:250 dilution in blocking solution, BD Biosciences, #610181) overnight at 4ºC. Cells were washed thrice for 5 minutes each wash with 1X PBS. Then, cells were incubated with goat anti-mouse CF640 conjugated secondary antibody (1:800 dilution in blocking solution; Life Technologies) for 1 hour and a half at room temperature in the dark. Also, Rhodamine-Phalloidin, Alexa 488 Phalloidin or Alexa 647 Phalloidin was used to stain F-actin for 20 min (1:25 dilution in 1X PBS, Life Technologies), at room temperature in the dark. Cells were incubated with DAPI for 1 min in the dark to stain the nucleus. Finally, coverslips were mounted using Prolong® Gold (Life Technologies) and kept on a flat surface in the dark at 4ºC until image acquisition.

Image Acquisition and Processing

Images were acquired using an inverted Zeiss microscope (AxioObserver Z1) using Axiovision 4.8.2 software (Zeiss) equipped with a Plan-Apo 63x oil

immersion objective with a numerical aperture of 1.4. 35 Z-stacks with a step size of 0.240 µm were acquired using a QuantEM 512SC camera (Photometrics) with 2 by 2 binning for translation site visualization, or Cool Snap HQ^2 (Photometrics) camera for indirect immunofluorescence visualization with 2x2 binning. Camera options: digital and electron-multiplying (EM) gains were kept constant across a single set of experiments (e.g. one experimental set for β-actin translation sites: control , 50 µg/ml DECMA-1, 100 µg/ml DECMA-1, 200 µg/ml DECMA-1; 3 hours post-contact). Filter cube sets used: Far-red channel, 49 (Zeiss); green channel, 38HE (Zeiss); red channel, Ex:560/40, Em:630/75; and, blue channel, 49 (Zeiss). Exposure times for all the channels were keep constant across a single set of experiments without saturating any images. Image saturation was checked using the dynamic range indicator “OverExp” option on the live window in the Axiovision 4.8.2 software (Zeiss).

Image stacks were processed using the Zeiss AxioVision 4.8.2 3D Deconvolution algorithm with the following parameters: theoretical PSF, autolinear normalization, constrained iterative and medium strength setting for all fixed images.

Fluorescence Covariance Index (Fluorescence Covariance Index) Analyses

Processed images were exported into Volocity® 6.1 (PerkinElmer). Under the measurements window, two distinct cellular compartments, cell periphery and the cytoplasm (interior of the cell excluding the periphery and the nucleus), were defined using the freehand region of interest tool for each cell in an image stack. Pearson’s correlation coefficient (for two protein pairs) was computed using the

Calculate Object Colocalization tool. Peripheral and cytoplasmic Pearson's Correlation (Pearson's correlation coefficient) values were exported as a comma separated value format (*.csv). A MATLAB (MathWorks®) custom written script was used to extract Pearson's correlation coefficient values and calculate Fluorescence Covariance Index values for each cell (**Appendix 4**).

β-actin monomer synthesis sites quantification

Processed (deconvoluted) images were opened in ImageJ (NIH). To determine cell-cell contacts differential interference contrast (DIC) channel was used. Fluorescence signal from the red channel was quantified since *de novo* β-actin monomer synthesis sites were taken in this channel. Under the Analyze tab in ImageJ the scale was set to distance in pixels 1, known distance 0.25 (AxioVision information for image has the μm/pixel), pixel aspect ratio 1, and unit length to μm. A Z-plane was selected in which cell-cell contacts were in focus using DIC channel. This Z-plane was used to quantify *de novo* β-actin monomer synthesis sites. Translation sites are characterized by clusters of puncta that surround a significantly bright punctum or pixel (Gutierrez et al., 2014). Region of interests were drawn from the cell-cell contact until 5 μm back along the cell-cell contact site. The total area (25 μm^2) of the region of interest was calculated by multiplying the x and y values.

Western Blotting

Total cell lysates for various time points of the Ca^{2+} switch assay (steady state, low calcium, 1, 2 and 3 hours after Ca^{2+} repletion) were collected and probed for β-actin by immunoblot. Briefly, the cells were washed 3 times with 1X PBS. After

complete removal of the wash solution, the cells were placed on ice and incubated with RIPA buffer (150 mM sodium chloride, 1.0% Triton X-100, 0.5% sodium deoxycholate, 0.1% sodium dodecyl sulfate, 50 mM Tris-base pH 8.0) with phosphatase and proteinase inhibitors (Thermo Scientific Cat# 78443). For **Figure 18**, cells were lysed in SDS lysis buffer (25 mM Tris-base, 2 mM EDTA, 95 mM of sodium chloride, 1% sodium dodecyl sulfate) with phosphatase and proteinase inhibitors (Thermo Scientific Cat# 78443). Cell lysates were scraped off the plate and collected into sterile pre-chilled microfuge tubes. The lysed suspensions were passed 3-4 times through a 28G½ needle attached to a 1 mL syringe in ice, this was repeated every 10-15 min, thrice. Then lysates were centrifuged at 6,000 rpm for 15 min at 4°C and the supernatant collected into a clean pre-chilled microfuge tubes. Protein concentration was measured using the Bicinchoninic Acid (BCA) assay method as per manufacturer's specifications (Thermo Scientific). The samples were denatured using sample loading buffer (250 mM Tris-base pH 6.8, 10% sodium dodecyl sulfate, 30% glycerol, 0.02% bromophenol blue and 25% β-mercaptoethanol). Equal total protein for each sample (5 µg) was loaded into each well of a 10% or 12% SDS-PAGE gel. Proteins transferred onto a PVDF membrane (Bio-Rad) with 0.2 µm pore size at 90 volts for 1 hour and a half, and then, the membrane was blocked in 5% skim milk (Bio-Rad) 1X TBS-T buffer for one hour at room temperature. The membranes were incubated with mouse anti-β-actin (1:30,000; Sigma-Aldrich, A5316) in 5% skim milk in 1X TBS-T buffer overnight at 4ºC. Next day, membranes were washed with 1X TBS-T thrice, 5 min per wash. Then, membranes were incubated with secondary antibody Goat anti-mouse tagged to Horse Radish Peroxidase (1:15,000) for 1 hour at room

temperature (GE Healthcare). Next, membranes were washed with 1X TBS-T thrice, 5 min per wash followed by chemiluminescence detection (Pierce Western blotting substrate as per manufacturer's specifications) and exposure on X-ray film. X-ray film was scanned and converted into an 8-bit image, quantification of the probed antigen was done in ImageJ (NIH). Using the gel analysis tool in Image J, the intensity of each band relative to the controls was measured to get the relative protein density in each lane.

Statistical Analyses

Statistics data analysis was performed using GraphPad Prism 7 software (GraphPad Software, Inc).

For E-cadherin overexpression studies, 3 independent set of experiments were performed (e.g. one set: steady state, low calcium, 1 hour recovery, 2 hours recovery, 3 hours recovery). Mean FCI values at each time point were compared using the non-parametric One-Way Anova, Krustal-Wallis test.

For E-cadherin function blocking studies, 3 independent set of experiments. Mean FCI values at each time point and treatment condition were compared using unpaired t-test with Welch's correction.

For β-actin translation site studies, 3 independent set of experiments were performed (e.g. one set: control, 50 µg/ml of DECMA-1, 100 µg/ml of DECMA-1, 200 µg/ml of DECMA-1). Mann-Whitney statistical test was used to compare number of β-actin translation sites at cell-cell contact 3 hours post-contact.

Preliminary Data: For the Western blotting during calcium switch experiments, 3 experimental replicates were performed on the same day (e.g. one set: steady state, low calcium, 1 hour recovery, 2 hours recovery, 3 hours recovery). Relative total protein density values were calculated and analyzed using one-way ANOVA and Dunnett post-test or unpaired t-test.

Significance was set at $p < 0.05$ for all statistical analyses.

CHAPTER 3: E-cadherin expression and binding function spatially regulate β-actin translation initiation signal, Src, following *de novo* epithelial cell-cell contact

INTRODUCTION

Adherens junctions are a major class of cell adhesion complexes observed in epithelial tissues (Nagafuchi, 2001; Takeichi, 2014). They are composed of the transmembrane adhesion receptor E-cadherin and the adaptor proteins β-catenin and α-catenin that bind linear actin filaments at cell-cell contact sites. Catenins are the best understood binding partners for classical cadherins, but many other molecules also interact with cadherins. These diverse binding partners connect E-cadherin with key cellular processes such as cell adhesion and signaling. In regard to signal transduction, diverse signaling tyrosine kinases and phosphatases are found and activated in a cadherin dependent manner (McLachlan and Yap, 2007). For instance, Src is found and activated at cadherin based contacts (McLachlan et al., 2007; McLachlan and Yap, 2011; Truffi et al., 2014). There are two main phosphorylation sites on Src known to regulate activity. When Src tyrosine residue 527 is phosphorylated by C-terminal Src kinase (CSK), Src adopts an inactive closed conformation (Xu et al., 1997). Dephosphorylation of Src tyrosine residue 527 causes Src to adopt an open conformation allowing the kinase domain of Src to autophosphorylate itself at tyrosine residue 416 resulting in Src kinase activation (Roskoski, 2004; Yeatman, 2004). When E-cadherin function is inhibited following *de novo* cell-cell contact, a decrease in Src signaling was observed along with the loss of E-cadherin cell-cell contacts in MCF-7 (metastatic breast cancer) cell line

(McLachlan et al., 2007; McLachlan and Yap, 2011). These studies suggest Src has to be active at the right time and place for the cell to properly form adherens junctions. Importantly, these studies showed E-cadherin function is required to active Src, which is the permissive signal to initiate β-actin monomer synthesis (Hüttelmaier et al., 2005). Taken together these studies establish a connection between E-cadherin, Src signaling and β-actin monomer synthesis at cell-cell contacts.

The mechanisms which regulate the precise relationship between E-cadherin, Src signaling and β-actin monomer synthesis at cell-cell contacts remains poorly understood. Thus, I investigated the extent to which E-cadherin activates Src during adherens junction assembly following *de novo* cell-cell contacts. Consequently, I investigated the extent to which E-cadherin protein expression or homophilic binding spatially regulates Src kinase activity following *de novo* cell-cell contact.

RESULTS:

Active Src, a putative β-actin monomer synthesis initiation signal, localizes to epithelial cell-cell contacts.

In Chapter 2, I demonstrated E-cadherin expression and homophilic binding are required to localize β-actin monomer synthesis to *de novo* cell-cell contact sites **(Figures 17 and 19)**. It is well established that E-cadherin adhesion activates the β-actin monomer synthesis initiation signal, Src, at *de novo* cell-cell contacts in the human breast adenocarcinoma MFC-7 cell line during *de novo* junction assembly (Hüttelmaier et al., 2005; McLachlan et al. 2007). In addition, chemically inhibiting Src kinase activity reduced adherens junction assembly (Gutierrez et al., 2014). As a consequence of the loss of adherens junction complexes, I observed a reduction in the number of cell-cell contact localized β-actin monomer synthesis (**Figure 17 and Figure 19**). Consequently, I examined the spatial distribution of β-actin monomer initiation signaling complex (E-cadherin/Src) during Ca^{2+} switch experiments using Fluorescence Covariance Index analysis of E-cadherin and pY416-Src immunofluorescence in MDCK cells (Andreeva et al., 2014; Vedula et al., 2016; Volberg et al., 1986). To identify the dynamic range of the phospho-Src antibody immunofluorescence signal, I determined the dose response between Src inhibitor and the band intensity for phospho-Src using immunoblotting analysis. Tissues assembled from MDCK cells were incubated in regular media containing increasing concentrations (22nM, 44nM, 88nM) of Src inhibitor-1 for 3 hours during *de novo* adherens junction assembly. Then, cells were lysed and relative protein expression levels of active Src were analyzed using Western blot (**Figure 22**). MDCK cells incubated with 22nM Src Inhibitor-1 during 3 hours post-contact

showed no significant difference in protein relative density for active Src in comparison to MDCK cells incubated with DMSO (**Figure 22A and 22A': DMSO and 22 nM Src Inh-1**). When higher concentrations of Src Inhibitor-1 were used, I observed significant decreases in active Src (pY416-Src) protein relative densities (**Figure 22A and 22A': DMSO, 44nM Src Inh-1 and 88nM Src Inh-1**). Importantly, no changes in total Src protein expression levels were observed (**Figure 22B and 22B'**). As a control, tissues assembled from MDCK cells were analyzed to see if a change in Src activity at 3 hours post-contact was due to DMSO treatment, since DMSO was used as a vehicle to facilitate transport of Src Inhibitor-1 into the cells (**Figure 22C and 22D**). MDCK cells treated with DMSO for 3 hours during *de novo* junction assembly did not have a significant change of active Src or total Src protein levels demonstrating the observed decreased in inhibitor studies are caused by the inhibitor and not the vehicle (**Figure 22C' and 22D'**).

After establishing the dynamic range of phospho-Src (pY416) antibody sensitivity I investigated the spatial distribution of active Src in tissues assembled from MDCK cells during calcium switch assays. In steady state tissues, E-cadherin/active Src signaling complex is mainly present at cell-cell contacts with little cytoplasmic localization (**Figure 23: SS, blue arrows**). Quantitatively, E-cadherin/active Src signaling complex localization at the cell-cell contacts is about twice the amount relative to the cytoplasm (**Figure 23B**). Addition of low calcium culture medium (4 mM EGTA; see Materials and Methods) to these cells for 1 hour resulted in the breakdown of intercellular junctions characterized by a decrease in E-cadherin and active Src (pY416-Src) at cell-cell contacts and by an increase in

cytoplasmic staining (**Figure 23A: LC**). Consequently, when E-cadherin binding function was inhibited, through the removal of calcium, a delocalized active Src was observed (**Figure 23B: LC**). 1 hour post-contact, E-cadherin and active-Src remain diffusely localized throughout the whole cell (**Figure 23A: 1 hr**). As a result, the asymmetric distribution of E-cadherin/active-Src signaling complex is still lacking; this is demonstrated by similar Pearson's correlation coefficient values at the cell periphery in comparison to the cytoplasm (**Figure 23B: 1hr**). 2-hours post-contact, even though there is little change in active-Src localization with E-cadherin at cell-cell contacts, a small decrease in cytoplasmic localization is observed (**Figure 23A and Figure 23B: 2hr)**. In contrast, 3 hours post-contact, the permissive signal Src localization with E-cadherin is greater at cell-cell contact zones than compared with 1 and 2 hours post-contact (**Figure 23B**). Additionally, the increased localization of active Src at E-cadherin sites (**Figure 23B: 3 hr**) correlates with β-actin monomer synthesis at 3 hours post-contact following *de novo* cell-cell contacts (**Figure 19**). Importantly, the asymmetric distribution of E-cadherin/active-Src signaling complex at 3 hours post-contact generates a peak for E-cadherin mediated localized Src signal (**Figure 26: Control**), which has previously been shown to be the peak for average number of β-actin monomer synthesis sites per cell-cell contact at 3 hours post-contact (Gutierrez et al., 2014). Furthermore, the cell-cell contact amount of Src signal at E-cadherin sites 3 hours post-contact is similar to steady state MDCK cells (**Figure 26**); demonstrating that the cells have re-established the localization of Src signaling predominately at cell-cell contacts.

E-cadherin homophilic binding is required for active Src, the β-actin monomer synthesis initiation signal, localization to epithelial cell-cell contacts.

To further investigate the role of E-cadherin in localizing active-Src to *de novo* cell-cell contacts, I performed E-cadherin and active-Src immunofluorescence staining during Ca^{2+} switch experiments when E-cadherin binding is inhibited using DECMA-1 (**Figures 24 and 25**). At suboptimal concentrations of binding inhibitor 1 hour post-contact, E-cadherin and active-Src remain diffusely localized throughout the whole cell (**Figure 24A**). The asymmetric distribution of E-cadherin/active-Src signaling complex is lacking. This is demonstrated by similar peripheral and cytoplasmic Pearson's correlation coefficient values (**Figure 24B: 1hr**). 2-hours post-contact there is no change in active-Src localization with E-cadherin at cell-cell contacts, but a small decrease in cytoplasmic localization is observed (**Figure 24A and Figure 24B: 2 hr**). In contrast, at 3 hours post-contact, the cobblestone phenotype is observed with active-Src localization with E-cadherin sites to *de novo* cell-cell contacts with little localization in the cytoplasm (**Figure 24A and Figure 24B: 3hr**). Overall, active Src signaling localization with E-cadherin at cell-cell contacts is similar during *de novo* adherens junction assembly when E-cadherin function is inhibited (**Figure 23B: 1hour, 2 hours, 3 hours**). At the same time, active Src cytoplasmic localization with E-cadherin during *de novo* adherens junction assembly decreases (**Figure 24B: 1hour, 2 hours, 3 hour**). As a result, when E-cadherin binding activity is blocked, E-cadherin/active-Src complex assembly progresses normally until 2 hours post-contact, but at 3 hours post-contact E-cadherin/active-Src complex assembly decreases as shown by the

Fluorescence Covariance Index values (**Figure 26: compare Control versus 100 µg/ml DECMA-1**). Within 1 and 2 hours post-contact, optimal concentrations of binding inhibitor did not have an effect on E-cadherin/active Src complex assembly at *de novo* cell-cell contacts. In contrast, 3 hours post-contact, the asymmetric distribution of E-cadherin/active Src signaling complex was completely abolished (**Figure 25A and Figure 25B**). As a consequence, Fluorescence Covariance Index value of cells treated with optimal concentration of binding inhibitor during junction assembly remain close to zero at 3 hours post-contact (**Figure 26: 200 µg/ml DECMA-1**). These data demonstrate E-cadherin binding function is required for active-Src localization at E-cadherin cell-cell contact sites during *de novo* adherens junction assembly. Importantly, these data also demonstrate the relationship between E-cadherin/active Src signaling complex and β-actin monomer synthesis cell-cell contact localization during *de novo* adherens junction assembly. Consequently, cells in which E-cadherin function is inhibited are expected to have lower Src activity at cell-cell contacts resulting in reduced β-actin monomer synthesis.

In this study, I had shown E-cadherin function inhibition decreases Src activity at cell-cell contacts (**Figure 25**) without affecting total β-actin protein expression levels during junction assembly (**Figure 20**). The undetectable change in β-actin protein expression might be due to an increase in Src protein expression since this is the permissive signal for β-actin monomer synthesis (Hüttelmaier et al., 2005; McLachlan and Yap, 2011). Consequently, to investigate if Src protein expression levels are increased when E-cadherin function is inhibited during junction assembly, Western blots probing for total Src during calcium switch experiments

were performed **(Figure 27)**. Preliminary data shows total Src protein expression levels remained unchanged during the course of the calcium switch experiment either in the presence (+) or absence (-) of E-cadherin binding inhibitor DECMA-1 (**Figure 27A: immunoblot on top; Figure 27B**). Since no change was observed in total Src protein levels during calcium switch assays, I decided to look at active Src. Active Src protein levels increase during low calcium, but decrease during adherens junction assembly by ~25% in wild type MDCK cells (**Figure 27A: bottom immunoblot; Figure 27C: gray bars**). This preliminary data shows E-cadherin function inhibition has no effect in total Src activity during *de novo* adherens junction assembly either in the presence (+) or absence (-) of E-cadherin binding inhibitor (**Figure 27A: bottom immunoblot; Figure 27C: Ca^{2+} repletion**). Intriguingly, steady state treated MDCK cells with E-cadherin function blocking antibodies for 3 hours showed an increase in Src activity in comparison to control steady state MDCK cells (**Figure 27C: SS**). Taken together, these data suggest that the regulation of cell-cell contact localized Src signaling activation by E-cadherin plays an important role in *de novo* adherens junction assembly.

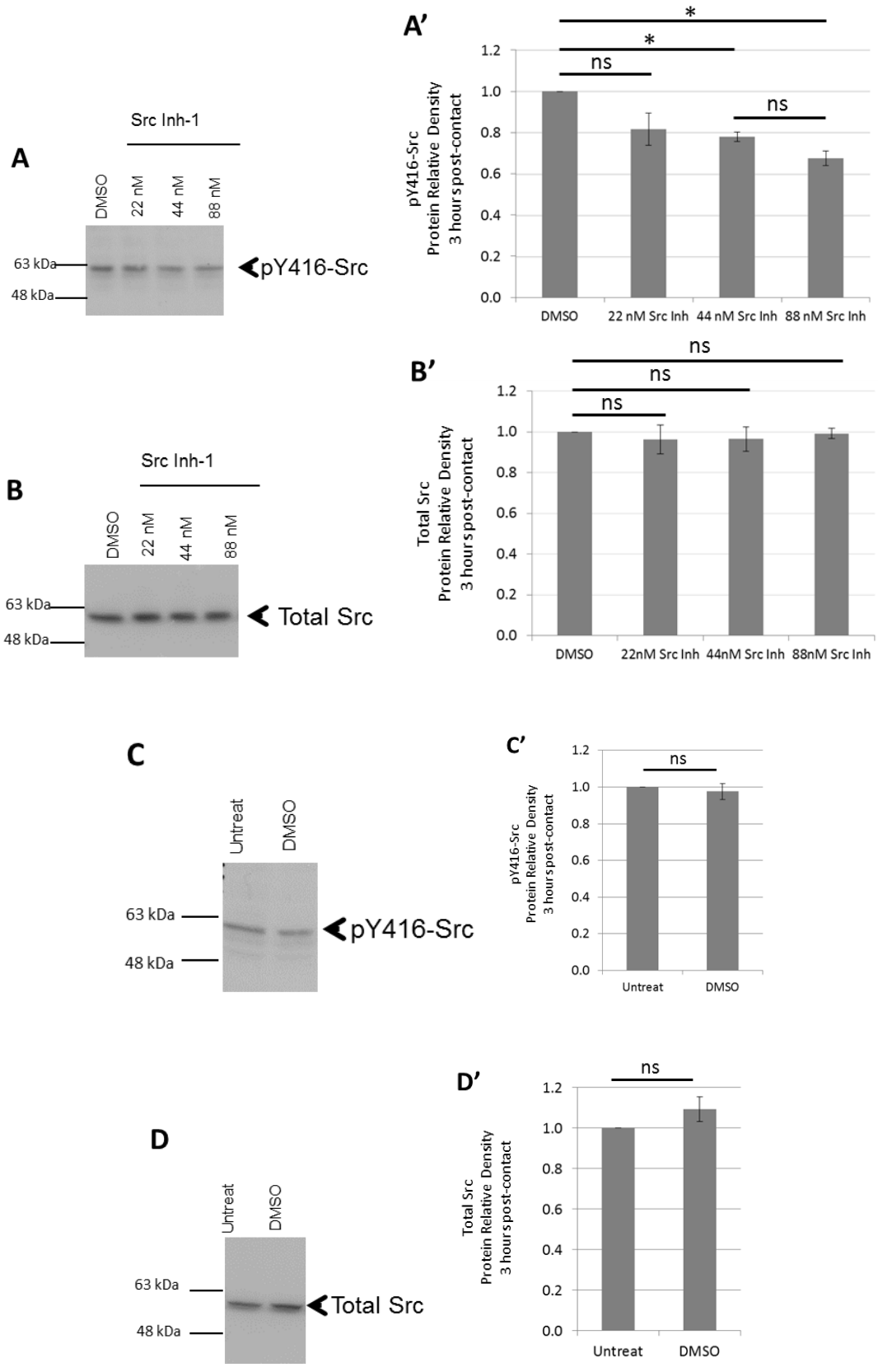
A
Src Inh-1
DMSO
22 nM
44 nM
88 nM
63 kDa
48 kDa
pY416-Src
A'
*
*
ns
ns
pY416-Src Protein Relative Density 3 hours post-contact
DMSO
22 nM Src Inh
44 nM Src Inh
88 nM Src Inh
B
Src Inh-1
DMSO
22 nM
44 nM
88 nM
63 kDa
48 kDa
Total Src
B'
ns
ns
ns
Total Src Protein Relative Density 3 hours post-contact
DMSO
22nM Src Inh
44nM Src Inh
88nM Src Inh
C
Untreat
DMSO
63 kDa
48 kDa
pY416-Src
C'
ns
pY416-Src Protein Relative Density 3 hours post-contact
Untreat
DMSO
D
Untreat
DMSO
63 kDa
48 kDa
Total Src
D'
ns
Total Src Protein Relative Density 3 hours post-contact
Untreat
DMSO

Figure 22: Src Inhibitor-1 decreases the density of immunoblot-detected active Src bands.

Wild type MDCK cells incubated with recovery media 3 hours post-contact containing DMSO (control), 22nM, 44nM and 88nM of Src inh-1 were lysed. Cell lysates were analyzed using Western blot technique and probed for active Src (pY416-Src) **(A)** and total Src **(B)**.

(A') Protein relative density quantifications for immunoblot shown in **A** exhibited significantly lower Src phosphorylation in cell lysates treated with 44nM and 88nM Src inh-1 in comparison to the control (DMSO).

(B') Protein relative density quantifications for Total Src for immunoblot shown in **B** revealed no significant change in total Src protein expression.

Wild type MDCK cells incubated with recovery media for 3 hours post-contact containing with DMSO (control) or without DMSO. Cell lysates were analyzed using Western blot and probed for active Src (pY416-Src) **(C)** and total Src **(D)**.

(C') Protein relative density quantifications for immunoblot shown in **C** exhibited no change in Src phosphorylation of cell lysates with DMSO (control) or without DMSO. **(D')** Protein relative density quantifications for Total Src for Western blot shown in **D** revealed no significant change in total Src protein expression. Protein relative density analysis of pY416-Src and total Src were performed using ImageJ. Error bars represent mean ± SEM based on 3 experimental replicates. Unpaired T-test result: * $P<0.05$;

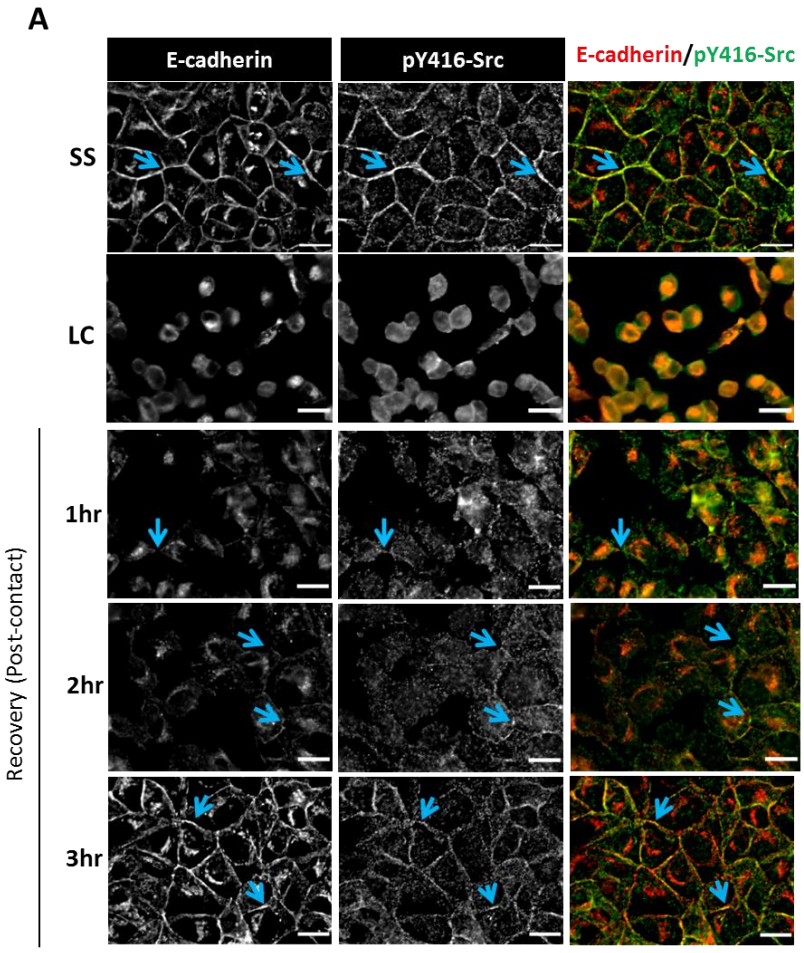
A
E-cadherin
pY416-Src
E-cadherin/pY416-Src
SS
LC
1hr
2hr
3hr
Recovery (Post-contact)

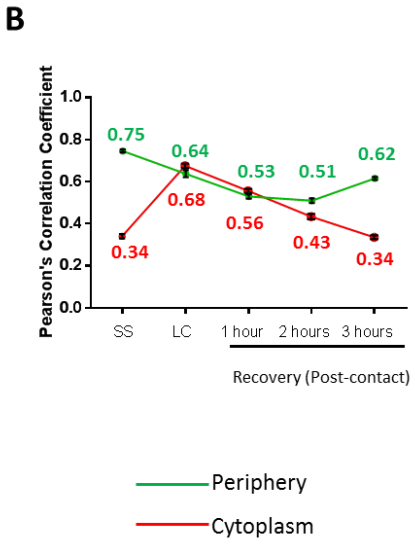
B
Pearson's Correlation Coefficient
1.0
0.8
0.6
0.4
0.2
0.0
0.75
0.64
0.53
0.51
0.62
0.68
0.56
0.43
0.34
0.34
SS
LC
1 hour
2 hours
3 hours
Recovery (Post-contact)
Periphery
Cytoplasm

Figure 23: E-cadherin and active Src (pY416-Src) increase at epithelial cell-cell contact zones following *de novo* adherens junction assembly in wild type MDCK cells.

Indirect immunofluorescence staining on wild type MDCK cells for E-cadherin (red) and active-Src (pY416-Src, green) during calcium switch assay. SS = steady state, LC = low calcium, 1 hour, 2 hour and 3 hours post-contact.

(A) Micrographs represent deconvoluted single plane images for MDCK cells during calcium switch assay. 2 and 3 hours post-contact active Src and E-cadherin begin to accumulate at cell-cell contacts (blue arrows). Scale bar in all images = 20μm.

(B) Change in Pearson's correlation coefficient values for E-cadherin and active-Src in the periphery and the cytoplasm measured for wild type MDCK cells shown in panel **A**. Points represent mean ± SEM. Note that 3 hours post contact Pearson's correlation coefficient values in the periphery increase while Pearson's correlation coefficient values in the cytoplasm decrease.

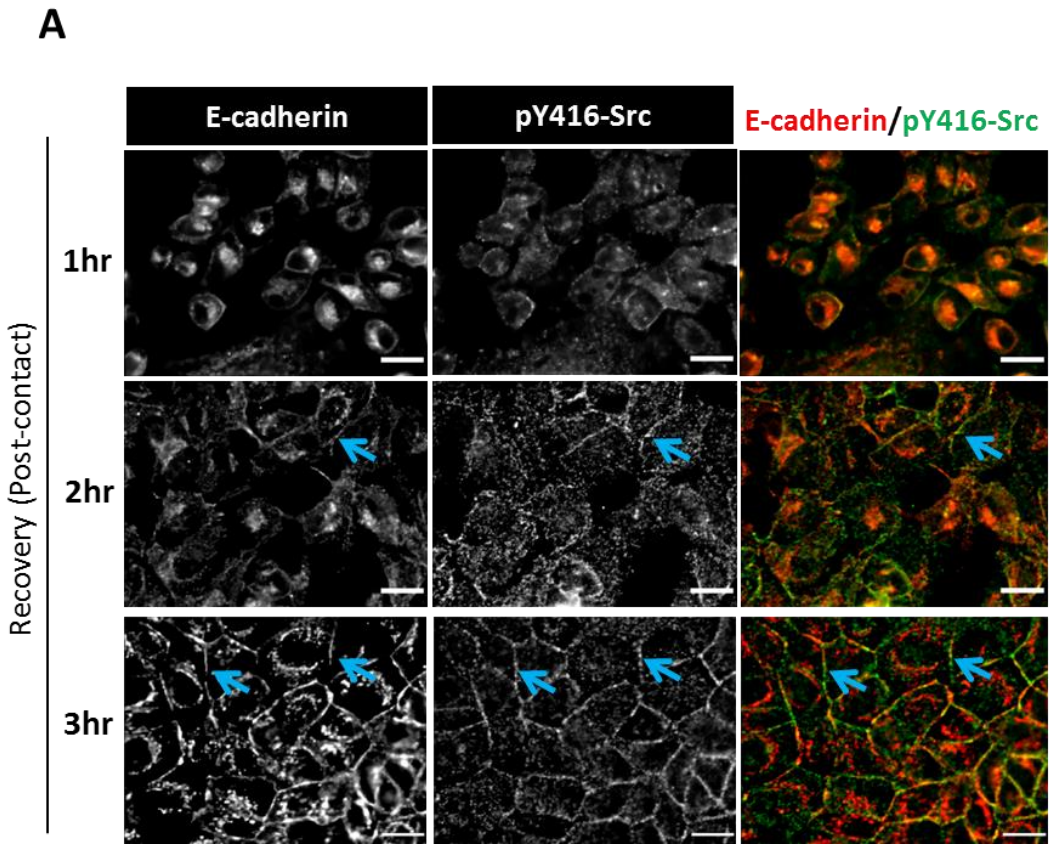
A
E-cadherin
pY416-Src
E-cadherin/pY416-Src
Recovery (Post-contact)
1hr
2hr
3hr

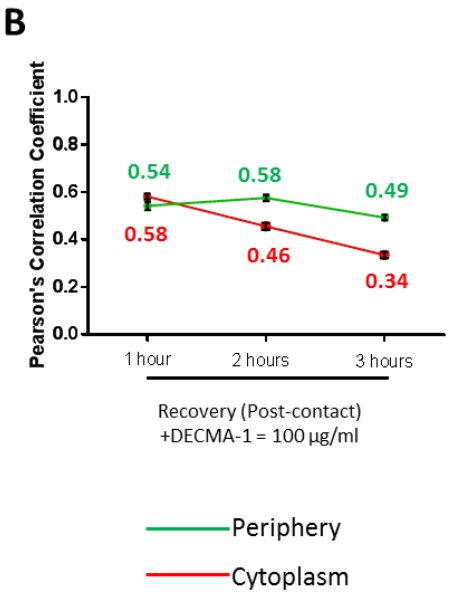
B
Pearson's Correlation Coefficient
1.0
0.8
0.6
0.4
0.2
0.0
0.54
0.58
0.49
0.58
0.46
0.34
1 hour
2 hours
3 hours
Recovery (Post-contact)
+DECMA-1 = 100 µg/ml
Periphery
Cytoplasm

Figure 24: Active Src and E-cadherin localization at the cell-cell contacts is perturbed when E-cadherin function is blocked during *de novo* cell-cell contact formation.

Indirect immunofluorescent staining for E-cadherin (red) and active-Src (pY416-Src, green) using wild type MDCK cells treated with E-cadherin function blocking antibodies (DECMA-1, final concentration of 100 µg/ml) following *de novo* cell-cell contact.

(A) Micrographs represent deconvoluted single plane images for MDCK cells 1 , 2 and 3 hours post-contact with E-cadherin function blocking antibodies. Note that there is a decrease at 3 hours post-contact of pY416-Src and E-cadherin at cell-cell contacts (blue arrows). Scale bar in all images = 20µm.

(B) Change in Pearson's correlation coefficient values for E-cadherin and active-Src in periphery and cytoplasm measured for MDCK cells shown in panel **A**. Points represent mean ± SEM. Note that 3 hours post-contact Pearson's correlation coefficient values in the periphery decreases.

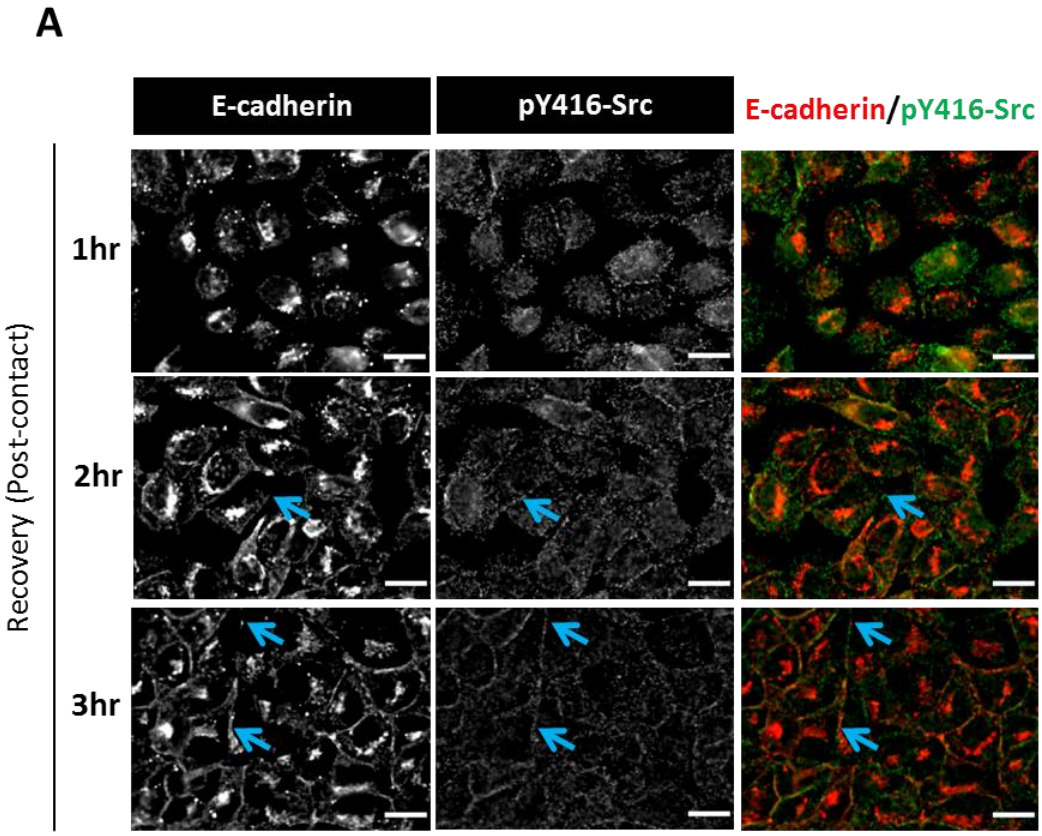
A
E-cadherin
pY416-Src
E-cadherin/pY416-Src
Recovery (Post-contact)
1hr
2hr
3hr

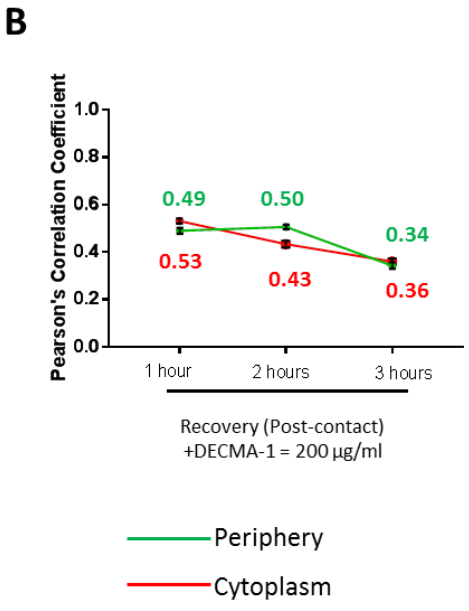
B
Pearson's Correlation Coefficient
1.0
0.8
0.6
0.4
0.2
0.0
0.49
0.50
0.34
0.53
0.43
0.36
1 hour
2 hours
3 hours
Recovery (Post-contact)
+DECMA-1 = 200 µg/ml
Periphery
Cytoplasm

Figure 25: Active Src and E-cadherin localization at the cell-cell contacts is completely abolished when E-cadherin function is optimally inhibited during *de novo* cell-cell contact formation.

(A) Micrographs represent deconvoluted single plane images for wild type MDCK cells incubated with higher concentrations of E-cadherin function blocking antibodies at 1 , 2 and 3 hours following *de novo* cell-cell contact. Note that there is a higher decrease 3 post-contact of active-Src and E-cadherin at cell-cell contacts (blue arrows) in comparison to the controls (**Figure 23**: 3hr, blue arrows) and to MDCK cells treated with 100 µg/ml of DECMA-1 (**Figure 24**: 3hr, blue arrows). Scale bar in all images = 20µm.

(B) Change in Pearson's correlation coefficient values for E-cadherin and active-Src in the periphery and the cytoplasm measured for MDCK cells shown in panel **A**. Points represent mean ± SEM. Note 3 hours post-contact Pearson's correlation coefficient values in the periphery has a similar trend as the Pearson's correlation coefficient values in the cytoplasm.

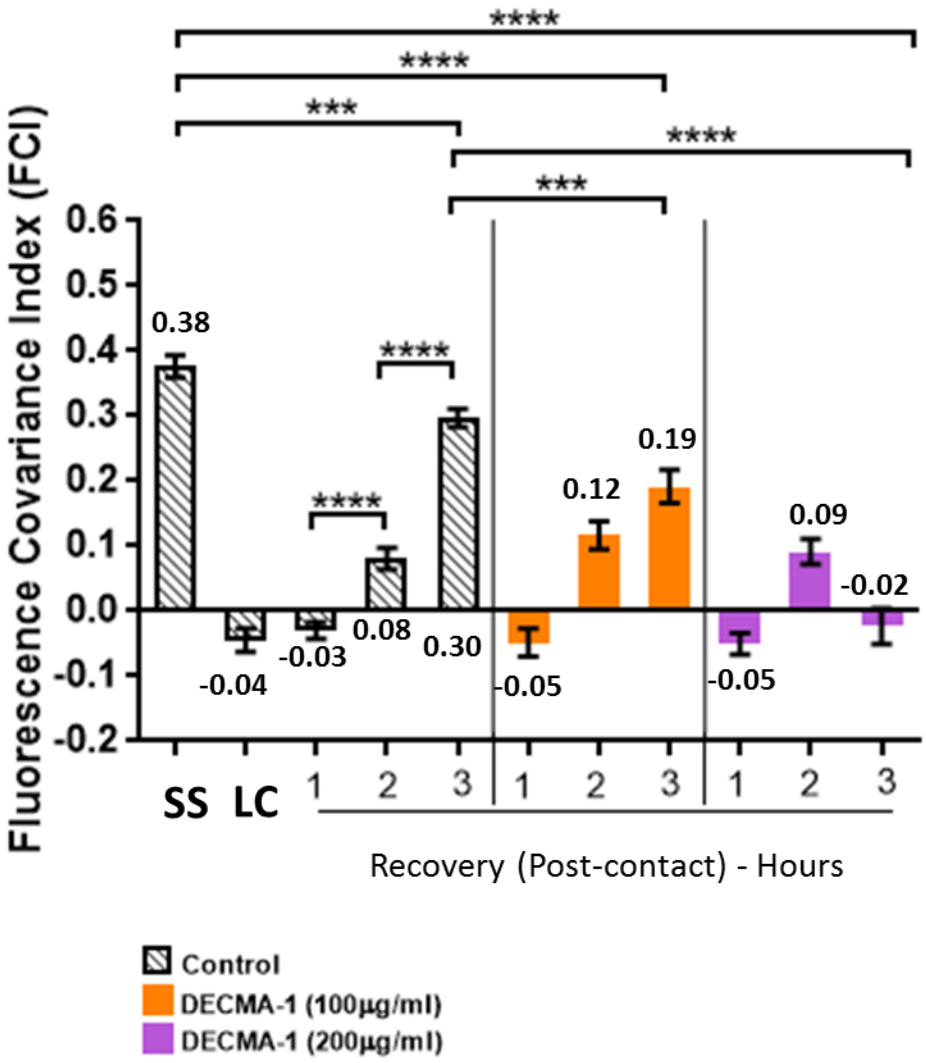
****
****
***
****
***
Fluorescence Covariance Index (FCI)
0.6
0.5
0.4
0.3
0.2
0.1
0.0
-0.1
-0.2
0.38
-0.04
-0.03
****
0.08
0.30
****
-0.05
0.12
0.19
-0.05
0.09
-0.02
SS LC 1 2 3 1 2 3 1 2 3
Recovery (Post-contact) - Hours
Control
DECMA-1 (100µg/ml)
DECMA-1 (200µg/ml)

Figure 26: FCI analyses of E-cadherin and Active Src (pY416-Src) during *de novo* adherens junction assembly. Mean FCI measurements for E-cadherin and active Src from cells in **Figures 23**, **24** and **25**, showed significant decrease of active Src (pY416-Src) and E-cadherin at cell-cell contacts when E-cadherin function is inhibited. Striped pattern bars represent cells without DECMA-1 treatment (control), orange bars represent cells with 100 µg/mL of DECMA-1 treatment, magenta bars represent cells with 200 µg/mL of DECMA-1 treatment. Error bars show mean ± SEM based on three independent experiments. Unpaired t-test with Welch's correction result: *** $P<0.001$; **** $P<0.0001$. Steady state n = 125, low calcium n = 98, 1 hour control n = 141, 2 hour control n = 99, 3 hour control n = 175. Orange bars (100 µg/mL of DECMA-1): 1 hour n=83, 2 hours n=82, 3 hours n=76. Magenta bars (200 µg/mL of DECMA-1): 1 hour n=126, 2 hours n=100, 3 hours n=110. The symbol n represents the total number of cells quantified.

The β-actin monomer synthesis permissive signal, Src, and F-actin colocalize at *de novo* cell-cell contact sites

It is well establish linear actin filament polymerization is required for adherens junction complex anchoring to F-actin. In this thesis I have shown E-cadherin homophilic binding is required for cell-cell contact localized Src activation resulting in β-actin monomer synthesis at cell-cell contacts and adherens junction complex assembly. It is also known E-cadherin adhesion activates Src (McLachlan et al., 2007). In addition another study found Src phosphorylates ZBP1 driving β-actin monomer synthesis (Hüttelmaier et al., 2005). However, the connection between E-cadherin adhesion activated Src and phosphorylation of ZBP1 driving β-actin monomer synthesis has not been addressed. Thus, I investigated the localization of E-cadherin receptor mediated activation of Src with F-actin. I was interested in this since Src is the permissive signal for β-actin monomer synthesis, I hypothesize this will result in adherens junction anchoring to F-actin. To investigate the relationship between E-cadherin receptor-mediated activation of Src signal for β-actin monomer synthesis and F-actin anchoring, I used calcium switch assays (see Materials and Methods for details). In MDCK cells where E-cadherin adhesion is normal, active Src and F-actin anchor are components of a cell-cell contact localized adherens junction complex assembled within 3 hours post-contact (Calcium repletion, **Figure 28: top panel, blue arrows)**. In contrast, when E-cadherin function is blocked I demonstrated using Pearson's Correlation analyses, the number of adherens junction complex containing active Src and F-actin at cell-cell contacts significantly decreases within 3 hours post-contact (**Figure 28**). Similar to blocking E-cadherin homophilic binding, when E-cadherin is knocked

down the complex between active Src and F-actin at cell-cell contacts significantly decreases in comparison to cells normally expressing E-cadherin (**Figure 29**).

Since these experiments are heavily dependent on E-cadherin protein expression, total E-cadherin protein levels were analyzed using immunoblotting following *de novo* cell-cell contacts. It was observed the amount of E-cadherin protein knockdown is consistent during calcium switch assays (**Figure 30A: top immunoblot; Figure 30B**). Once I established E-cadherin protein downregulation is consistent during calcium switch assays, I determined if cell-cell contact localized active Src goes down (**see Figure 29**) due to a decrease in total Src protein expression or through a delocalization event. Surprisingly, total Src protein expression remains the same in cells where E-cadherin is knockdown and in cells expressing proper E-cadherin protein amounts during calcium switch assays (**Figure 30A: bottom immunoblot; Figure 30C**). Thus, downregulation of Src signal at cell-cell contacts when E-cadherin is knocked down is due to a delocalization event, ultimately resulting in β-actin monomer delocalization from cell-cell contacts. Interestingly, this is exactly what happens to β-actin translation sites when E-cadherin binding is inhibited for 3 hours post-contact (**Chapter 2, Figure 19**). Importantly, as a control experiment, MDCK cells were transfected with a combination of scrambled shRNA and scrambled siRNA and subjected to a calcium switch assay to test whether E-cadherin and β-actin protein expression levels were affected in comparison to wild type MDCK cells (**Figure 30D**). Relative protein density analyses for E-cadherin and β-actin during calcium switch assays in cells transfected with a combination of scrambled shRNA and scrambled siRNA

were not significantly different in comparison to the wild type MDCK cells (**Figure 30D' and 30D"**).

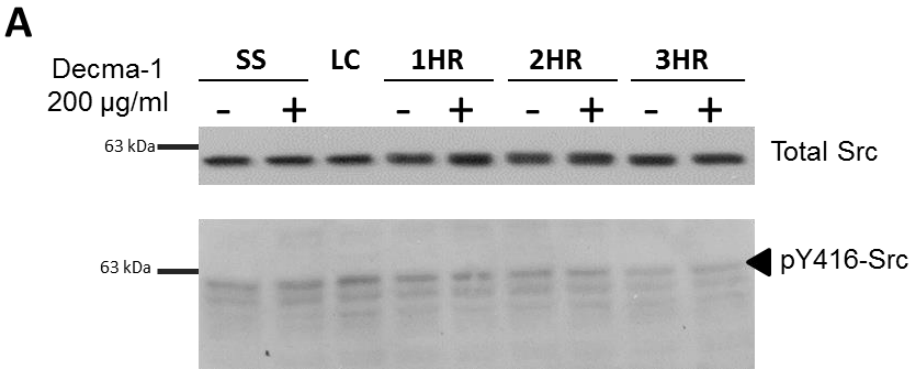
A
Decma-1
200 µg/ml
SS
LC
1HR
2HR
3HR
- + - + - + - +
63 kDa
Total Src
63 kDa
pY416-Src

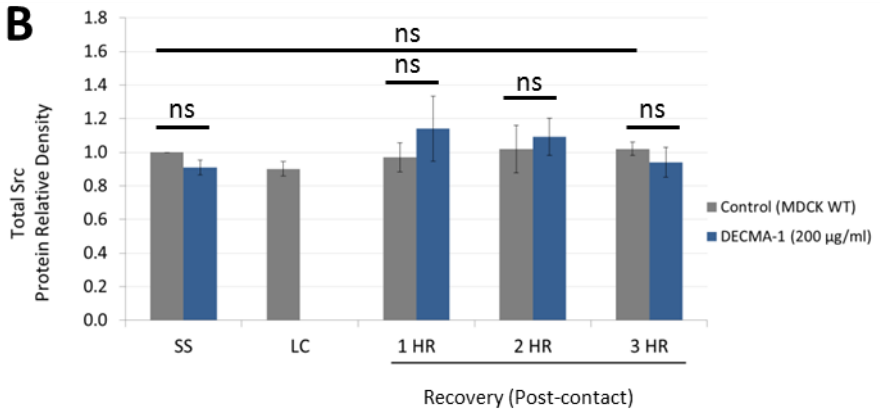
B
Total Src
Protein Relative Density
1.8
1.6
1.4
1.2
1.0
0.8
0.6
0.4
0.2
0.0
ns
ns
ns
ns
ns
SS
LC
1 HR
2 HR
3 HR
Recovery (Post-contact)
Control (MDCK WT)
DECMA-1 (200 µg/ml)

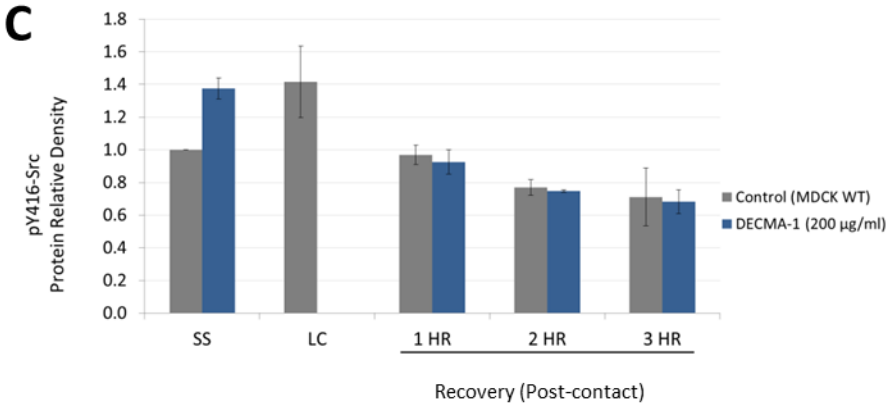
C
pY416-Src
Protein Relative Density
1.8
1.6
1.4
1.2
1.0
0.8
0.6
0.4
0.2
0.0
SS
LC
1 HR
2 HR
3 HR
Recovery (Post-contact)
Control (MDCK WT)
DECMA-1 (200 µg/ml)

Figure 27: E-cadherin loss of function does not affect total Src protein expression or total active-Src (pY416-Src) during *de novo* adherens junction assembly.

(A) Wild type tissues assembled from MDCK cells were subjected to a calcium switch assay. Whole cell lysates at steady state (SS), low calcium (LC) and 1 , 2 and 3 hours (3HR) post-contact with (+) or without DECMA-1(-) treatment were analyzed using Western blot technique.

(B) Protein relative density quantifications for Total Src for immunoblot shown in **A** (top immunoblot) revealed no significant change in protein expression.

(C) Preliminary data showing protein relative density quantifications for active-Src (pY416-Src) for immunoblot shown in **A** (bottom immunoblot), exhibited no change in Src activity during calcium switch assay in comparison to the controls **(compare grey bars vs. blue bars)**.

Protein relative density analysis of pY416-Src and total Src were performed using ImageJ. Error bars represent mean ± SEM based on 3 experimental replicates. Unpaired T-test result: * $P<0.05$.

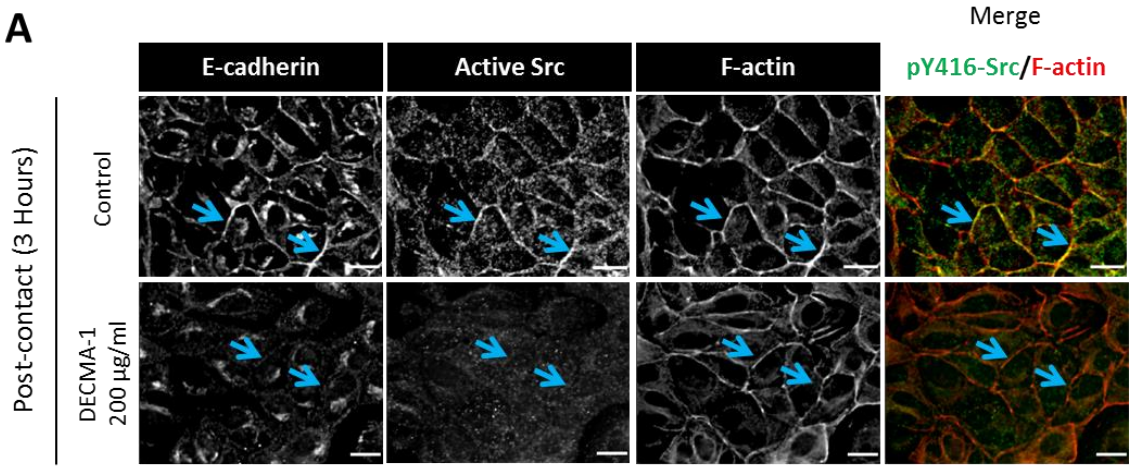
A
Merge
E-cadherin
Active Src
F-actin
pY416-Src/F-actin
Post-contact (3 Hours)
Control
DECMA-1
200 µg/ml

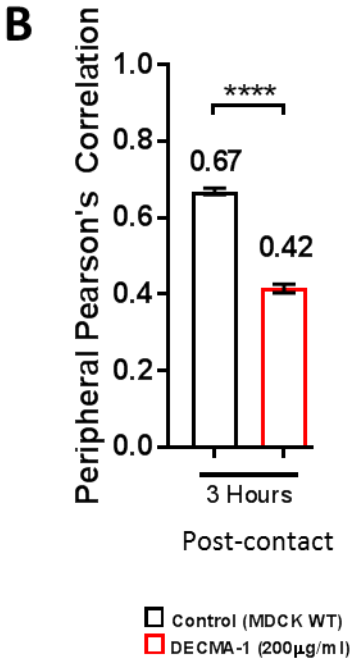
B
Peripheral Pearson's Correlation
1.0
0.8
0.6
0.4
0.2
0.0
****
0.67
0.42
3 Hours
Post-contact
Control (MDCK WT)
DECMA-1 (200µg/ml)

Figure 28: E-cadherin function is required to localize active Src and F-actin to cell-cell contacts during *de novo* adherens junction assembly.

Immunofluorescent staining for E-cadherin (Cy5), pY416-Src (active Src; green) and rhodamine phalloidin (red) using wild type MDCK cells 3 post-contact.

(A) Micrographs represent deconvolved single plane images for MDCK cells at 3 hours post-contact with E-cadherin function blocking antibodies (bottom) or without E-cadherin function blocking antibodies (top). **Merge**: Note that there is a decrease in colocalization of pY416-Src and F-actin fluorescent staining at cell-cell contacts when E-cadherin function is inhibited (**bottom panel**: blue arrows) in comparison to the controls (**top panel**, blue arrows). Scale bar in all images = 20μm.

(B) Mean peripheral Pearson's correlation coefficient measurements for F-actin and pY416-Src from figures in **panel A**; showed significant decrease of active Src (pY416-Src) and F-actin at cell-cell contacts when E-cadherin function is blocked. Unpaired T-test ****$p<0.0001$. Error bars represent mean ± SEM from 3 independent experiments. 3 hr (n=196); 3 hr DECMA-1 (n=110). Where n represents the total number of cells quantified.

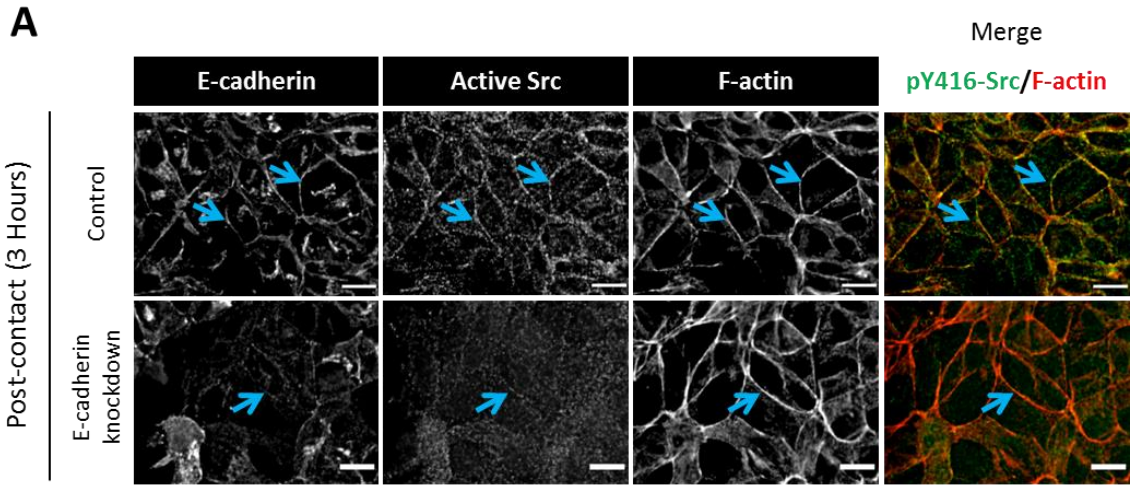
A
Merge
E-cadherin
Active Src
F-actin
pY416-Src/F-actin
Post-contact (3 Hours)
Control
E-cadherin knockdown

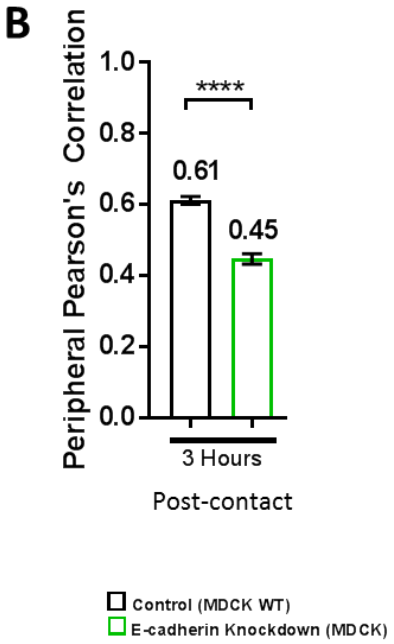
B
Peripheral Pearson's Correlation
1.0
0.8
0.6
0.4
0.2
0.0
****
0.61
0.45
3 Hours
Post-contact
Control (MDCK WT)
E-cadherin Knockdown (MDCK)

Figure 29: E-cadherin protein expression is required to localize active Src and F-actin at cell-cell contacts during de novo adherens junction assembly. Immunofluorescent staining for E-cadherin (Cy5), pY416-Src (active Src-green) and rhodamine phalloidin (red) using MDCK cells 3 hours post-contact.

(A) Micrographs represent deconvolved single plane images for MDCK cells at 3 hours post-contact (top panel) and in MDCK cells where E-cadherin protein expression has been knockdown (bottom panel). **Merge**: Note that there is a decrease in pY416-Src and F-actin colocalization 3 hours following *de novo* cell-cell contact at intercellular contacts when E-cadherin protein expression is reduced (**A**, **bottom panel**: blue arrows) in comparison to the controls (**A**, **top panel**, blue arrows).

(B) Mean peripheral Pearson's correlation coefficient measurements for F-actin and pY416-Src from images in panel **A**, showed significant decrease of active Src (pY416-Src) and F-actin at cell-cell contacts when E-cadherin protein expression is knockdown. Unpaired T-test **** $p < 0.0001$. Scale bar in all images = 20μm. Error bars represent mean ± SEM from a single experiment. 3 hr, n=69; 3 hr, E-cadherin knockdown, n=81. Where n represents the total number of cells quantified.

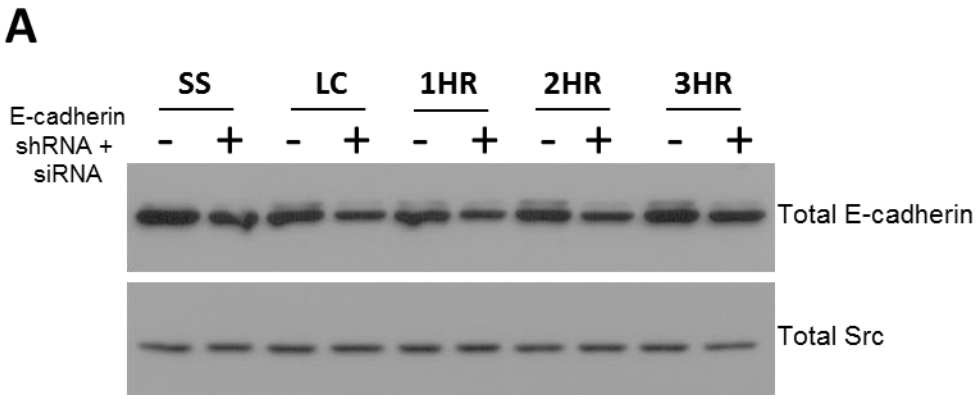
A
SS
LC
1HR
2HR
3HR
E-cadherin shRNA + siRNA
- + - + - + - + - +
Total E-cadherin
Total Src

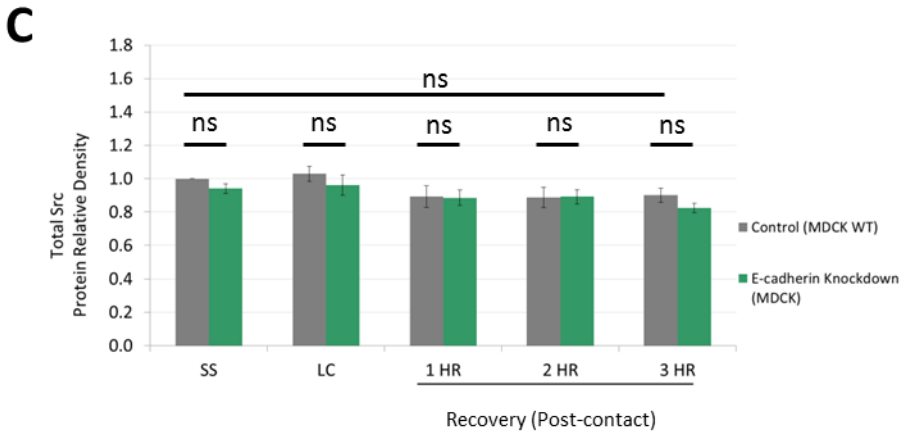
C
Total Src Protein Relative Density
1.8
1.6
1.4
1.2
1.0
0.8
0.6
0.4
0.2
0.0
ns
ns ns ns ns ns
SS
LC
1 HR
2 HR
3 HR
Recovery (Post-contact)
Control (MDCK WT)
E-cadherin Knockdown (MDCK)

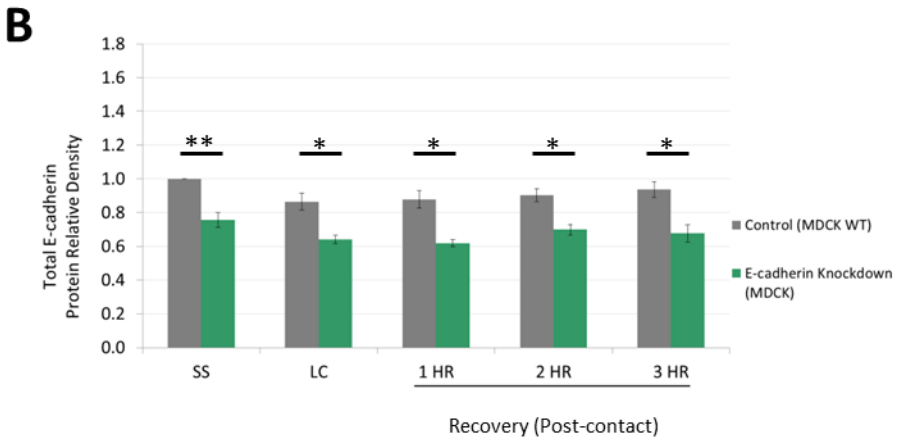
B
Total E-cadherin Protein Relative Density
1.8
1.6
1.4
1.2
1.0
0.8
0.6
0.4
0.2
0.0
** * * * *
SS
LC
1 HR
2 HR
3 HR
Recovery (Post-contact)
Control (MDCK WT)
E-cadherin Knockdown (MDCK)

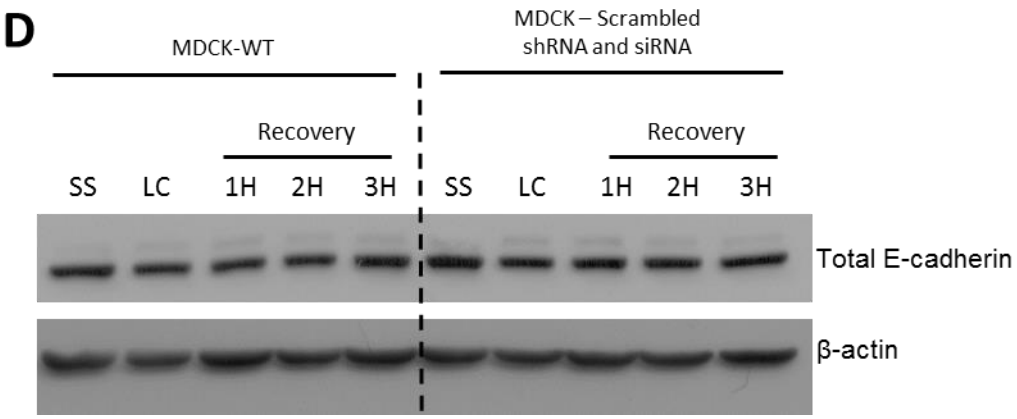
D
MDCK-WT
MDCK – Scrambled shRNA and siRNA
Recovery
Recovery
SS
LC
1H
2H
3H
SS
LC
1H
2H
3H
Total E-cadherin
β-actin

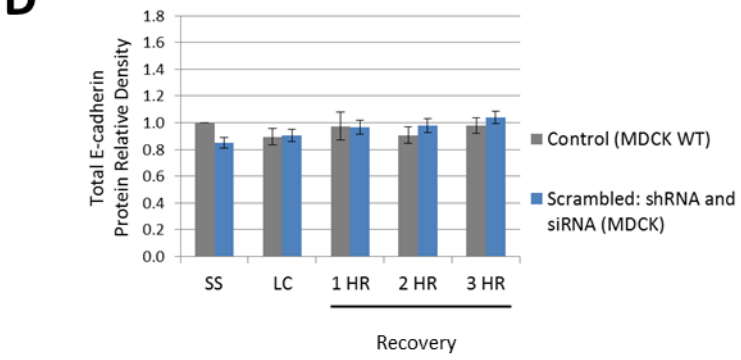
D'
Total E-cadherin Protein Relative Density
1.8
1.6
1.4
1.2
1.0
0.8
0.6
0.4
0.2
0.0
SS
LC
1 HR
2 HR
3 HR
Recovery
Control (MDCK WT)
Scrambled: shRNA and siRNA (MDCK)

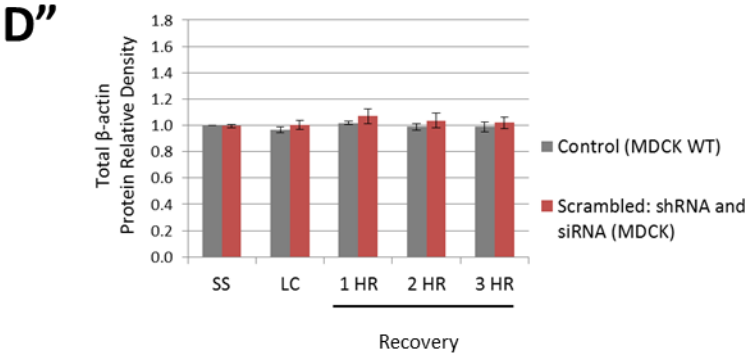
D"
Total β-actin Protein Relative Density
1.8
1.6
1.4
1.2
1.0
0.8
0.6
0.4
0.2
0.0
SS
LC
1 HR
2 HR
3 HR
Recovery
Control (MDCK WT)
Scrambled: shRNA and siRNA (MDCK)

Figure 30: Total Src protein expression levels during *de novo* adherens junction assembly do not change when E-cadherin protein expression is reduced.

(A) Whole cell lysates of wild type MDCK cells and MDCK cells transiently co-transfected with E-cadherin shRNA-A + E-cadherin siRNA-B (E-cadherin knockdown) at steady state (SS), low calcium (LC) and 1, 2 and 3 hours (3H) post-contact. Cell lysates were analyzed using Western blot and probed for total E-cadherin and total Src.

(B) Protein relative density analysis of E-cadherin demonstrates that E-cadherin protein expression has been knockdown effectively during the calcium switch assay in comparison to the controls.

(C) Relative protein levels of total Src from the same lysates showed no change in protein expression during *de novo* adherens junction assembly.

(D) Whole cell lysates of wild type MDCK cells and MDCK cells transiently co-transfected with scrambled shRNA-A + scrambled siRNA-B at steady state (SS), low calcium (LC) and 1, 2 and 3 hours (3H) post-contact. Cell lysates were analyzed using Western blot technique and probed for total E-cadherin and β-actin. Protein relative density analysis of E-cadherin **(D')** and β-actin **(D")** from the same lysates showed in panel **(D)** demonstrated no change in E-cadherin and β-actin protein expression between cells treated with scrambled shRNA-A and siRNA -B and wild type MDCK cells (Control). Relative protein levels analyses were performed using ImageJ. Error bars in all graphs represent mean ± SEM based on 3 experimental replicates. Unpaired T-test yielded not a significant difference in

total protein expression between treatments and during different time points of the calcium switch assay for **(‘D)** and **(D”)**.

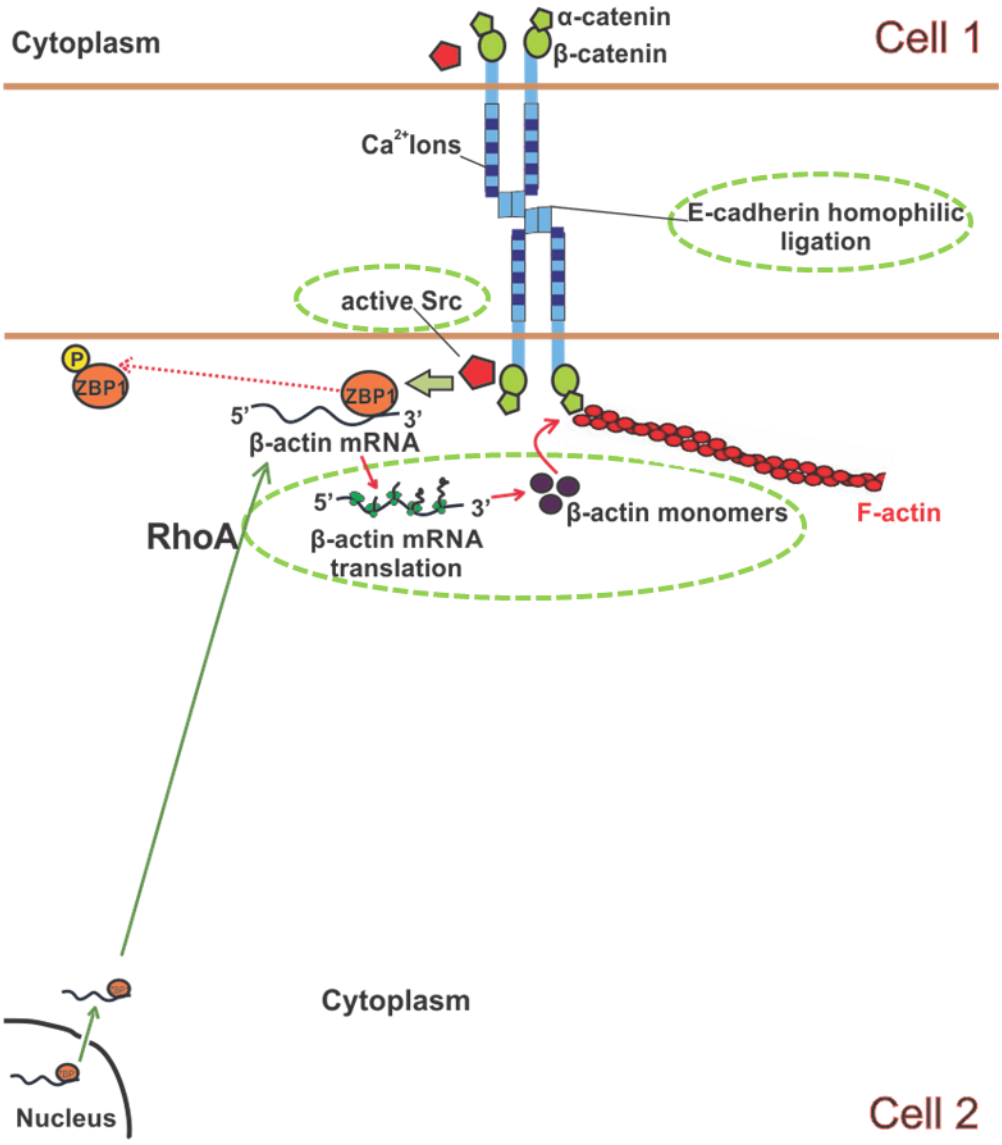
Cytoplasm
α-catenin
β-catenin
Cell 1
Ca2+Ions
E-cadherin homophilic ligation
active Src
P
ZBP1
ZBP1
5'
3'
β-actin mRNA
5'
3'
β-actin mRNA translation
β-actin monomers
F-actin
RhoA
Cytoplasm
Nucleus
Cell 2

Figure 31: (Summary of proposed working model and findings) E-cadherin function regulates Src activity for de *novo* adherens junction assembly. E-cadherin function regulates Src activity and β-actin monomer synthesis at cell-cell contact zones which drives *de novo* adherens junction assembly (dotted green circles). As mentioned before, RhoA triggers the targeting of the β-actin mRNA/ZBP1 complex to cell-cell contact zones. In addition, active Src phosphorylates ZBP1, which is bound to the β-actin mRNA, promoting β-actin monomer synthesis. Briefly, I proposed a working model in which E-cadherin activates RhoA and Src at *de novo* cell-cell contacts required for cell-cell contact localized β-actin monomer synthesis resulting in adherens junction complex anchoring to F-actin.

DISCUSSION

E-cadherin homophilic binding localizes the β-actin monomer synthesis initiation E-cadherin/active-Src complex to *de novo* cell-cell contact sites

Previously, we demonstrated RhoA and Src signaling are required to localize β-actin monomer synthesis to *de novo* epithelial cell-cell contact sites (Gutierrez et al., 2014). Also, in Chapter 2, I show there is a reciprocal relationship between E-cadherin binding and *de novo* cell-cell contact localized β-actin monomer synthesis in tissues assembled from MDCK cells. For this reason, I characterized the molecular mechanism of β-actin monomer synthesis at *de novo* cell-cell contacts. Blocking E-cadherin adhesive function significantly decreases the amount of signaling competent Src anchored to E-cadherin at *de novo* cell-cell contact sites in a DECMA-1 dose dependent manner (**Figure 26**). In cells with normal E-cadherin function, the asymmetric distribution of E-cadherin/active Src signaling complex favoring cell-cell contact generates a peak for E-cadherin mediated localization of active Src signaling at 3 hours post-contact. In fact, the dose dependent reduction in the accumulation of E-cadherin/active Src at cell-cell contacts is not affected during the first 2 hours following *de novo* cell-cell contact (**Figure 26**). However, the dose dependent reduction in E-cadherin function decreased E-cadherin/active-Src signaling complex accumulation at cell-cell contacts 3 hours post-contact (**Figure 26**). Interestingly, the dose dependent reduction in the number of *de novo* cell-cell contact localized β-actin monomer synthesis sites at 3 hours post-contact coincides with the peak generated by E-cadherin/active Src signaling complex localization at cell-cell contacts (**Figure 19B and Figure 26**). Remarkably, active RhoA under steady state conditions is

uniformly distributed throughout the cell. In contrast, during junction assembly RhoA is targeted near cell-cell contact zones (Gutierrez et al., 2014). Together these data suggest Src and RhoA signaling are required for cell-cell contact localized β-actin monomer synthesis at 3 hours post-contact. In addition, these data demonstrate E-cadherin adhesive function is required to accumulate the β-actin monomer synthesis initiation signal, Src, to *de novo* cell-cell contact sites in tissues assembled from MDCK cells.

The β-actin monomer synthesis initiation signal, Src, and F-actin are components of a common complex at *de novo* cell-cell contact sites

E-cadherin can be visualized only at early stages of cell-cell contacts using TIRF (internal reflection fluorescence microscopy), but at later stages of cell-cell contact formation, E-cadherin was only visible using widefield fluorescence microscopy (Yamada and Nelson, 2007).This suggests newly assembled contact moved upward, away from the substratum as the contact expanded (Yamada and Nelson, 2007). Active Src and F-actin can be found not only at cell-cell contacts, but they are also found at the basal cytoplasm, for example in cell-extracellular matrix contacts such us focal adhesions (Hu et al., 2014; Saleh et al., 2015). Moreover, focal adhesions are formed at the edges of the expanding contacts while focal adhesions at the center of the contact disassembled (Yamada and Nelson, 2007). I observed adherens junction maturation occurs ~3 hours post-contact. At this time point the contribution of Src signal and F-actin anchor coming from the basal cytoplasm below cell-cell contact zones will be minimal. Thus, I characterized the localization of Src signal with F-actin anchor at cell-cell contacts in tissues composed of MDCK cells.

Using fluorescence microscopy, I was able to determine the localization of active Src and F-actin in tissues assembled from MDCK cells that had undergone calcium switch assay. 3 hours following *de novo* cell-cell contact, active Src and F-actin were localized with E-cadherin at cell-cell contacts in cell that have proper E-cadherin function. When E-cadherin binding function is effectively inhibited, active Src localization with F-actin at cell-cell contacts is significantly decreased (**Figure 28: blue arrows**). Similarly, when E-cadherin is knocked down, active Src localization with F-actin at cell-cell contacts significantly decreases (**Figure 29: blue arrows**). Also, I showed E-cadherin protein downregulation or E-cadherin function inhibition results in Src signal delocalization from *de novo* cell-cell contacts, ultimately resulting in β-actin monomer delocalization from cell-cell contacts. In addition, preliminary data showed no change in total Src protein expression levels or changes in active Src when E-cadherin function was inhibited (**Figure 27**). This further verifies that Src signal localization at cell-cell contacts is important for adherens junction assembly in MDCK cells.

Model of E-cadherin adhesion mediated cell-cell contact localized β-actin monomer synthesis

Increasing evidence shows cadherins themselves can transduce cellular signals (McLachlan and Yap, 2007). For instance, an independent study found that RPTPα, a protein tyrosine phosphatase receptor, is in close proximity to E-cadherin and has a role in controlling Src activity downstream of E-cadherin at cell-cell contacts (Gomez et al., 2015; McLachlan and Yap, 2011; Truffi et al., 2014). Thus, in the context of above cited studies and data presented in this study, it is tempting to propose E-cadherin homophilic binding activates Src at *de novo* cell-

cell contacts. Then, active Src phosphorylates ZBP1 which is bound to the β-actin mRNA through its zipcode sequence. This initiates β-actin monomer synthesis at *de novo* cell-cell contacts leading to assembly of F-actin to anchor adherens junction complexes (**Figure 31**). Thus, the ability of cells to assemble adherens junction complexes depends on the presence of E-cadherin mediated RhoA and Src signaling resulting in β-actin monomer synthesis. When and where E-cadherin mediated activation of RhoA and Src signals occurs following *de novo* cell-cell contacts has not been well characterized. I postulate a model which specifies the localization of active RhoA and Src downstream E-cadherin adhesion following *de novo* cell-cell contact. In this thesis I showed E-cadherin/active Src signal complex formation favoring *de novo* cell-cell contacts was observed to be highest in steady state MDCK cells (**Figure 26**). In previous research studies we showed cell-cell contact localized β-actin monomer synthesis and active RhoA are absent in steady state cells (Gutierrez et al., 2014). In contrast, 3 hours post-contact following *de novo* cell-cell contacts, active RhoA (Gutierrez et al., 2014) and active Src, which are responsible for targeting β-actin mRNA and for β-actin monomer synthesis respectively are present along cell-cell contacts. Thus, in steady state MDCK cells where adherens junctions complexes are already formed, active RhoA signaling and β-actin monomer synthesis are absent at cell-cell contact zones depicted by the negative symbols in parenthesis (**Figure 32: Steady State**). When synchronized *de novo* cell-cell contact is initiated in tissues composed of MDCK cells (calcium switch), lamellipodia overlap between contacting cells is observed, and this is mediated by Rac1 and Arp2/3 (**Figure 32: Contact Initiation** (Kovacs et al., 2002; Yamada and Nelson, 2007)). Also at this stage, the cells are sensing

one another possibly through E-cadherin homotypic interactions (Collins et al., 2017). Also, a modest increase in *de novo* cell-cell contact localized active RhoA is observed. Interestingly, Rho signaling has been postulated to be responsible for β-actin transcript localization (**Figure 32: Contact Initiation;** Latham et al., 2001). During contact expansion, few E-cadherin based cell-cell contacts are observed. α-catenin concentration has to be significantly higher at nascent cell-cell contacts to form homodimers and suppress Arp2/3-mediated actin polymerization; resulting in the transition from active lamellipodia to their inhibition and bundling of actin filaments (Drees et al., 2005). This is accompanied by a modest increase in RhoA and Src signaling at cell-cell contacts leading to the appearance of contact localized β-actin monomer synthesis (**Figure 32: Contact Expansion**). During junction maturation, the assembly of adherens junction complexes significantly increases along with an increase in cell-cell contact localized RhoA (Gutierrez et al., 2014) and Src signaling which results in an increase of cell-cell contact localized β-actin monomer synthesis (**Figure 32: Maturing Junction**). The local synthesis of β-actin monomers drives F-actin polymerization required to anchor adherens junction complexes to *de novo* cell-cell contact sites during adherens junction maturation.

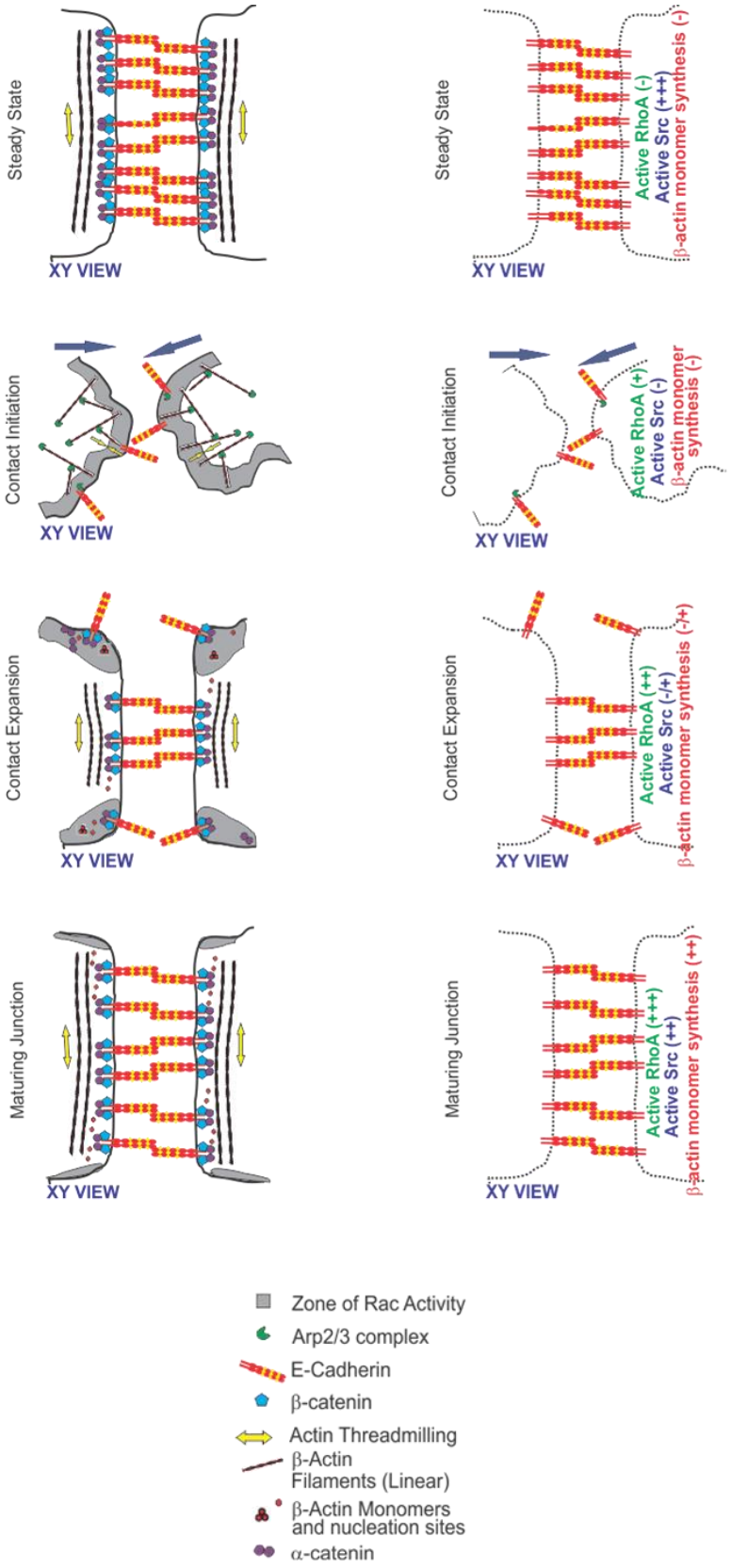
Steady State
XY VIEW
Steady State
Active RhoA (-)
Active Src (+++)
β-actin monomer synthesis (-)
XY VIEW
Contact Initiation
XY VIEW
Contact Initiation
Active RhoA (+)
Active Src (-)
β-actin monomer synthesis (-)
XY VIEW
Contact Expansion
XY VIEW
Contact Expansion
Active RhoA (++)
Active Src (-/+)
β-actin monomer synthesis (-/+)
XY VIEW
Maturing Junction
XY VIEW
Maturing Junction
Active RhoA (+++)
Active Src (++)
β-actin monomer synthesis (++)
XY VIEW
Zone of Rac Activity
Arp2/3 complex
E-Cadherin
β-catenin
Actin Threadmilling
β-Actin Filaments (Linear)
β-Actin Monomers and nucleation sites
α-catenin

Figure 32: Model of cell-cell contact localized β-actin monomer synthesis mediated by E-cadherin adhesion.

Schematic showing the three stages of de novo adherens junction assembly: contact initiation, contact expansion, and junction maturation. Contact initiation is characterized by branched actin network at the leading edge of the cells. E-cadherin clustering mediates actin filament remodeling from branched array to linear filaments that anchor adherens junctions complexes to F-actin, leading to the contact expansion phase. This is followed by an inhibition of protrusive activity and junction maturation. In addition, cells are able to form *de novo* adherens junction complexes by localizing E-cadherin mediated activation of RhoA and Src signals leading to β-actin monomer synthesis. As a consequence, the number of adherens junction complexes being anchored to F-actin increases, leading to junction maturation.

MATERIALS AND METHODS

For function blocking studies:

For calcium switch experiments, 75,000 wild type MDCK cells were seeded in a 24-well plate containing glass coverslips (No 1, Fisher Scientific). Cells were grown in regular growth media for 2 days at 37°C, 5% CO_2, and 95% humidity to form a monolayer ~90% confluent. Calcium switch procedure was done as described previously. For function blocking studies, an E-cadherin function blocking antibody, DECMA-1, (Sigma-Aldrich, product # U3254) was diluted in regular growth media without antibiotics to three final concentrations: 50 µg/ml (suboptimal concentration), 100 µg/ml (suboptimal concentration) and 200 µg/ml (optimal concentration). These diluted E-cadherin function blocking antibodies were added to the cells during *de novo* junction assembly. For control cells, wild type MDCK cells were used.

Indirect Immunofluorescence

Cells were fixed at room temperature in 4% paraformaldehyde in 1XPBS pH 7.4 for 20 min at different time points of the calcium switch experiment for E-cadherin function blocking studies (described previously in Chapter 3, Materials and Methods section). 0.5% Triton-X was used to permeabilize cells for 2 min at room temperature. Followed by blocking with 1% BSA diluted in 1X PBS pH 7.4 for 1 hour at room temperature. Then, cells were incubated in rabbit polyclonal anti-pY416-Src (active Src) primary antibody (1:50 dilution in blocking solution; Cell Signaling Technology, #2101) overnight at 4ºC. Cells were washed thrice for 5 minutes each wash with 1X PBS. Then, cells were then incubated with secondary

antibody, goat anti-rabbit conjugated to Cy3 or 488 fluorophores (1:800 dilution in blocking solution, Life Technologies) for 1 hour and a half at room temperature in the dark. Alexa Flour 488 Phalloidin or Alexa Flour 647 Phalloidin from ThermoFisher Scientific (1:25 dilution in 1X PBS) was used to stain F-actin for 20 min. at room temperature in the dark. DAPI was used to stain the nucleus. Finally, coverslips were mounted using Prolong® Gold (Life Technologies) and kept on a flat surface in the dark at 4ºC until image acquisition.

Image Acquisition and Processing

Images were acquired using an inverted Zeiss microscope (AxioObserver Z1) using Axiovision 4.8.2 software (Zeiss) equipped with a Plan-Apo 63x oil immersion objective with a numerical aperture of 1.4. 35 Z-stacks with a step size of 0.240 µm were acquired using a Cool Snap HQ^2 (Photometrics) camera with 2 by 2 binning for indirect immunofluorescence visualization. Camera digital gain was kept constant across a single set of experiments (e.g., one experimental set: calcium switch performed on MDCK control cells and calcium switch performed on MDCK cells treated with DECMA-1). Filter cube sets used: Far-red channel, 49 (Zeiss); green channel, 38HE (Zeiss); red channel, Ex:560/40, Em:630/75; and, blue channel, 49 (Zeiss). Exposure times for all the channels were kept constant across a single set of experiments without saturating any images. Image saturation was checked using the dynamic range indicator “OverExp” option on the live window in the Axiovision 4.8.2 software (Zeiss).

Image stacks were processed using the Zeiss AxioVision 4.8.2 Deconvolution algorithm with the following parameters: theoretical PSF, autolinear

normalization, constrained iterative and medium strength setting for all fixed images.

Fluorescence Covariance Index Analyses

Deconvolved images were exported into Volocity® 6.1 (PerkinElmer). Under the measurements window, two distinct cellular compartments, cell periphery and the cytoplasm (interior of the cell excluding the periphery and the nucleus), were defined using the freehand region of interest tool for each cell in an image stack. Pearson's correlation coefficient (for two protein pairs) was computed using the Calculate Object Colocalization tool. Peripheral and cytoplasmic Pearson's Correlation values were exported as a comma separated value format (*.csv). A MATLAB (MathWorks®) custom written script was used to extract Pearson's correlation coefficient values and calculate Fluorescence Covariance Index values for each cell.

Western Blotting

Western Blot was done as described previously (Chapter 2: Materials and Methods section). To detect active Src, 20 µg of total protein was loaded per well. Primary antibodies were rabbit anti-pY418-Src (1:1000; Cell Signaling Technology, #2101), mouse anti-total Src (1:10,000; Cell Signaling Technology, #2110), mouse anti-β-actin (1:30,000; Sigma-Aldrich, A5316) and mouse anti-E-cadherin (1:25,000; BD Transduction Laboratories™, Cat # 610181). Secondary antibodies included HRP-conjugated goat anti-mouse (1:15,000; GE Healthcare) and HRP-conjugated goat anti-rabbit (1:5,000; GE Healthcare). Total Src and its phosphorylated active form were probed in the same immunoblot to make sure that our antibodies were

detecting the expected molecular weight band ~60 kDa for both antibodies (**Appendix 3A: yellow box)**. Note that as decreasing concentrations of primary and secondary antibodies for active Src and total Src are used, unspecific banding patterns below the expected molecular weight for Src begin to disappear (**Appendix 3B and 3C**). Relative total protein density values were calculated and analyzed using ImageJ.

Src Inhibition

For calcium switch experiments, 250,000 wild type MDCK cells were seeded in a 6-well plate containing glass coverslips (N_o1, Fisher Scientific). Cells were grown in regular growth media for 2 days at 37°C, 5% CO_2, and 95% humidity to form a monolayer ~90% confluent. Cells were quickly washed with 1X PBS pH 7.4 and medium containing 4 mM EGTA (low calcium media: 13.37g/L of DMEM, 2g/L of sodium bicarbonate and the final concentration of 4 mM EGTA) was added for 1 hour. Then, cells were washed quickly once again with 1X PBS pH 7.4. Next, regular growth medium containing different concentrations of Src inhibitor, 22 nM, 44 nM and 88 nM, was added for 3 hours (Src Inhibitor-1-≥98% (HPLC) Sigma-Aldrich Product # S2075). Control was DMSO diluted in regular media, this solution was added to the cells for 3 hours post-contact. At the end of the 3 hour post-contact period, cells were lysed and total Src and active protein levels were analyzed by Western blot as described previously.

Statistical Analyses

Statistics data analysis was performed using GraphPad Prism 7 software (GraphPad Software, Inc).

For E-cadherin function blocking studies, 3 independent set of experiments were done. Mean FCI values at each time point and treatment condition were compared using unpaired t-test with Welch's correction. A p value of less than 0.05 ($p<0.05$) was considered significantly different.

Preliminary Data: For the Western blotting during calcium switch experiments, 3 experimental replicates were performed on the same day. Relative total protein density values were calculated and analyzed using unpaired t-test.

Significance was set at $p <0.05$ for all statistical analyses.

CHAPTER 4: Spatially regulated β-actin monomer synthesis and dynamin-mediated endocytosis are dynamically balanced during the assembly of functional epithelial monolayers.

Experiments included in this chapter are taken from and are published in Cruz et al., Cytoskeleton (2015); 72:597-608.

INTRODUCTION

Dynamic interactions between cadherin-catenin complexes and linear actin filaments regulate epithelial homeostasis (Cavey et al., 2008; Van Roy and Berx, 2008). Central to these interactions is the transmembrane adhesion/signaling receptor E-cadherin. Consequently, transcriptional repression by E-cadherin promoter and post-translational control of E-cadherin regulate epithelial to mesenchymal transition and cancer invasion (Blanco et al., 2002; Cano et al., 2000; Korpal et al., 2008; Lombaerts et al., 2006; Thiery, 2003). Conversely, blocking E-cadherin recycling at the cell surface by inhibiting endocytosis, increases E-cadherin transdimer formation and F-actin anchoring thereby stabilizing adherens junction complexes (Troyanovsky et al., 2006; Harris and Tepass, 2010). The contribution of E-cadherin endocytosis to the maintenance of mature adherens junctions in epithelia has been well studied (de Beco et al., 2009). However, its role in balancing actin anchoring of cadherin-catenin complexes during *de novo* adherens junction formation has yet to be explored. The main questions I investigated were: 1) Does dynamin-mediated endocytosis opposes F-actin anchoring of cadherin-catenin complexes in cells with partial

delocalization of β-actin monomer synthesis? 2) Does increased cadherin clustering at the cell surface drive actin anchoring of cadherin-catenin complexes? 3) What is the extent to which complete delocalization of β-actin monomer synthesis supersedes adherens junction assembly when endocytosis is inhibited? 4) What is the relationship between tissue barrier integrity and endocytosis inhibition?

RESULTS

Partial delocalization of β-actin monomer synthesis in MDCK cells impairs their ability to assemble a functional epithelial monolayer

Partially delocalizing β-actin monomer synthesis in tissues assembled from MDCK cells which contain a population of β-actin transcripts lacking 3'UTR targeting information (Δ3'UTR β-actin) generates a dominant negative adherens junction assembly phenotype (Gutierrez et al., 2014). Expressing β-actin transcripts lacking targeting information in epithelial and myoblast cells delocalizes β-actin translation (Gutierrez et al., 2014; Rodriguez et al., 2006). In Chapter 2, I demonstrated E-cadherin is required for cell-cell contact localized β-actin monomer synthesis during *de novo* adherens junction assembly. Of note, total β-actin protein expression is similar in tissues assembled from cells properly targeting β-actin translation versus cells impaired in their ability to target β-actin translation (Ballestrem et al., 1998; Gutierrez et al., 2014). To further investigate the function of E-cadherin in regulating cell-cell contact localized β-actin monomer synthesis, adherens junction complex assembly was assesed in tissues assembled from MDCK cells partially perturbed in their ability to target β-actin monomer synthesis. Cells that properly localize β-actin translation to cell-cell contacts exhibit strong E-cadherin with F-actin localization at cell-cell contacts (**Figure 33A: top panel**). In addition, these cells contain stress fibers in the basal cytoplasm (**Figure 33A: bottom panel**). By contrast, I observed cells with partially delocalized β-actin translation showed significant but weaker E-cadherin localization with F-actin at cell-cell contacts (**Figure 33B: top panel**). Also, fewer stress fibers were observed in the cytoplasm of these cells (**Figure 33B: bottom panel**). Importantly, cells with

partial delocalization of β-actin monomer synthesis exhibit lamellar protrusive activity that is largely absent in cells properly localizing β-actin monomer synthesis to cell-cell contacts (**Figure 33B: white arrowheads**). Cells impaired in their ability to localize β-actin monomer synthesis exhibited decreased adherens junction complex assembly at cell-cell contact zones evidenced by lower Fluorescence Covariance Index values compared to cells properly localizing β-actin translation (**Figure 33C**). Additionally, monolayers assembled from cells partially impaired in their ability localize β-actin translation were only 66% the height of monolayers assembled from cells expressing properly localizing β-actin translation (**Figures 33A and 33B: compare ΔZ**). These results indicate partially delocalizing β-actin monomer synthesis causes defects in the junction maturation stage of adherens junction assembly. Moreover, the in vitro tissue permeability to fluorescent dextran was ~5 times higher in confluent monolayers assembled from cells with partially delocalized β-actin translation (**Figure 33D**). Interestingly, low Fluorescence Covariance Index values correlated with the observed reduction in epithelial barrier permeability demonstrating this metric has value in quantifying gain or loss of tissue function.

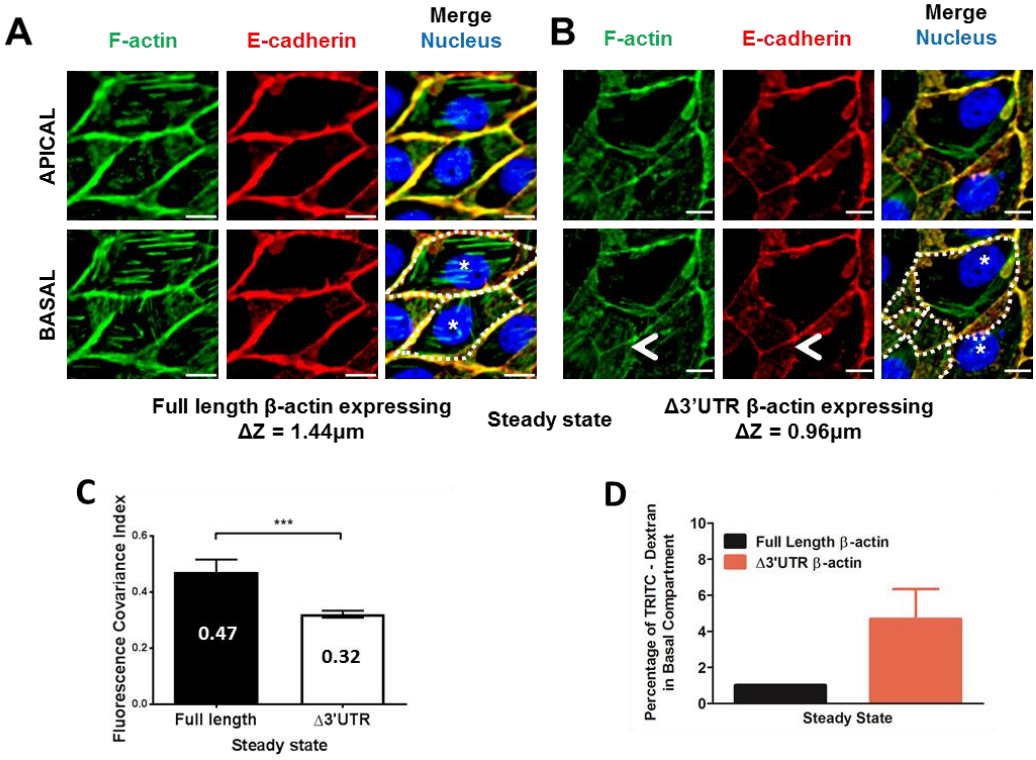
A
F-actin
E-cadherin
Merge
Nucleus
APICAL
BASAL
B
F-actin
E-cadherin
Merge
Nucleus
Full length β-actin expressing
ΔZ = 1.44μm
Steady state
Δ3'UTR β-actin expressing
ΔZ = 0.96μm
C
Fluorescence Covariance Index
0.6
0.4
0.2
0.0
***
0.47
0.32
Full length
Δ3'UTR
Steady state
D
Percentage of TRITC - Dextran in Basal Compartment
10
8
6
4
2
0
Full Length β-actin
Δ3'UTR β-actin
Steady State

Figure 33: MDCK cells with partial delocalization of β-actin monomer synthesis shows adherens junction assembly defects.

(A) Immunofluorescent co-staining of MDCK cells with proper localization of β-actin translation (expressing full length β-actin mRNA) for E-cadherin (red), F-actin (green) and nucleus (blue). Stress fibers are more prominent in the basal compartment, while E-cadherin and F-actin co-stain cell-cell interfaces in the apical and basal compartments.

(B) MDCK cells with partially delocalized β-actin translation (expressing Δ3'UTR β-actin mRNA) fixed at steady state and co-stained for F-actin (green), E-cadherin (red) and Nucleus (blue). Lamellar overlap from neighboring cells is visible in the basal compartment although E-cadherin and F-actin still co-stain at the cell-cell interfaces but to a lesser extent. Dotted white lines indicate cell boundaries and * indicates nucleus of individual cells. Note lamellar protrusions from adjacent cells (white arrowhead). ΔZ represents the distance between the apical and basal planes. Cells that properly localize β-actin monomer synthesis (full length β-actin mRNA) are taller than those with partially delocalized β-actin translation (Δ3'UTR β-actin mRNA), indicating defects in apical lifting.

(C) Mean FCI values for E-cadherin and F-actin for full length β-actin mRNA (n=29) and Δ3'UTR β-actin mRNA (n=314) expressing cells fixed at steady state. Unpaired T-test result: * **P<0.0006. Bars represent Mean ± S.E.M. Scale bars 10μm. The symbol n represents the number of cells quantified in each case.

(D) Graph illustrating the percent of TRITC-dextran in the bottom compartment in an *in vitro* permeability assay at steady state (SS) in cells that properly localize β-actin monomer synthesis (Full length β-actin) and cells with partial delocalization of

β-actin monomer synthesis (Δ3'UTR β-actin). Bars represent mean ± S.E.M. I would like to acknowledge Dr. Natasha Gutierrez for performing the permeability assays.

Inhibiting dynamin mediated endocytosis rescues the epithelial adherens junction assembly defect caused by partially delocalizing β-actin monomer synthesis

To study adherens junction assembly dynamics in epithelial MDCK monolayers with partially delocalized β-actin translation, calcium switch experiments were performed (Volberg et al., 1986). The extent of adherens junction assembly was assessed using Fluorescence Covariance Index analysis for E-cadherin and F-actin (Vedula et al., 2016). Cells with partially delocalized β-actin monomer synthesis begin to accumulate E-cadherin and F-actin at cell-cell contacts within 1 hour post-contact with accumulation continuing the 2nd hour post-contact (**Figure 34A: 1 hour and 2 hour panels**). Quantitatively, this increase in adherens junction complex assembly is shown by the increase in colocalization of E-cadherin and F-actin at cell-cell contacts within 2 hours post-contact (**Figure 34B, periphery**). Interestingly, 3 hours post-contact the extent of E-cadherin localization with F-actin at cell-cell contacts is similar to that observed 2 hours post-contact (**Figure 34A: 3 hours**). Due to an increase in lamellar protrusive overlapping (**Figure 34A: 3 hours, white arrowhead**), cytoplasmic E-cadherin and F-actin colocalization was highest 3 hours post-contact (**Figure 34B**). As a consequence, in tissue composed of cell partially delocalizing β-actin monomer synthesis, adherens junction complex assembly increases the first 2 hours post-contact but decreases in the 3rd hour post-contact. Quantitatively, this is demonstrated by Fluorescence Covariance Index values which increase the first 2 hours post-contact, and decrease significantly 3 hours post-contact (**Figure 37A**). In addition, in tissues assembled from cells partially delocalizing β-actin

monomer synthesis, tissue height is low in comparison to cells properly localizing β-actin translation (**Figures 34A and 33A: compare ΔZ**).

To further study E-cadherin's role in regulating cell-cell contact localized β-actin monomer synthesis, endocytosis was chemically inhibited in tissues assembled from cells partially delocalizing β-actin monomer synthesis. The rationale was blocking E-cadherin endocytosis from the cell surface increases E-cadherin transdimer formation and F-actin anchoring (Troyanovsky et al., 2006; Harris and Tepass, 2010). Dynasore, a small molecule inhibitor of Dynamin's GTPase function, was used to inhibit dynamin-mediated endocytosis of E-cadherin (Macia et al., 2006; Cruz et al., 2015). Adding 40 μM dynasore, following *de novo* cell-cell contact to cells partially delocalizing β-actin translation had little effect on the contact initiation or contact expansion phases of adherens junction assembly (**Figure 35A: 1 hour and 2 hour panels**). These cells reached a height of 1.44 μM, similar to cells properly targeting β-actin monomer synthesis (**Figure 33A**). However, these cells are impaired in their ability to shut off lamellar protrusive activity on their basal surface (**Figure 35A: 3 hour panel, white arrow**). E-cadherin's colocalization with F-actin at cell-cell contacts increased from 1 to 3 hours post-contact (**Figure 35B**). In contrast, E-cadherin's cytoplasmic colocalization with F-actin was low 1 and 2 hours post-contact (**Figure 35B**). Importantly, due to the presence of extensive lamellar protrusions 3 hours post-contact, I observed E-cadherin and F-actin fluorescence correlations increased in the cytoplasm, while fluorescence correlations also increased in the periphery (**Figure 35B: 3 hours**). Consistent with normal contact initiation followed by contact expansion the number of adherens junction complex assembly increased

up to 2 hours post-contact (**Figure 37B**). However, the number of adherens junction complex assembly at cell-cell decreased 3 hours post-contact (**Figure 37B**). This demonstrates there is a defect in adherens junction maturation when E-cadherin endocytosis was inhibited with this concentration of dynasore. To further investigate the relationship between E-cadherin endocytosis and spatially localized β-actin monomer synthesis, I doubled the concentration of dynasore to 80 μM. At this concentration of dynasore, I observed a significant increase in E-cadherin colocalization with F-actin at cell-cell contacts during *de novo* adherens junction assembly (**Figure 36A**). Consequently, I observed fewer lamellar protrusions 3 hours post-contact (**Figure 36A: 3 hours**). Additionally, these cells assembled tissues as tall as cells properly localizing β-actin translation (**Figure 36A and Figure 33A**). E-cadherin colocalization with F-actin remained low in the cytoplasm, while E-cadherin localization with F-actin at cell-cell contacts progressively increased from 1 to 3 hours post-contact (**Figure 36B**). Consequently, the phases of adherens junction complex assembly: contact initiation, contact expansion and cell-cell contact maturation, progressed normally at this concentration of endocytosis inhibitor. Quantitatively, Fluorescence Covariance Index values significantly increased during the 3 hours post-contact (**Figure 37C**). Together, these results indicate inhibiting endocytosis rescues adherens junction assembly in cells with partially delocalized β-actin monomer synthesis.

β-actin mRNA zipcode function and dynamin mediated endocytosis balance each other to drive adherens junction maturation

Previously it was shown MDCK cells partially delocalizing β-actin monomer synthesis (Δ3'UTR β-actin) express ~20% of the exogenous 3'UTR truncated β-

actin and express ~80% of the endogenous β-actin protein (Gutierrez et al., 2014). Consequently, when E-cadherin endocytosis is blocked this endogenous β-actin mRNA remains available to localize to cell-cell contacts. This result in the production of actin filaments at cell-cell contacts and when combined with decreased E-cadherin endocytosis, tips the balance toward anchoring cadherin-catenin complexes to F-actin. To completely delocalize endogenous β-actin mRNA, I used β-actin mRNA zipcode antisense oligonucleotides to mask β-actin/ZBP1 interactions (Gutierrez et al., 2014; Shestakova et al., 2001). Tissues assembled from MDCK cells partially delocalizing β-actin monomer synthesis were pretreated with β-actin mRNA zipcode antisense oligonucleotides. This resulted in a significant increase of lamellar protrusive activity 3 hours post-contact in the basal cytoplasm in comparison to cells properly localizing β-actin monomer synthesis (**Figure 38A: white arrow; Figure 33A**). Adding 80 μM dynasore to cells treated with antisense oligonucleotides resulted in taller cells, but lamellar protrusive activity was still active 3 hours post contact (**Figure 38B: white arrow**). These data demonstrate adherens junction complex assembly at cell-cell contacts is inhibited when β-actin monomer synthesis is completely delocalized even when endocytosis is strongly inhibited demonstrated by low Fluorescence Covariance Index values (**Figure 38C**). These results show the dominant negative adherens junction assembly phenotype caused by partially delocalizing β-actin translation can be rescued by inhibiting endocytosis but this rescue is critically dependent on the expression of a population of properly localizing β-actin transcripts.

The dynasore dependent rescue of adherens junction assembly in Δ3'UTR β-actin mRNA expressing cells requires functional E-cadherin

Dynamin inhibitors block the recycling of several transmembrane proteins including E-cadherin. The next question to ask is whether global inhibition of dynamin-mediated endocytosis or more specifically, E-cadherin function at the cell surface, was required for rescuing adherens junction assembly in cells with partial defects in localizing β-actin translation. To ask this question, DECMA-1, an E-cadherin function blocking antibody (Vestweber and Kemler, 1985) was used in these cells when endocytosis is inhibited following *de novo* cell-cell contact. To visualize the formation of *de novo* cell-cell contacts, live cell imaging experiments following *de novo* cell-cell contact with cells expressing Δ3'UTR β-actin mRNA encoding β-actin with an eGFP-fusion tag were utilized. In cells treated with vehicle alone (DMSO), contact initiation followed by contact expansion was observed as an increase in distance between cell vertices (**Figure 39A: yellow arrows**). However, during the contact expansion phase, cell-cell contact localized β-actin decreases. Also, neighboring cells continued to overlap and failed to reach the junction maturation phase (**Figure 39A**). Cells treated with 80 μM dynasore, also exhibited contact initiation followed by contact expansion. This was followed by junction maturation seen as the accumulation of linear β-actin cables running along the cell-cell interface (**Figure 39B: yellow arrows**). Additionally, lamellar protrusive activity decreased as cells reached the junction maturation stage ~3 hours post-contact (**Figure 39B: dotted yellow lines**). By contrast, treating cells with DECMA-1 and 80 μM of dynasore following *de novo* cell-cell contact completely abolished contact expansion and the rescue of junction maturation

(**Figure 39C: yellow arrows**). These data show inhibiting Dynamin-mediated endocytosis requires E-cadherin homophilic binding function to rescue adherens junction assembly in cells with partially delocalized β-actin translation.

Barrier integrity fails to recover when β-actin translation is delocalized during *de novo* adherens junction assembly in MDCK cell monolayers even with endocytosis inhibition

Epithelial cells self-assemble tissues variably resistant to molecular diffusion. At the molecular level, E-cadherin controls tissue self-assembly via its role in regulating cell-cell adhesions (Acharya et al., 2017). Therefore, cells with defective epithelial cell-cell adhesion machinery often exhibit tissue self-assembly defects. Interestingly, we observed an adherens junction assembly defect while characterizing β-actin monomer synthesis delocalization via mRNA zipcode masking during epithelial Ca^{2+} switch experiments (Gutierrez et al., 2014). To determine the effect on inhibiting E-cadherin endocytosis in cells with partially delocalized β-actin monomer synthesis, permeability barrier was measured using TRITC-dextran during calcium switch assays (**Figure 40**). Cells partially defective in their ability to localize β-actin monomer synthesis exhibited higher permeability to fluorescent dextran 4 hours post-contact compared to cells with no defects in localizing β-actin translation (**Figure 40: compare β-actin $_{(Unmasked)}$ versus Δ3'UTR β-actin**). Inhibiting endocytosis during *de novo* cell-cell contact using dynasore (80 μM final concentration) in cells with partially delocalized β-actin monomer synthesis rescued the epithelial barrier integrity defects observed within the first 3-4 hours post-contact (**Figure 40: compare Δ3'UTR β-actin versus Δ3'UTR β-actin with dynasore 80 μM**). Importantly, these results further

demonstrate Fluorescence Covariance Index values are a good proxy for monolayer barrier function (**Figure 37A and Figure 37C**). A complete delocalization of cell-cell contact localized β-actin monomer synthesis using β-actin mRNA zipcode antisense oligonucleotides abolished the rescue of barrier integrity observed when endocytosis is inhibited (**Figure 40: Δ3'UTR β-actin with dynasore 80 μM + β-actin mRNA zipcode antisense**). Taken together, these data show inhibiting the dynamin-mediated endocytosis rescues of adherens junction assembly and tissue permeability barrier in cells with partially delocalized β-actin monomer synthesis; and this requires E-cadherin homophilic binding function.

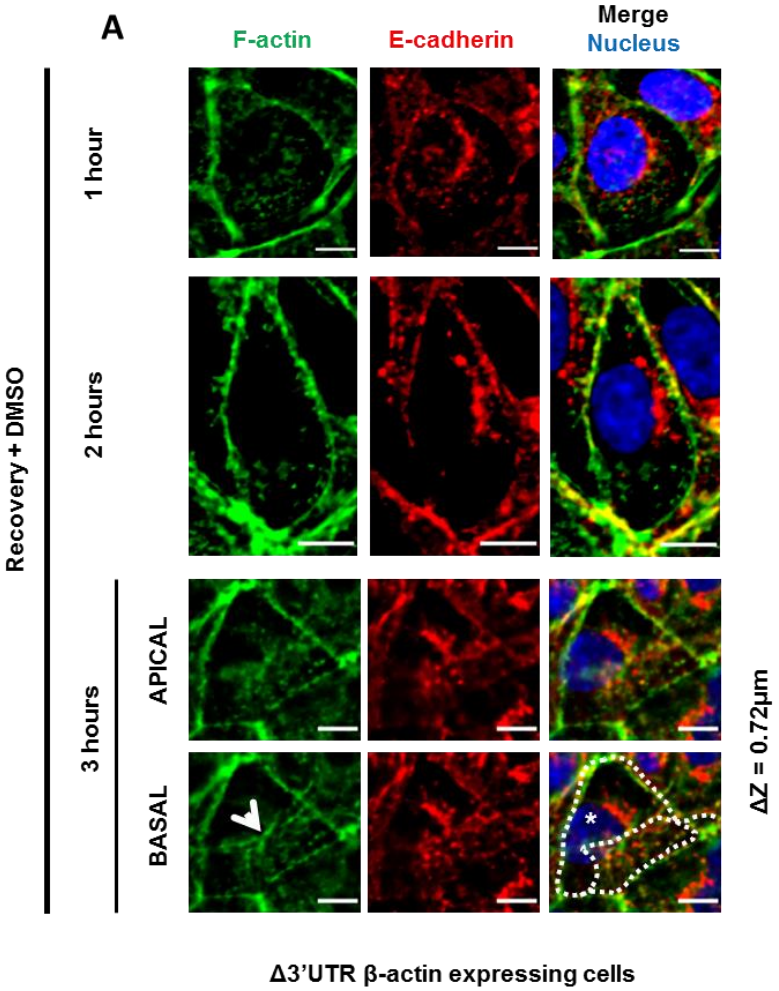
A
F-actin
E-cadherin
Merge
Nucleus
Recovery + DMSO
1 hour
2 hours
3 hours
APICAL
BASAL
ΔZ = 0.72µm
Δ3'UTR β-actin expressing cells

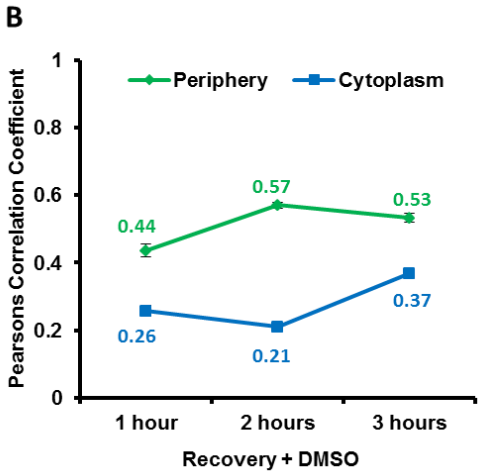
B
Periphery
Cytoplasm
Pearsons Correlation Coefficient
1
0.8
0.6
0.4
0.2
0
0.44
0.57
0.53
0.26
0.21
0.37
1 hour
2 hours
3 hours
Recovery + DMSO

Figure 34: Partially delocalized β-actin monomer synthesis causes adherens junction assembly defects during *de novo* adherens junction assembly.

(A) MDCK cells with partial delocalization of β-actin monomer synthesis (Δ3'UTR β-actin) fixed at 1, 2 and 3 hours post-contact (recovery) and co-stained for F-actin (Green), E-cadherin (Red), and Nucleus (Blue). Dotted white lines indicate cell boundaries and * indicates nucleus of individual cells.

(B) Change in cytoplasmic and peripheral Pearson's correlation coefficient values for F-actin and E-cadherin from cells shown in panel **A**. Points represent mean ± SEM. Note 3 hours recovery Pearson's correlation coefficient values in the periphery do not increase while PCC values in the cytoplasm increase due to lamellar overlap from neighboring cells in the basal compartment (white arrowhead in panel **(A)**).

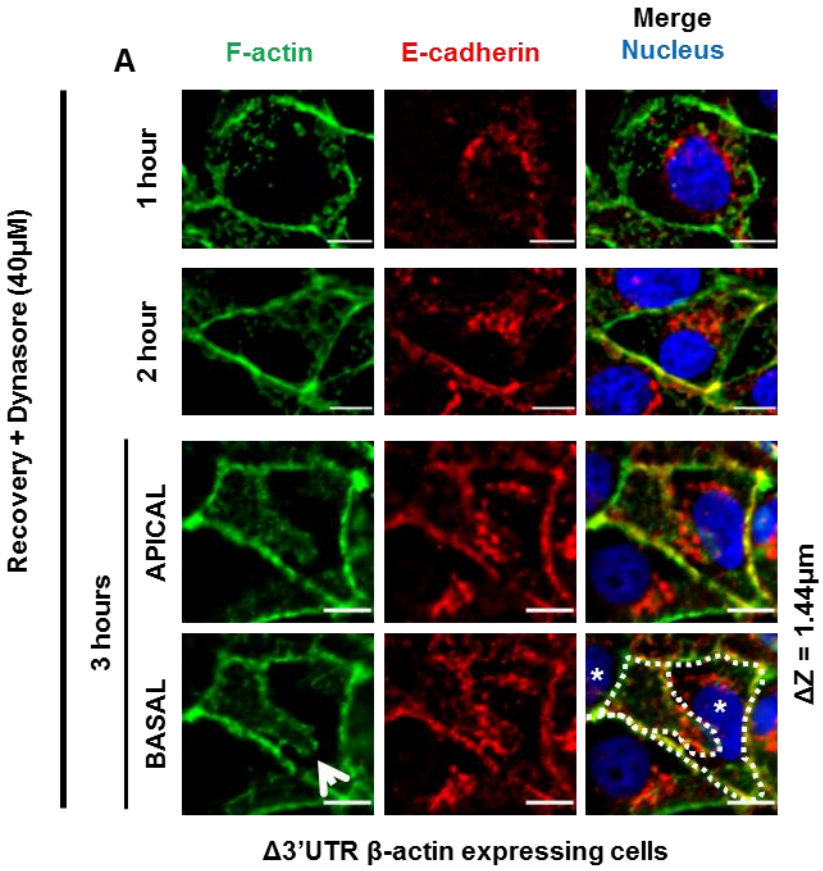
A
F-actin
E-cadherin
Merge
Nucleus
Recovery + Dynasore (40μM)
1 hour
2 hour
3 hours
APICAL
BASAL
ΔZ = 1.44μm
Δ3'UTR β-actin expressing cells

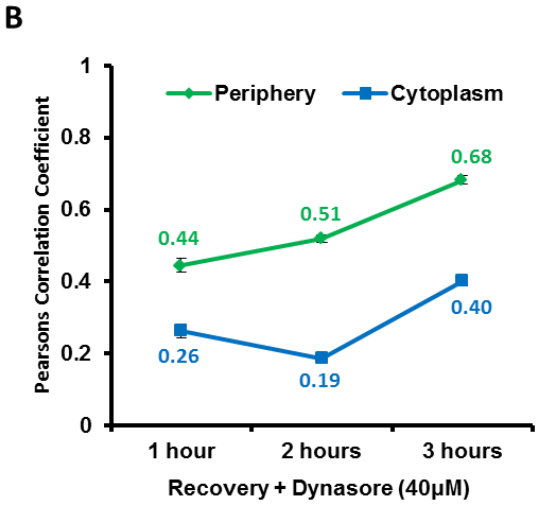
B
Periphery
Cytoplasm
Pearsons Correlation Coefficient
1
0.8
0.6
0.4
0.2
0
0.44
0.51
0.68
0.26
0.19
0.40
1 hour
2 hours
3 hours
Recovery + Dynasore (40μM)

Figure 35: MDCK cells partially delocalizing β-actin monomer synthesis treated with 40 μM dynasore still present adherens junction assembly effects.

(A) Micrographs of MDCK cells with partially delocalized β-actin translation (Δ3'UTR β-actin) 1, 2 and 3 hours post-contact with 80 μM dynasore and co-stained for F-actin (Green), E-cadherin (Red), and Nucleus (Blue). Dotted white lines indicate cell boundaries and * indicates nucleus of individual cells. ΔZ represents the distance between the apical and basal planes.

(B) Change in cytoplasmic and peripheral Pearson's correlation coefficient values for F-actin and E-cadherin from cells shown in panel **A**. Points represent mean ± SEM. Note 3 hours recovery Pearson's correlation coefficient values in the periphery remain high while Pearson's correlation coefficient values in the cytoplasm increase due to lamellar overlap from neighboring cells in the basal compartment (white arrowhead in panel **(A)**).

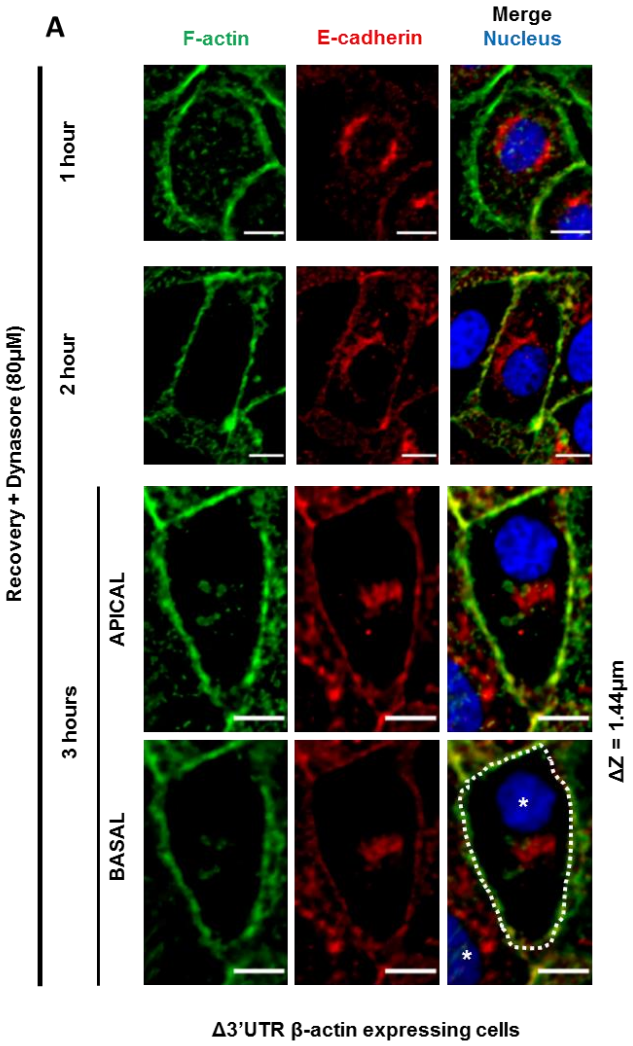
A
F-actin
E-cadherin
Merge
Nucleus
1 hour
2 hour
3 hours
APICAL
BASAL
Recovery + Dynasore (80μM)
ΔZ = 1.44μm
Δ3'UTR β-actin expressing cells

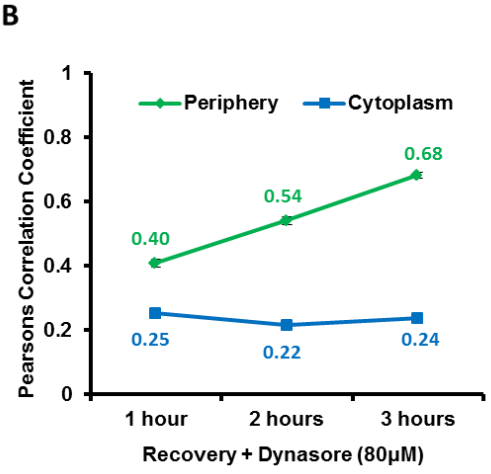
B
Periphery
Cytoplasm
Pearsons Correlation Coefficient
1
0.8
0.6
0.4
0.2
0
0.68
0.54
0.40
0.25
0.22
0.24
1 hour
2 hours
3 hours
Recovery + Dynasore (80μM)

Figure 36: Effectively inhibiting dynamin mediated endocytosis rescues adherens junction assembly defects caused by partially delocalized β-actin monomer synthesis.

(A) Micrographs of MDCK cells with partially delocalized β-actin translation (Δ3'UTR β-actin) 1, 2 and 3 hours recovery with 80 μM dynasore and co-stained for F-actin (Green), E-cadherin (Red), and Nucleus (Blue). Scale bars = 10 μm. Dotted lines indicate cell boundaries and * indicates nucleus of individual cells. ΔZ represents the distance between the apical and basal planes. Note the lamellar overlap is reduced of cells treated with 80 μM dynasore in comparison to cells treated with DMSO (**Figure 34**).

(B) Change in cytoplasmic and peripheral Pearson's correlation coefficient values for F-actin and E-cadherin from cells shown in panel **A**. Points represent mean ± SEM. Note 3 hours recovery Pearson's correlation coefficient values in the periphery increase while PCC values in the cytoplasm remain low.

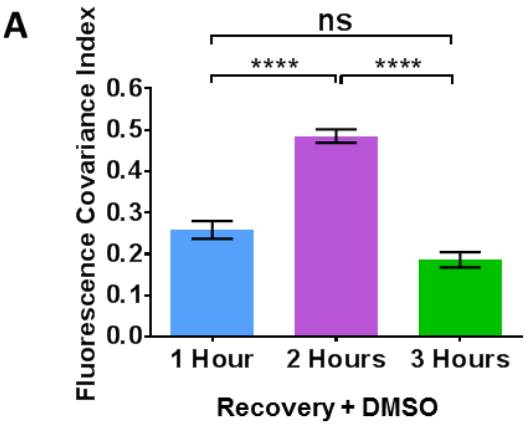
A
ns
****
****
Fluorescence Covariance Index
0.6
0.5
0.4
0.3
0.2
0.1
0.0
1 Hour
2 Hours
3 Hours
Recovery + DMSO

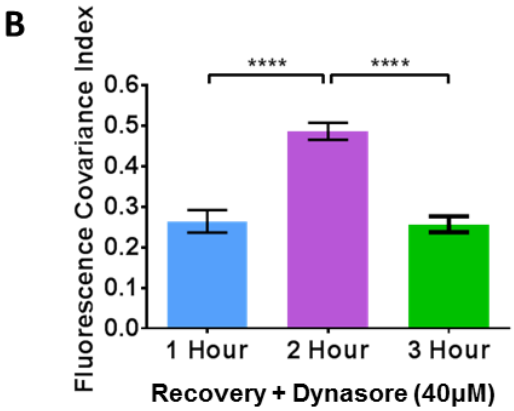
B
****
****
Fluorescence Covariance Index
0.6
0.5
0.4
0.3
0.2
0.1
0.0
1 Hour
2 Hour
3 Hour
Recovery + Dynasore (40µM)

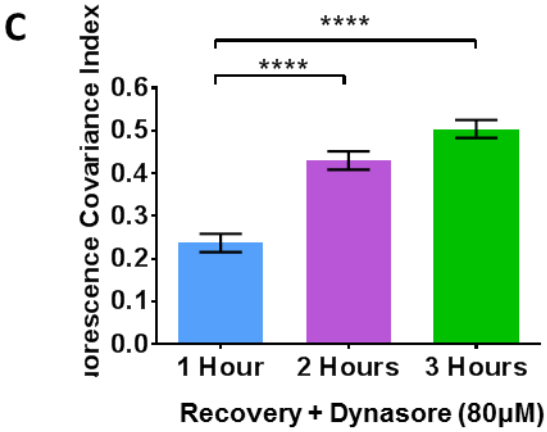
C
****
****
lorescence Covariance Index
0.6
0.5
0.4
0.3
0.2
0.1
0.0
1 Hour
2 Hours
3 Hours
Recovery + Dynasore (80µM)

Figure 37: FCI analyses of E-cadherin and F-actin during de novo adherens junction assembly in cells partially delocalizing β-actin monomer synthesis.

(A) Mean FCI values for E-cadherin and F-actin when β-actin monomer synthesis is partially delocalized during adherens junction assembly (quantifications are from cells shown in **Figure 34A**). A Kruskal-Wallis test yielded a *p*-value < 0.0001. Dunn's post-hoc multiple comparison test results with **** $p < 0.0001$ and *ns*: not significant indicated on the graph. 1 hour (n = 97), 2 hours (n = 229), 3 hours (n = 192).

(B) Mean FCI values for E-cadherin and F-actin in cells treated with 40μM dynasore when β-actin monomer synthesis is partially delocalized during adherens junction assembly (quantifications are from cells shown in **Figure 35A**). One-way ANOVA result was statistically significant ($F_{2, 302} = 35.7$, $p<0.0001$). Tukey's post-hoc multiple comparison test results with **** $P<0.0001$ are indicated on the graph. 1 hour (n = 86); 2 hours (n = 117); 3 hours (n = 102).

(C) Mean FCI values for E-cadherin and F-actin in cells treated with 80μM dynasore when β-actin monomer synthesis is partially delocalized during adherens junction assembly (quantifications are from cells shown in **Figure 36A**). One-way ANOVA result was statistically significant ($F_{2, 457} = 41.06$, $p<0.0001$). Tukey's post-hoc multiple comparison test results with *** $P<0.0001$ are indicated on the graph. Note: MDCK cells with partial β-actin monomer synthesis delocalization treated with 80 μM dynasore are able to assemble and anchor adherens complexes to F-actin. All bar graphs represent mean ± SEM. 1 hour (n = 201); 2 hours (n = 147); 3 hours (n = 112).

The symbol n represents the number of cells quantified in this figure.

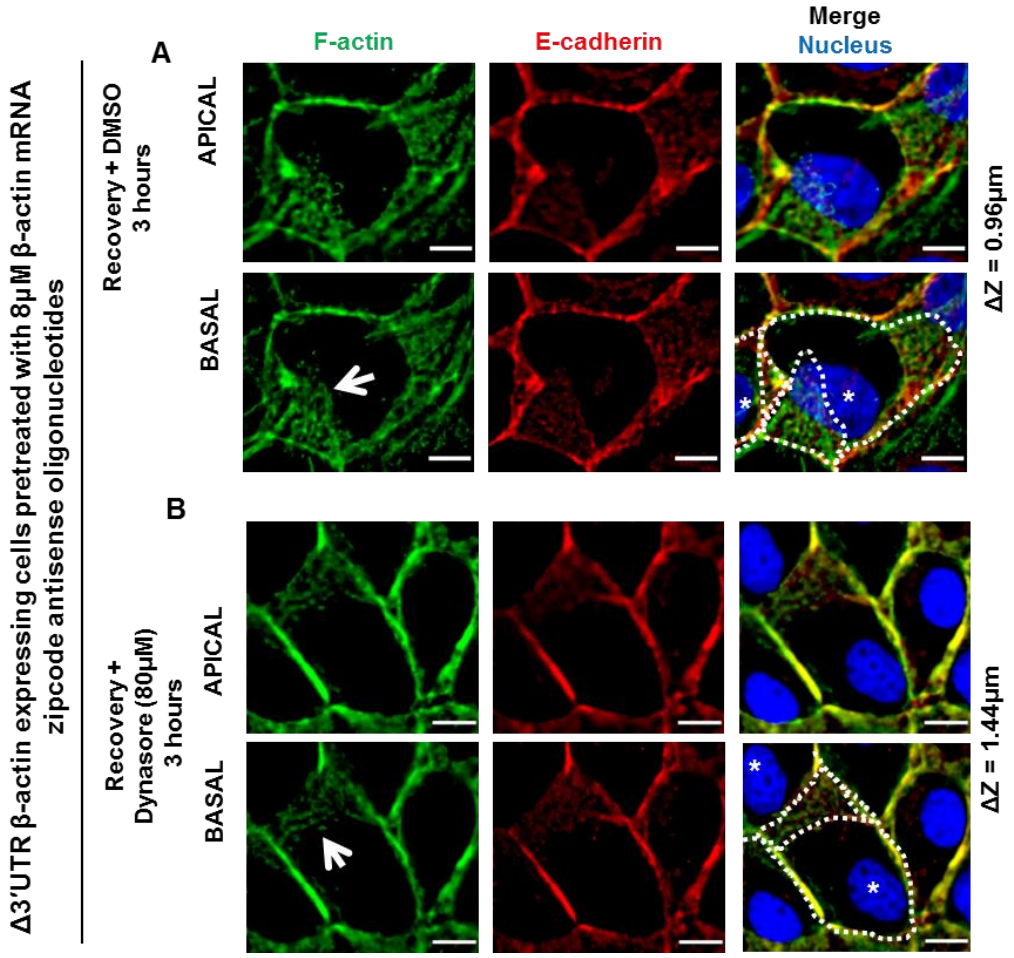
Δ3'UTR β-actin expressing cells pretreated with 8μM β-actin mRNA zipcode antisense oligonucleotides
A
Recovery + DMSO 3 hours
APICAL
BASAL
F-actin
E-cadherin
Merge
Nucleus
ΔZ = 0.96μm
B
Recovery + Dynasore (80μM) 3 hours
APICAL
BASAL
ΔZ = 1.44μm

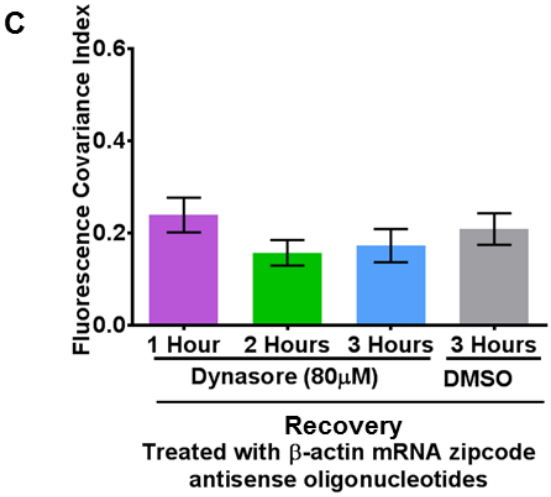
C
Fluorescence Covariance Index
0.6
0.4
0.2
0.0
1 Hour
2 Hours
3 Hours
3 Hours
Dynasore (80μM)
DMSO
Recovery
Treated with β-actin mRNA zipcode antisense oligonucleotides

Figure 38: Delocalizing β-actin translation blocks *de novo* adherens junction assembly even with endocytosis inhibition.

MDCK cells partially delocalizing β-actin translation (Δ3'UTR β-actin) were pretreated with β-actin mRNA zipcode antisense oligonucleotides for 3 hours post-contact with: **(A)** DMSO or **(B)** 80 μM dynasore. Then, cells were immunostained for F-actin (green), E-cadherin (red), and Nucleus (blue). Scale bars = 10 μm. Dotted lines indicate cell boundaries and * indicates nucleus of individual cells. ΔZ represents the distance between the apical and basal planes. Note the lamellar protrusions in the cells in panel **A** and **B** are seen in the basal compartment (white arrows).

(C) Mean FCI values for E-cadherin and F-actin from cells shown in panels **A** and **B**. Bars represent mean ± SEM. One-way ANOVA results for dynasore with β-actin mRNA zipcode antisense oligonucleotides treatment indicates no significant difference with time in FCI values. Unpaired student T-test indicates no significant variation between dynasore with antisense oligonucleotides and DMSO with antisense oligonucleotides treatment 3 hours post-contact. 1 hour dynasore + antisense oligonucleotides (n = 29); 2 hours dynasore + antisense oligonucleotides (n = 29); 3 hours dynasore + antisense oligonucleotides (n = 28); 3 hours DMSO + antisense oligonucleotides (n = 22). The symbol n represents the number of cells quantified.

I would like to acknowledge Neel Shah and Dr. Pavan Vedula for obtaining data presented in this figure.

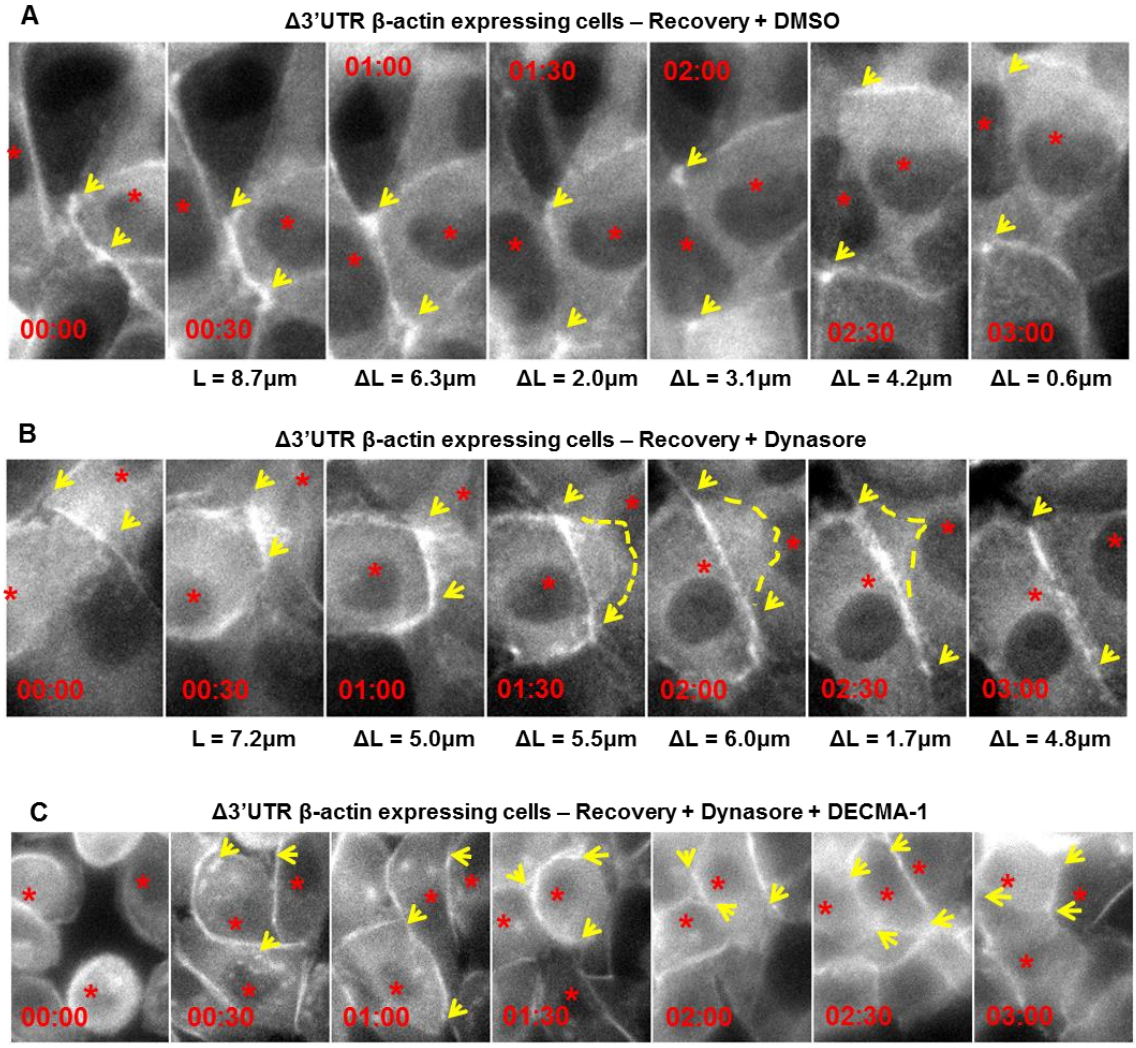
A
Δ3'UTR β-actin expressing cells – Recovery + DMSO
00:00
00:30
01:00
01:30
02:00
02:30
03:00
L = 8.7μm
ΔL = 6.3μm
ΔL = 2.0μm
ΔL = 3.1μm
ΔL = 4.2μm
ΔL = 0.6μm
B
Δ3'UTR β-actin expressing cells – Recovery + Dynasore
00:00
00:30
01:00
01:30
02:00
02:30
03:00
L = 7.2μm
ΔL = 5.0μm
ΔL = 5.5μm
ΔL = 6.0μm
ΔL = 1.7μm
ΔL = 4.8μm
C
Δ3'UTR β-actin expressing cells – Recovery + Dynasore + DECMA-1
00:00
00:30
01:00
01:30
02:00
02:30
03:00

Figure 39: Inhibition of E-cadherin endocytosis is required to rescue adherens junction assembly in cells partially delocalizing β-actin monomer synthesis.

Montage of MDCK cells with partially delocalized β-actin translation (Δ3'UTR β-actin mRNA that encodes an eGFP-fusion tag), following *de novo* cell-cell contact. Cells were treated with: **(A)** DMSO or **(B)** 80 μM Dynasore or **(C)** DMSO + 100 μg/ml DECMA-1 with calcium repletion. Time is indicated as duration post-initial contact (hh:mm). L is an estimate of contact length and ΔL represents the increase in length with respect to the previous frame. Arrows point to expanding contacts. Note in cells treated with DMSO, there is overlap of neighboring cells while in cells treated with 80 μM dynasore, contact expansion is followed by a decrease in lamellar protrusive activity (dotted yellow line). Treating cells with DECMA-1 completely abolishes contact expansion as seen by the lack of continued expansion of the filamentous actin along the cell-cell interface. The data represents a qualitative assessment of lamellar retraction followed by contact expansion upon inhibition of endocytosis in cells expressing Δ3'UTR β-actin mRNA following *de novo* cell-cell contact. Three independent experiments were performed for each condition in A, B, and two independent experiments for C. I would like to acknowledge Pavan Vedula for obtaining data presented in this figure.

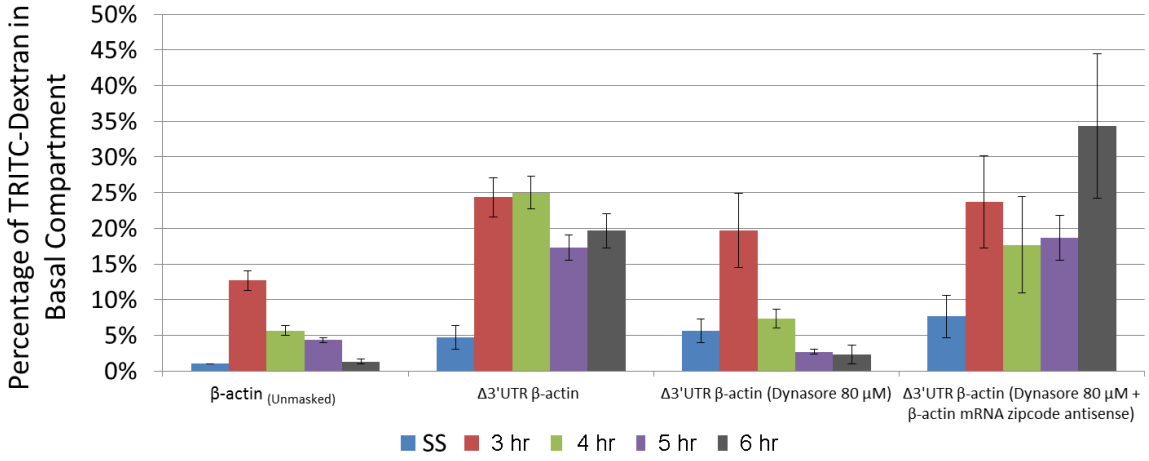
Percentage of TRITC-Dextran in Basal Compartment
50%
45%
40%
35%
30%
25%
20%
15%
10%
5%
0%
β-actin (Unmasked)
Δ3'UTR β-actin
Δ3'UTR β-actin (Dynasore 80 μM)
Δ3'UTR β-actin (Dynasore 80 μM + β-actin mRNA zipcode antisense)
SS
3 hr
4 hr
5 hr
6 hr

Figure 40: Barrier integrity fails to recover when β-actin translation is completely delocalized during *de novo* adherens junction assembly even with endocytosis inhibition.

Graph illustrating the percent of TRITC-dextran in the bottom compartment in an *in vitro* permeability assay at steady state (SS), 3 hour (3hr), 4 hours (4 hr), 5 hours (5 hr) and 6 hours (6 hr) post-contact with FL-β-actin eGFP MDCK cells (Unmasked), Δ3'UTR β-actin MDCK cells, Δ3'UTR β-actin MDCK cells with 80 μM dynasore and Δ3'UTR β-actin MDCK cells with 80 μM dynasore and β-actin mRNA zipcode antisense oligonucleotides. Bars show mean ± SEM based on three independent experiments. Note that treating the cells with partial delocalization of β-actin monomer synthesis with dynasore rescued the barrier integrity defect. However when β-actin monomer synthesis is completely delocalized even with dynasore addition, the permeability barrier defect during junction assembly cannot be rescued. I would to acknowledge Natasha Gutierrez for obtaining data presented in this figure.

DISCUSSION

E-cadherin anchoring to actin and E-cadherin endocytosis: The Yin and Yang of Adherens junction assembly

It has been proposed and observed E-cadherin endocytosis contributes significantly to the dynamics of adherens junctions (Troyanovsky et al., 2006). E-cadherin clustering at cell-cell contact sites increases α-catenin recruitment, which is required for inhibiting lamellar protrusions (Drees et al., 2005). E-cadherin that is not anchored at the cell surface is internalized by dynamin-mediated endocytosis and is either recycled or degraded (Cavey et al., 2008; Harris and Tepass, 2010). In fact, when E-cadherin is unable to form transdimers, it gets preferentially internalized (Izumi et al., 2004). In addition, endocytosis is required for redistributing E-cadherin to mature junctions (de Beco et al., 2009). Thus, E-cadherin endocytosis has two significant roles in regulating E-cadherin. The first, a rapid turnover during the initial phase of adherens junction assembly following cell-cell contact where Rac1 activity is high; and second, to recycle E-cadherin at mature junctions following disassembly of transdimers. Interestingly, it has been shown cells impaired in their ability to locally synthesize β-actin monomers results in reduced cadherin localization at the cell-cell contacts (Gutierrez et al., 2014; Rodriguez et al., 2006). As a result, epithelial monolayers composed of cells with partially delocalized β-actin translation are unable to recruit and anchor α-catenin to cell-cell contacts and turn off lamellar protrusions following *de novo* cell-cell contact. Thus, cells with partial delocalization of β-actin monomer synthesis undergo contact initiation and contact expansion but fail to progress to junction maturation due to lamellar overlap and increased E-cadherin endocytosis (**Figure**

33). A new generation dynamin inhibitor, hydroxy-Dynasore aka Dyngo 4a, was also used in this system, in MDCK cells with partial delocalization of β-actin monomer synthesis (Cruz et al., 2015; Mccluskey et al., 2013). The results obtained were similar to those observed when cells with partial delocalization of β-actin acting monomer synthesis were treated with dynasore following *de novo* cell-cell contact (**Figure 36**). In these cells, contact initiation and contact expansion were observed at 1 and 2 hours following *de novo* cell-cell contact. Cadherin based lamellar protrusive activity decreased significantly 3 hours post-contact (**Figure 36**). These results confirm inhibiting Dynamin-mediated endocytosis rescues adherens junction assembly defects caused by partially delocalizing β-actin monomer synthesis.

Interestingly, recent studies have demonstrated E-cadherin based intercellular junctions are modulated in a force-dependent manner (Ladoux et al., 2010). As cells pull on cadherin adhesions, internal tension increases due to more recruitment of adhesion proteins. As a consequence, a continued buildup on actomyosin contractility occurs which is required for contact expansion and junction maturation (Ladoux et al., 2010; Papusheva and Heisenberg, 2010). In fact, actin anchored cadherin-catenin complexes induce a myosin II-dependent feedforward loop that drives additional cadherin-catenin and actin filament anchoring. The resulting expansion and maturation of adherens junctions is required for epithelial structure and function (Smutny et al., 2010; Yonemura et al., 2010). Cell height in cells with partial delocalization of β-actin monomer synthesis and endocytosis inhibition was higher in comparison to cells with partial delocalization of β-actin monomer synthesis (**Figure 36A and 34A: 3 hours**).

Furthermore, cell height in MDCK cells with partial delocalization of β-actin monomer synthesis with endocytosis inhibition was the same in comparison to cells that had no defects in localizing β-actin monomer synthesis (**Figure 36A and Figure 33A**). Moreover, tissue barrier integrity is perturbed in cells partially delocalizing β-actin monomer synthesis and is restored when endocytosis is inhibited in these cells during *de novo* adherens junction assembly (**Figure 40**). Atomic force microscopy measurements during the formation of intercellular contacts revealed that myosin II tension is highest at ~2 hours during junction assembly (Harris et al., 2014). Also, previous studies had shown that nascent adhesion complexes are trafficked from basal to apical cell compartment as the cells lift (Hong et al., 2010; Kametani and Takeichi, 2007). Interestingly, constitutively active Rac1 depletes E-cadherin from intercellular contacts by increasing its internalization dependent on the stability of the mature contact (Akhtar and Hotchin, 2001). Thus, it is tempting to hypothesize partially delocalizing β-actin monomer synthesis prevents cells from lifting due to a decrease in adherens junction complex stability and insufficient tension, resulting in permeability and adherens junction assembly defects.

In Chapter 3, I proposed a model in which I specify the localization of active RhoA and Src downstream E-cadherin adhesion following *de novo* cell-cell contact. Briefly, E-cadherin/active Src signal complex formation favoring cell-cell contacts was observed to be highest in steady state MDCK cells (**Figure 26**). However, in previous research studies we showed cell-cell contact localized β-actin monomer synthesis and active RhoA are absent in steady state cells (Gutierrez et al., 2014). In contrast, following *de novo* cell-cell contact active RhoA

and Src are present at intercellular contacts; this coincides with the observed cell-cell contact localized β-actin monomer synthesis 3 hours post-contact (**Figure 19**). Thus, for *de novo* adherens junction complex assembly and anchoring to F-actin to occur, the following molecular events are necessary: E-cadherin mediated localization of RhoA and Src signal at cell contacts and cell-cell contact localized β-actin monomer synthesis. During contact expansion, E-cadherin based cell-cell contacts are observed. α-catenin concentration has to be significantly higher at nascent cell-cell contacts to form homodimers and suppress Arp2/3-mediated actin polymerization; resulting in the transition from active lamellipodia to their inhibition and bundling of actin filaments (Drees et al., 2005). This will result in actin filament remodeling that further drives E-cadherin clustering at the cell surface to oppose E-cadherin endocytosis, the negative contributor; and drives adherens junction assembly in epithelial cells (**Figure 41**). The balance tips if filament assembly and remodeling is blocked either pharmacologically using Latrunculin A and Cytochalasin B (Ballestrem et al., 1998; Wu et al., 2015) or by inhibiting cell-cell contact localized β-actin monomer synthesis (Gutierrez et al., 2014). The result is that cells are unable to transition from contact expansion to contact maturation owing to endocytosis of cadherin-catenin complexes, which now supersedes weak cadherin-catenin complexes that are bound to actin at cell-cell contacts.

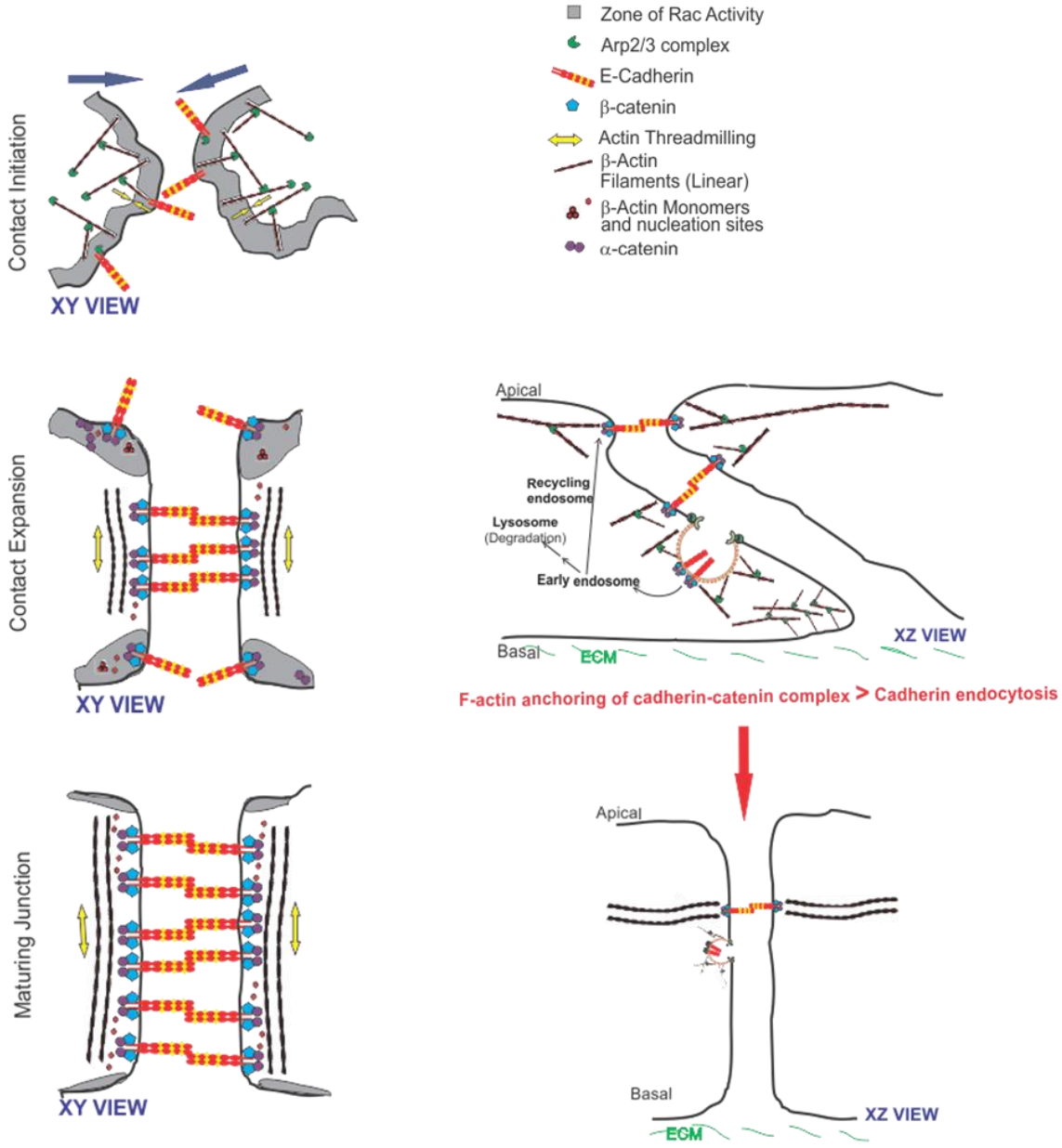
Zone of Rac Activity
Arp2/3 complex
E-Cadherin
β-catenin
Actin Threadmilling
β-Actin Filaments (Linear)
β-Actin Monomers and nucleation sites
α-catenin
Contact Initiation
XY VIEW
Contact Expansion
XY VIEW
Maturing Junction
XY VIEW
Apical
Recycling endosome
Lysosome (Degradation)
Early endosome
Basal
ECM
XZ VIEW
F-actin anchoring of cadherin-catenin complex > Cadherin endocytosis
Apical
Basal
ECM
XZ VIEW

Figure 41: Actin mediated E-cadherin clustering and E-cadherin endocytosis balance each other during adherens junction assembly.

Schematic showing the three stages of de novo adherens junction assembly: contact initiation, contact expansion, and junction maturation. Contact initiation is characterized by branched actin network at the leading edge of the cells. E-cadherin clustering mediates actin filament remodeling from branched array to linear filaments which anchor adherens junction complexes to F-actin, leading to the contact expansion phase. This is followed by an inhibition of protrusive activity and junction maturation. Endocytosis acts to remove E- cadherin-catenin complexes that are not actin anchored or are less stable. However, cells that are able to form *de novo* adherens junction complexes by localizing E-cadherin mediated activation of RhoA and Src signals leading to β-actin monomer synthesis, will supersede E-cadherin endocytosis from the cell surface to drive adherens junction anchoring to F-actin.

MATERIALS AND METHODS

Cell Culture

MDCK-NBL-2 (Madin-Darby Canine Kidney-NBL-2 from ATCC®CCL - 34™) is a parental epithelial cell line that will form a polarized monolayer (Dukes et al., 2011). MDCK epithelial cells were cultured in regular growth media (13.37 g/L of DMEM (Corning cellgro®), 1% penicillin/streptomycin (Corning cellgro®), 10% FBS (Corning cellgro®) and 2 grams/L of sodium bicarbonate) in a 100 x 20 mm cell culture dish. For cell passage, when the cells were ~80-90% confluent, regular growth media was removed and cells washed twice with 1X PBS pH 7.4. Then, 2 mL of 0.25% Trypsin EDTA pH 8.0 was added to the plate and incubated at room temperature for ~20-30 minutes. When the cells fully lifted from the plate, 8 mL (150 x 25mm dish) of regular growth media was applied and the cells transferred to a 15 mL Falcon tube. The cells were centrifuged for 2 minutes at 1200 rpm, producing a white pellet. The supernatant was discarded and cell pellet was re-suspended in 1 mL of regular growth media. 10 µl of the re-suspended pellet was pipetted into the hemocytometer and counted. For cell passage one million cells were seeded onto 100 x 20 mm cell culture dish and grown for 2-3 days at 37°C, 5% CO_2 and 95% humidity atmosphere until they were ~80-90% confluent.

Generation of stable cell lines

MDCK-NBL-2 cells were transfected with the reporter plasmids TC-eGFP-β-actin full length (Addgene, plasmid #27123) and TC-eGFP-β-actin Δ3'UTR (Addgene, plasmid #27124) using Lipofectamine™ 2000 (Invitrogen) according to manufacturer's guidelines (Gutierrez et al., 2014). All the stable cell lines were

sorted using FACS and the high βactin expressing cells were used for the experiments shown in **Figures 33 to 39**. Cell culture and passage was done as described previously. With the exception that these cells were cultured in regular growth media with G418 at a final concentration of 500 µg/ml to select transfected clones (stable MDCK cell lines).

Calcium Switch Assays

Cells were plated at a density of 250,000 cells per well in a six-well plate onto No 1 coverslips (Fisher Scientific) and grown for 48 h in regular growth medium with final concentration of 500 µg/ml G418. Cells were washed with 1XPBS, and medium without serum supplemented with 4 mM EGTA was added for 1 h. Regular growth medium containing G418 at a final concentration of 500 µg/ml was added to initiate *de novo* adherens junction assembly. Additionally, either DMSO (Sigma–Aldrich) or Dynasore (Sigma–Aldrich) at a concentration of 40 µM or 80 was added during calcium repletion. Pretreatment of cells with β-actin mRNA zipcode antisense oligonucleotide treatment was carried out in regular growth medium with 8 µM of oligonucleotides for 12 hours prior to start the calcium switch assay. Regular growth medium with fresh β-actin antisense oligonucleotides were added every 4 hours. This was followed by a calcium switch as described above maintaining oligonucleotides in the medium throughout the course of the experiment.

Live Cell Imaging

Cells were seeded at a density of 250,000 in 35-mm Mat-Tek dishes with glass cover bottom (MatTek Corp.) for 48 h and were subject to low calcium treatment as

described above. FluorBrite DMEM (Life Technologies) supplemented with 10% FBS and OxyFluor (Oxyrase) at 1% (v/v) was used as calcium repletion medium to minimize phototoxicity and photobleaching. Images were acquired on an inverted widefield Zeiss microscope (Zeiss AxioOb- server.Z1) equipped with an incubator chamber (37°C and 5% CO_2) was used. A 63X water immersion objective, NA 1.33 was used. QuantEM 512SC camera (Photometrics) was used with no binning. Time-lapse images were taken in GFP channel (Filter Set 38HE, item number 489038- 9901-000, Carl Zeiss) at 5-min intervals for 12 h. DECMA-1 antibody (Sigma–Aldrich) was used at a 100 µg/ml following calcium repletion.

Immunofluorescence

Cells were fixed at room temperature in 4% (w/v) paraformaldehyde in 1XPBS (pH 7.4) for 20 min at room temperature. A 0.5% Triton-X was used to permeablize the cells for 2 min at room temperature. Followed by blocking in 1% (w/v) BSA in 1X PBS, pH 7.4, cells were incubated in mouse monoclonal anti-E-cadherin primary antibody (1:250 dilution in blocking solution, BD Bio- sciences, #610181) overnight at 4°C. Cells were then incubated with goat anti-mouse Cy5 (Life Technologies) conjugated secondary antibody (1:800 dilution in blocking solution, Life Technologies) for 1 1/2 hours at room temperature. Rhodamine-Phalloidin (1:40 dilution in 1X PBS, Life Technologies) was used to stain F-actin for 40 min. at room temperature. DAPI was used to stain the nucleus. Finally, coverslips were mounted using Prolong® Gold (Life Technologies).

Image Acquisition and Processing

Images were acquired using an inverted Zeiss microscope (AxioObserver Z1) using Axiovision 4.8.2 software (Zeiss) equipped with a Plan-Apo 63x oil immersion objective with a numerical aperture of 1.4. 35 Z-stacks with a step size of 0.240 μm were acquired using Cool Snap HQ^2 (Photometrics) camera for indirect immunofluorescence visualization with 2x2 binning. Digital gain (camera option) was kept constant across a single set of experiments (e.g., calcium switch in DMSO treated cells and calcium switch in dynasore treated cells). Filter cube sets used: Far-red channel, 49 (Zeiss); green channel, 38HE (Zeiss); red channel, Ex:560/40, Em:630/75; and, blue channel, 49 (Zeiss). Exposure times for all the channels were kept constant across a single set of experiments without saturating any images. Image saturation was checked using the dynamic range indicator "OverExp" option on the live window in the Axiovision 4.8.2 software (Zeiss).

Image stacks were processed using the Zeiss AxioVision 4.8.2 Deconvolution algorithm with the following parameters: theoretical PSF, autolinear normalization, constrained iterative and medium strength setting for all fixed images.

Fluorescence Covariance Index (Fluorescence Covariance Index) Analyses

Deconvoluted images were exported into Volocity® 6.1 (PerkinElmer). Under the measurements window, two distinct cellular compartments, cell periphery and the cytoplasm (interior of the cell excluding the periphery and the nucleus), were defined using the freehand region of interest tool for each cell in an image stack. Pearson's correlation coefficient (for two protein pairs) was computed using the Calculate Object Colocalization tool. Peripheral and cytoplasmic Pearson's

Correlation (Pearson's correlation coefficient) values were exported as a comma separated value format (*.csv). A MATLAB (MathWorks®) custom written script was used to extract Pearson's correlation coefficient values and to calculate Fluorescence Covariance Index values for each cell.

In Vitro Permeability Assay

MDCK cells expressing Δ3'UTR β-actin were plated at 700,000 cells per Transwell® support (0.4-lmpore size, Corning) in a 6-well plate and incubated for 48 hours. A calcium switch was performed as described above using regular growth medium. Then, 5 mg/ml of 3000 MW TRICT-dextran was added in 1,2,3 and 4 hours after calcium repletion in the top compartment for 2 hours (TRICT-dextran was diluted in FluorBrite DMEM (Life Technologies) supplemented with 10% FBS (Corning cellgro®), 1X penicillin/streptomycin (Corning cellgro®)). 200 µL samples were taken from the top and bottom compartments and put into a 96-well plate. Fluorescence intensity was measured using a GloMax plate reader (Promega). The ratio of the fluorescence intensities in the bottom and top compartments was taken and multiplied by 100 to get the percent of TRITC-dextran in the bottom compartment.

For β-actin mRNA zipcode oligonucleotides experiments, 8 µM phosphorothioate modified

β-actin antisense 5' CGCAACTAAGTCATAGTC 3',

β-actin sense 5'GACTATGACTTAGTTGCG 3',

scrambled 5' ACTGCAACGTCGTATACA 3'.

Pretreatment of cell oligonucleotides were done twice, for 4 hours each, prior to the calcium switch experiments in regular growth media. Throughout the calcium switch, cells remained in 8 μM antisense, or scrambled oligonucleotides.

CHAPTER 5: CONCLUSION AND FUTURE DIRECTIONS

Conclusions

E-cadherin binding localizes β-actin monomer synthesis to *de novo* cell-cell contacts to localize actin filament remodeling during adherens junction assembly

In chapter 2, I demonstrate E-cadherin localizes β-actin monomer synthesis to *de novo* epithelial cell-cell contact sites. It is well known E-cadherin is an important upstream effector of *de novo* adherens junction assembly. E-cadherin localizes to *de novo* cell-cell contacts by anchoring to the actin cytoskeleton (Chen et al., 2014; Cruz et al., 2015; Grieve and Rabouille, 2014; Gutierrez et al., 2014; Wu et al., 2015). Importantly, E-cadherin-F-actin anchoring regulates epithelial tissue adhesive function. For example, coupling cadherin adhesion to the actin cytoskeleton reinforces tissue adhesiveness (Desai et al., 2013; Hong et al., 2013). Therefore, E-cadherin-F-actin anchoring helps maintain tissue homeostasis since epithelial cell-cell contacts delicately balance mechanical stress and adhesion during tissue assembly and remodeling. Interestingly, in addition to its well-known role in adhesion via F-actin anchoring, E-cadherin specifies contractile actin filament assembly sites by regulating the activity of the linear actin filament polymerase mDia1 and the myosin IIA motor protein. In fact, blocking E-cadherin function decreased myosin IIA levels at MCF7 cell-cell junctions (Shewan et al., 2005). While mDia1 knockdown disrupted epithelial adherens junctions (Ayollo et al., 2009; Carramusa et al., 2007). Together these studies show E-cadherin

binding specifies actin cytoskeleton remodeling to assemble an actomyosin contractile network at cell-cell contact sites.

Previous studies determined that cell-cell contact-driven localization of β-actin monomer synthesis generates a monomer pool above the critical concentration for barbed end filament polymerization, sufficient to drive the assembly of unbranched actin filaments (Bonder et al., 1983; Gutierrez et al., 2014). Our studies demonstrate epithelial cells partially delocalizing β-actin monomer synthesis through β-actin mRNA zipcode deletion exhibited a significant decrease in adherens junction assembly (Gutierrez et al., 2014) and tissue permeability defects (Cruz et al., 2015). In Chapter 2, I presented data demonstrating that overexpressing E-cadherin rescues the epithelial adherens junction assembly and tissue barrier permeability defects caused by partially delocalizing β-actin monomer synthesis. Overexpressing E-cadherin in cells partially delocalizing β-actin monomer synthesis increased E-cadherin, β-actin and F-actin localization to *de novo* cell-cell contact sites. In a previous study, fluorescent speckle microscopy was used to detect labelled actin incorporation into actin filaments (Waterman-Storer et al., 1998). I speculate that eGFP β-actin monomers coming from the β-actin transcript lacking the zipcode were able to incorporate into actin filaments along with the endogenous β-actin containing the zipcode. Cells expressing endogenous levels of E-cadherin when β-actin monomer synthesis was partially delocalized presented with adherens junction assembly defects. Importantly, E-cadherin overexpression in these cells rescued epithelial adherens junction assembly and the tissue permeability barrier. In addition, there is a possibility that E-cadherin overexpression leads to an increase in RhoA and Src

signaling pathways at intercellular contacts in order to localize and release the translational repression of the endogenous β-actin transcript (Gutierrez et al., 2014; Latham et al., 2001; McLachlan and Yap, 2011; Rodriguez et al., 2006). Moreover, it should be noted that β-actin is present at intercellular contacts and in cytoplasmic stress fibers in small MDCK cell islets, whereas γ-actin is mainly localized to protrusive regions around islets (Dugina et al., 2009). Altogether, these studies suggest a role for E-cadherin in the coordinated regulation of signaling events required for β-actin monomer synthesis during adherens junction assembly.

To investigate the role of E-cadherin localized β-actin monomer synthesis during epithelial adherens junction assembly, I quantified the colocalization of E-cadherin and F-actin by measuring fluorescence signal using Pearson's correlation coefficient to calculate Fluorescence Covariance Index values (Vedula et al., 2016). The Fluorescence Covariance Index quantifies the colocalization of E-cadherin/F-actin at cell-cell contact with respect to the cytoplasm. As predicted, blocking E-cadherin homophilic binding (**Figure 19**) decreased adherens junction assembly evidenced by lower Fluorescence Covariance Index values (**Figure 15**). Interestingly, E-cadherin binding localizes the two most important signals required to localize β-actin monomer synthesis, RhoA and Src (Rodriguez et al., 2008). Active-RhoA localizes β-actin/ZBP1 mRNP complexes to the cell periphery in a myosin II dependent pathway (Latham et al., 2001). Then active-Src phosphorylates ZBP1 releasing the β-actin transcript to initiate translation (Hüttelmaier et al., 2005). Thus, overexpressing E-cadherin in cells partially delocalizing β-actin monomer synthesis stimulates sufficient RhoA and Src signal

activity at intercellular contacts to locally translate sufficient monomer from the endogenous zipcode-containing β-actin transcripts to fully drive filament polymerization and adherens junction complex anchoring (Gutierrez et al., 2014; Latham et al., 2001; McLachlan and Yap, 2011; Rodriguez et al., 2006).

In Chapter 2, I demonstrate the amount of cell-cell contact localized β-actin monomer synthesis correlates with both E-cadherin protein expression and homophilic binding activity (**Figure 17** and **Figure 19**). Consequently, cells with low E-cadherin protein expression or binding function delocalize β-actin monomer synthesis from cell-cell contact sites causing localized defects in polymerization of the linear actin filaments required for E-cadherin anchoring and formation of a functional tissue barrier. I note significant differences in the number of β-actin monomer synthesis sites on opposing sides of *de novo* epithelial intercellular contacts. Interestingly, the average difference in the number of β-actin monomer synthesis sites between contacting cells decreases when E-cadherin expression is reduced or when E-cadherin function is blocked (**Appendix 1 and 2**). Based on previous research studies mentioned above and the data presented here, it is tempting to propose the extent of linear actin filament assembly depends on the number of β-actin monomers being synthesized at opposing sides of *de novo* cell-cell contacts. As a result of the imbalance in β-actin monomer synthesis, tissues are able to equalize contractility on opposing sides of *de novo* contacts allowing for the maturation of adherens junction complex. Moreover, the increase in E-cadherin, β-actin monomer synthesis, and F-actin polymerization rescued the adherens junction assembly and barrier permeability defects in epithelial cells partially delocalizing β-actin monomer synthesis. Coupling our observations of E-

cadherin specifying β-actin monomer synthesis sites to the mechanosensitive receptor model produces a unified model where tension sensed through E-cadherin localizes molecular signals to localize β-actin monomer synthesis driving actin cytoskeleton remodeling required for adherens junction assembly. This model describes a novel pathway used by epithelial cells to regulate cell-cell adhesion in response to changes in tissue tension utilizing the mechanosensitive transmembrane receptor protein E-cadherin and mRNA zipcode mediated protein synthesis.

E-cadherin localizes β-actin monomer synthesis by localizing the translation initiation signal Src

After demonstrating E-cadherin localizes β-actin monomer synthesis to *de novo* cell-cell contacts, I investigated how this transmembrane receptor localizes protein synthesis. There is strong evidence demonstrating cadherins are important cellular signal transduction sites responsive to extracellular conditions (McLachlan and Yap, 2007). For instance, receptor tyrosine kinases and phosphatases are found at cell-cell adhesion sites in association with cadherin-catenin complexes. Importantly, it was shown E-cadherin recruits and activates receptor tyrosine phosphatases at cell-cell contact sites (McLachlan and Yap, 2007). Previous studies show E-cadherin activation of RPTPα is necessary for cell-cell contact localized Src signaling in MCF7 cells (McLachlan and Yap, 2011; Truffi et al., 2014). Importantly, chemically inhibiting Src signaling delocalizes β-actin monomer synthesis and inhibits *de novo* adherens junction formation in MDCK cells (Gutierrez et al., 2014) due to persistent ZBP1 binding to the β-actin mRNA zipcode which prevents translation (Chao et al., 2010). As mentioned before, when

the β-actin mRNA/ZBP1 complex reaches its destination, Src phosphorylates ZBP1 releasing the translational repression on the β-actin transcript to initiate monomer synthesis (Hüttelmaier et al., 2005). In Chapter 3, I demonstrate E-cadherin protein expression and homophilic binding are necessary to localize active Src to cell-cell contacts in MDCK tissues. The similar response profiles for localizing active Src and β-actin monomer synthesis to cell-cell contact sites in response to E-cadherin binding inhibition provides strong evidence supporting the model where E-cadherin binding localized Src to localize β-actin monomer synthesis.

E-cadherin localized β-actin monomer synthesis regulates epithelial tissue barrier permeability

Cell contacts are regularly formed, broken and rearranged during normal physiological processes and disease states. Adherens junctions have to be dynamic to allow for changes in cell-cell contact strength. One key mechanism to control adhesion strength is to regulate the amount of plasma membrane localized cadherin (Nanes and Kowalczk, 2012). E-cadherin clathrin-mediated endocytosis was first observed in MDCK cells, providing a mechanism to remove E-cadherin from the plasma membrane (Le et al., 1999; Nanes and Kowalczk, 2012). And blocking E-cadherin homophilic binding with E-cadherin function blocking antibodies stimulates E-cadherin clathrin-mediated endocytosis (Izumi et al., 2004). In Chapter 4, I presented data demonstrating when E-cadherin endocytosis is inhibited in MDCK cells that partially delocalize β-actin monomer synthesis, rescues adherens junction assembly defects following *de novo* epithelial cell-cell contact (**Figure 37**). Importantly, completely delocalizing β-actin monomer

synthesis prevents the endocytosis inhibition mediated rescue of adherens junction assembly (**Figure 38**). Based on these results, I hypothesize E-cadherin endocytosis and localized β-actin monomer synthesis are opposing parts of a common pathway, that is, blocking E-cadherin endocytosis in cells partially delocalizing β-actin monomer synthesis rescues adherens junction assembly, and completely delocalizing β-actin monomer synthesis abolishes the rescue of junction assembly by endocytosis inhibition. To further confirm this model, MDCK cells partially delocalizing β-actin monomer synthesis were subjected to calcium switch assays in the presence of both E-cadherin endocytosis and E-cadherin binding inhibitor. Simultaneously blocking E-cadherin endocytosis and E-cadherin binding, prevented cells transitioning from contact initiation to junction maturation stage of adherens junction assembly (**Figure 39**). This result further confirms E-cadherin is required to rescue adherens junction assembly in cells partially delocalizing β-actin monomer synthesis. Importantly, these results suggest actin mediated E-cadherin clustering at the cell surface and E-cadherin endocytosis during junction assembly balance each other. The actin cytoskeleton remodeling is driven, in part, by local increases in β-actin monomer concentration. As a result, localizing β-actin monomer synthesis to epithelial cell–cell contacts locally regulates the concentration of β-actin monomer to control actin filament polymerization (Condeelis and Singer, 2005; Gutierrez et al., 2014; Rodriguez et al., 2006). Previous studies showed knocking down β-actin expression by RNA interference or delocalizing its synthesis by mRNA zipcode masking in epithelial cells specifically impairs adherens junction assembly (Baranwal et al., 2012; Gutierrez et al., 2014; Kislauskis et al., 1994). Additionally, expressing β-actin

mRNA lacking its 3'UTR (Δ3'UTR), where the mRNA zipcode is located, impairs actin filament remodeling at the cell periphery reducing cadherin clustering at cell-cell contacts (Gutierrez et al., 2014; Lyubimova et al., 1999; Rodriguez et al., 2006). As a result, barrier integrity remains perturbed in cells partially delocalizing β-actin monomer synthesis following *de novo* cell-cell contact even with endocytosis inhibition.

Model of Adherens Junction complex assembly

Epithelial adherens junction assembly occurs in three stages: contact initiation, contact expansion and junction maturation (Adams et al., 1998; Kovacs et al., 2002; Baum and Georgiou, 2011). Contact initiation is characterized by E-cadherin puncta loosely holding contacting cells together (Gloushankova et al., 1997). Initial stable contact formation restrains retrograde actin flow resulting in local pooling of adhesion molecules that would normally be removed by the "actin current" (Krendel and Bonder, 1999). Concurrently, a circumferential actin cable is observed surrounding un-contacting single cells (Adams et al., 1998).

During contact expansion, E-cadherin binds to actin filaments and strengthens cell-cell interactions. In addition, E-cadherin homophilic binding activates Rac at the edges of the contact driving lamellar protrusions with surface exposed cadherin to promote contact expansion by lateral zipping (Kovacs et al., 2002). High α-catenin levels associated with E-cadherin adherens junction complexes at nascent cell-cell contacts suppresses Arp2/3-mediated actin polymerization inhibiting lamellar protrusion and stimulates actin filament bundling (Drees et al., 2005; Yamada et al., 2005). Cell-cell contact localized linear

actin bundles anchor cadherin-catenin complexes, and hence positively regulate adherens junction assembly (Gloushankova et al., 1997; Krendel and Bonder, 1999; Vasioukhin et al., 2000; Wu et al., 2015; Vedula et al., 2016). The formation of more structured actin bundles is due to the accumulation of cell adhesion molecules and actin filaments in the contact area. These actin bundles would then serve as precursors for the formation of circumferential bundles found in association with mature adherens junctions (Krendel and Bonder, 1999). Also, during the junction maturation stage, E-cadherin plaques present at the edges of the expanding contact coalesce to form multicellular vertices (Adams et al., 1998).

To add to the complexity of adherens junction formation and maintenance, endocytosis contributes significantly to assembling and maintaining adherens junction complexes at contacting plasma membranes (Troyanovsky et al., 2006). For example, endocytosis redistributes E-cadherin to mature junctions (de Beco et al., 2009). Unanchored surface-exposed E-cadherin is internalized by dynamin-mediated endocytosis from high Rac1 activity sites and is either recycled to the cell surface or degraded (Cavey et al., 2008; Harris and Tepass, 2010; Izumi et al., 2004). Thus, endocytosis recycles E-cadherin from mature junctions following trans dimer disassembly and during the initial phases of adherens junction assembly for rapid cadherin turnover (Hong et al., 2010).

The aim of this study was to identify new mechanisms underlying adherens junction assembly and maturation. A focus was on integrating and analyzing what was known previously about E-cadherin controlled key signaling events with new experimental knowledge. While much was known about the separate actions of E-

cadherin and cytoskeleton assembly, exact knowledge about the local regulation of the actin cytoskeleton from branched filaments to linear filaments controlled by E-cadherin had never been evaluated temporally using the same cell line under controlled conditions. Interestingly, I found a spatial correlation between the location of E-cadherin binding, active-Src and β-actin monomer synthesis at *de novo* cell-cell contact sites in the epithelial MDCK cell line. In summary, my work led me to create the following multi-phase model of spatial and temporal regulation of β-actin monomer synthesis during adherens junction assembly:

Contact Initiation Stage. When synchronized *de novo* cell-cell contact is initiated in tissues composed of MDCK cells (calcium switch), lamellipodia overlap between contacting cells is observed (**Figure 42: Contact Initiation**). The cells sense each other through E-cadherin homotypic interactions. The existing actin at these cell-cell contacts can anchor few adherens junction complexes to F-actin. Presumably, cells are trying to form initial contacts with the existing actin to localize β-actin mRNA/ZBP1 complexes by activating RhoA through E-cadherin. At this stage localized active Scr at cell-cell contacts is not required. To add to this model, Another study found initial contact between two adjacent lamellipodia from two different cells has no detectable myosin-II (Krendel and Bonder, 1999).

Contact expansion stage. More adherens junction complexes assemble throughout the contact zone. This drives actin filament remodeling, increased E-cadherin clustering, and continued adherens junction assembly at the cell surface (**Figure 42**). This continued adherens junction assembly is accompanied by modest increases in localized RhoA and Src at cell-cell contacts to initiate β-actin

monomer synthesis. Also, RhoA signaling is required to activate and localize F-actin polymerization factor proteins, such as mDia; and to initiate cytoskeletal contraction (**Figure 42: Contact Expansion;** Gutierrez et al., 2014).

Junction maturation stage. The assembly of adherens junction complexes significantly increases, with an increase in cell-cell contact localized RhoA (Gutierrez et al., 2014) and Src signaling, further driving cell-cell contact localized β-actin monomer synthesis (**Figure 42: Maturing Junction**) resulting in an increase in F-actin filament polymerization and actomyosin contractility. It was also observed that β-actin monomers are synthesized in different amounts on the opposing sides of the contacts (**Appendix 1 and 2**). Presumably, this equalizes force tension at the opposing sides of the contact; resulting in cells lifting and the subsequent establishment of apical and basal polarity and tissue permeability barrier.

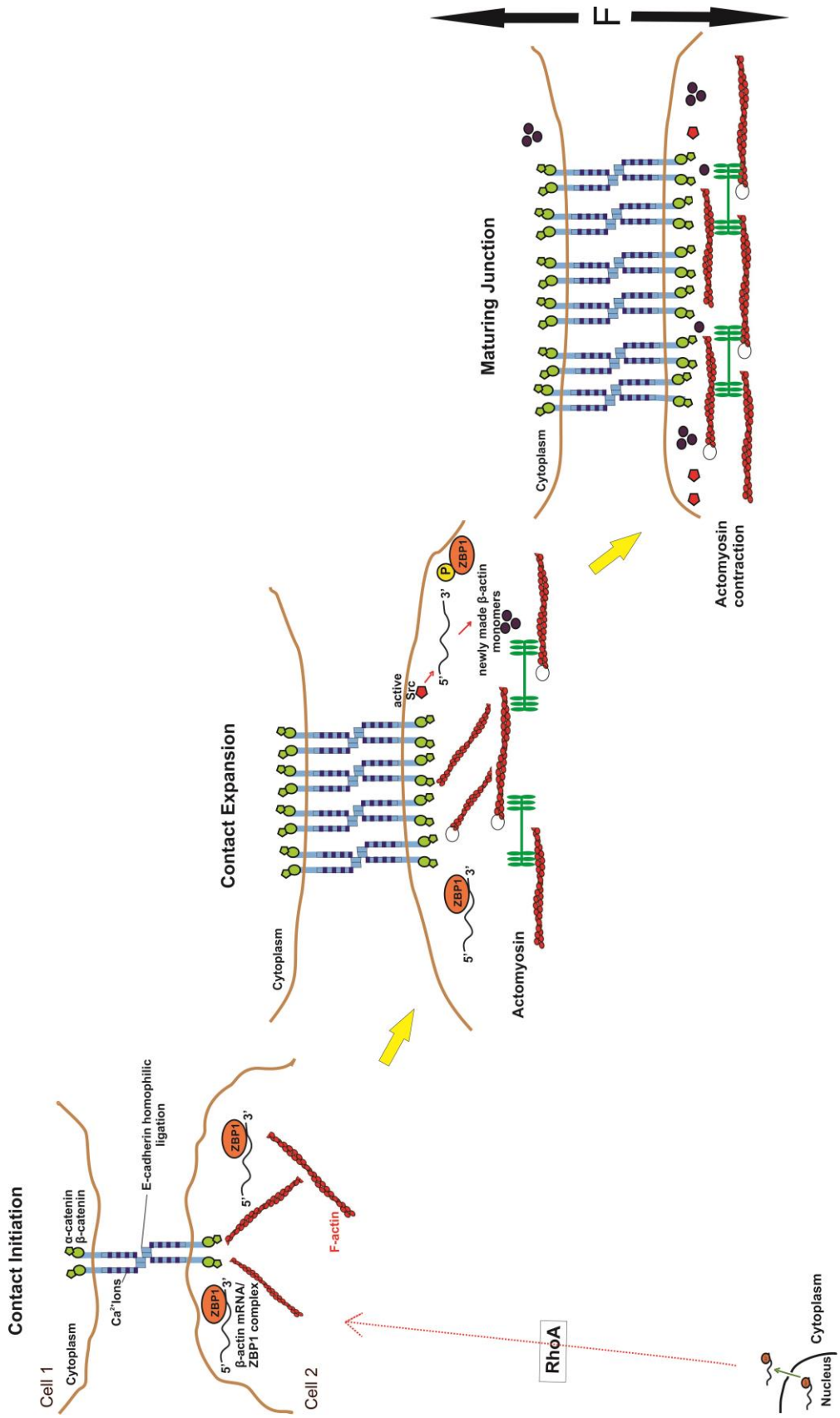
Contact Initiation
Cell 1
Cytoplasm
α-catenin
β-catenin
Ca2+ ions
E-cadherin homophilic ligation
ZBP1
3'
5'
β-actin mRNA/ ZBP1 complex
F-actin
Cell 2
Contact Expansion
Cytoplasm
active Src
P
newly made β-actin monomers
Actomyosin
Maturing Junction
Cytoplasm
Actomyosin contraction
F
RhoA
Cytoplasm
Nucleus

Figure 42: Model of adherens junction formation.

Schematic showing the three stages of *de novo* adherens junction assembly: contact initiation, contact expansion, and junction maturation. At nascent contacts, E-cadherin homophilic adhesion localizes RhoA activity at cell-cell contacts. E-cadherin clusters and increases its binding to other E-cadherin clusters on an opposite cell, leading to activation of localized RhoA and Src activity at *de novo* cell-cell contacts. Cells can form *de novo* adherens junction complexes by localizing E-cadherin mediated activation of RhoA and Src signals leading to β-actin monomer synthesis. The actomyosin network begins to organize in belt-like structures at cell-cell contacts. In addition, F-actin polymerization factors, such as mDIA (depicted as black circles near F-actin) presumably aids in the formation of filamentous actin using the newly synthesized β-actin monomers at cell-cell contacts. During junction maturation, the arrangement of epithelial cells at the apical domain is determined by E-cadherin homophilic binding and actomyosin contraction. For this to occur, the cells need to have equal force tension on opposing side of the contacts to lift and to eventually polarize.

Future Directions

Mechanisms of aberrant E-cadherin expression are still unclear. The loss of heterozygosity of 16q22 might be one of the steps for loss of tumor suppressive function of E-cadherin in addition with the presence of the mutated remaining allele. In the other hand, reduce dosage of the gene might result in reduced E-cadherin expression to a level below a critical threshold, which can be sufficient to impair E-cadherin functioning (Umbas et al., 1992). Presently this study can predict the number of contact localized translation sites when E-cadherin is perturbed during *de novo* cell-cell contact formation. In addition to studying E-cadherin mediated local β-actin translation, colocalization of junctional proteins and barrier integrity can be measured. For instance, previous studies in our laboratory had shown that E-cadherin overexpression in MDCK cells with partial delocalization of β-actin monomer synthesis rescues tissue barrier integrity and adherens junction assembly, (**Figure 4 and Figure 9**).

There is evidence that E-cadherin is under tension in steady state MDCK cells. Previous studies used an E-cadherin Tension Sensor Module construct (Borghi et al. 2012). When E-cadherin was under tension in MDCK cells the FRET index when down in control cells and in cells treated with cytochalasin B and ML-7 the FRET index partially increased (Borghi et al., 2012). In Chapter 2, I found that the number of β-actin monomer synthesis sites at opposing sides of cell-cell contact are different. I speculate during adherens junction assembly, cells try to have same tension on both sides of the contact by synthesizing locally different amounts β-actin protein monomers. When this process is disturbed, for instance

when E-cadherin function is inhibited, cells are not able to synthesize β-actin monomers to equalize tension on both sides of the contact. As a result, unequal tension on both sides of the contact prevents adherens junction maturation as the cells try to lift and polarize leading to breakage of newly formed cell-cell contacts. It would be interesting to use this E-cadherin sensor module construct and block E-cadherin function and see if this correlates with a decrease in tension during junction assembly.

Recent findings demonstrate local translation of β-actin and E-cadherin mRNAs mediated by ZBP1 influence actin dynamics and the formation of cell-cell adhesions (Wang et al., 2016). This could explain why similar effects are observed when E-cadherin function is perturbed (**Figure 15**) or when β-actin zipcode pathway is perturbed (**Figure 38**). Highly invasive breast adenocarcinoma cells present delocalized β-actin mRNA in comparison to non-metastatic medullary thyroid carcinoma cells (Shestakova et al., 1999). This finding confirms our results, pointing to the importance of β-actin monomer synthesis at the right time and place to make an organized and functional epithelial tissue. In another study, intestinal E-cadherin knockout mice present a severe body weight loss due to a compromise intestinal epithelial architecture (Schneider et al., 2010) similar when ZBP1 protein expression is reduced in mice pups (Hansen et al., 2004). It is interesting to note that while loss of E-cadherin in several studies has been shown not to induce EMT, it causes a significant disruption of the actin cytoskeleton (Chen et al., 2014) while ZBP1 has a metastatic suppression role (Nwokafor et al., 2016). Similar effects are observed when E-cadherin or ZBP-1 protein expression is downregulated can be an indication that these two molecules are in the same mechano-transduction

pathway, which is involved in adherens junction assembly. In the future, E-cadherin, β-actin and ZBP-1 protein and mRNA localization within cancer cells from epithelial origin could potentially serve as diagnostic markers for cancer aggressiveness.

Several studies have discussed the importance of signaling required for proper adherens junction assembly. For example, E-cadherin modulates RhoA and Src signaling at epithelial cell-cell contacts zones (Latham et al., 2001; Weber et al., 2011; McLachlan et al., 2007). This is required for local β-actin protein synthesis during adherens junction assembly (Gutierrez et al., 2014). Watanabe et al. (1999) came with a cooperation model in which Rho activates mDia1 to generate non-branching F-actin filament assembly. In parallel, RhoA activates ROCK which leads to Myosin phosphorylation and enhanced contractility. mDia1 and ROCK signaling pathways then work coordinately to form actin fibers of different thickness and densities (Watanabe et al., 1999). When mDia1 had a high activity or when its activity was decreased the integrity of cell-cell junctions was affected. In the other hand, moderate mDia1 activity resulted in intact adherens junctions (Carramusa et al., 2007). In addition, multiple myosin II isoforms accumulate at epithelial cell-cell junctions (Gomez et al., 2015). Moreover, myosin II isoforms have distinct roles during adherens junction assembly. Myosin IIA has a role in cadherin clustering, whereas myosin IIB has a role in increasing actin filament content and dynamics in MCF7 cell lines (Smutny et al., 2010). And both myosins, IIA and IIB, contribute to the generation of contractile tension at epithelial cell-cell contacts in MCF7 cell lines (Gomez et al., 2015). It would be interesting to test which myosin isoforms and actin polymerization factors contribute to E-

cadherin (e.g. formins such us mDia) clustering or/and the type of actin filaments being made in MDCK cells to have a more unified model of adherens junction assembly.

Bibliography

Acharya, B. R., Wu, S. K., Lieu, Z. Z., Parton, R. G., Grill, S. W., Bershadsky, A. D., Gomez, G. A and Yap, A. S. (2017). Mammalian Diaphanous 1 Mediates a Pathway for E-cadherin to Stabilize Epithelial Barriers through Junctional Contractility. *Cell Reports*, *18*(12), 2854–2867.

Adams, C. L., Chen, Y. T., Smith, S. J., and James Nelson, W. (1998). Mechanisms of Epithelial Cell–Cell Adhesion and Cell Compaction Revealed by High-resolution Tracking of E-Cadherin– Green Fluorescent Protein. *The Journal of Cell Biology*, *142*(4), 1105–1119.

Adams, S. R., Campbell, R. E., Gross, L. A., Martin, B. R., Walkup, G. K., Yao, Y., Llopis, J., and Tsien, R. Y. (2002). New biarsenical ligands and tetracysteine motifs for protein labeling in vitro and in vivo: Synthesis and biological applications. *Journal of the American Chemical Society*, *124*(21), 6063–6076.

Akhtar, N., and Hotchin, N. A. (2001). RAC1 regulates adherens junctions through endocytosis of E-cadherin. *Molecular Biology of the Cell*, *12*(4), 847–862.

Andreeva, A., Lee, J., Lohia, M., Wu, X., Macara, I. G., and Lu, X. (2014). PTK7-Src Signaling at Epithelial Cell Contacts Mediates Spatial Organization of Actomyosin and Planar Cell Polarity. *Developmental Cell*, *29*(1), 20–33.

Ayollo, D. V., Zhitnyak, I. Y., Vasiliev, J. M., and Gloushankova, N. A. (2009). Rearrangements of the Actin Cytoskeleton and E-Cadherin-Based Adherens Junctions Caused by Neoplasic Transformation Change Cell-Cell Interactions.

PLoS ONE, *4*(11).

Ballestrem, C., Wehrle-Haller, B., and Imhof, B. a. (1998). Actin dynamics in living mammalian cells. *Journal of Cell Science*, *111*, 1649–1658.

Baranwal, S., Naydenov, N. G., Harris, G., Dugina, V., Morgan, K. G., Chaponnier, C., and Ivanov, A. I. (2012). Nonredundant roles of cytoplasmic β- and γ-actin isoforms in regulation of epithelial apical junctions. *Molecular Biology of the Cell*, *23*(18), 3542–53.

Barlow, A. L., MacLeod, A., Noppen, S., Sanderson, J., and Guérin, C. J. (2010). Microscopy Microanalysis Colocalization Analysis in Fluorescence Micrographs : Verification of a More Accurate Calculation of Pearson ' s Correlation Coefficient. *Microscopy and Microanalysis*, *16*, 710–724.

Barry, A. K., Tabdili, H., Muhamed, I., Wu, J., Shashikanth, N., Gomez, G. A., Yap, A. S., Gottardi, C. J., de Rooij, J., Wang, N., and Leckband, D. E. (2014). α-Catenin cytomechanics-role in cadherin-dependent adhesion and mechanotransduction. *Journal of Cell Science*, *127*(8), 1779–1791.

Ben-Ari, Y., Brody, Y., Kinor, N., Mor, A., Tsukamoto, T., Spector, D. L., and Singer, R. H., and Shav-Tal, Y. (2010). The life of an mRNA in space and time. *Journal of Cell Science*, *123*(10), 1761–1774.

Biscardi, J. S., Belsches, A. P., and Parsons, S. J. (1998). Characterization of human epidermal growth factor receptor and c-Src interactions in human breast tumor cells. *Molecular Carcinogenesis*, *21*(4), 261–72.

Blanco, M. J., Moreno-Bueno, G., Sarrio, D., Locascio, A., Cano, A., Palacios, J.,

and Nieto, M. A. (2002). Correlation of Snail expression with histological grade and lymph node status in breast carcinomas. *Oncogene*, 21, 3241-3246 (Nature Publishing Group).

Bonder, E. M., Fishkind, D. J., and Mooseker, M. S. (1983). Direct Measurement of Critial Concentrations and Assembly Rate Constants at the two Ends of an Actin Filament. *Cell*, *34*, 491–501.

Borghi, N., Sorokina, M., Shcherbakova, O. G., Weis, W. I., Pruitt, B. L., James, W., and Dunn, A. R. (2012). Correction for Borghi et al., E-cadherin is under constitutive actomyosin-generated tension that is increased at cell-cell contacts upon externally applied stretch. *PNAS*, *109*(46), 19034–19034.

Braga, V. M. M., Machesky, L. M., Hall, A, and Hotchin, N. A. (1997). The Small GTPases Rho and Rac are required for the Establishment of Cadherin-dependent Cell-Cell Contacts (1997). *The Journal of Cell Biology*, *137*(6), 1421–31.

Brouxhon, S. M., Kyrkanides, S., Teng, X., Raja, V., O'Banion, M. K., Clarke, R., Byers, S., Silberfeld, A., Tornos, C,m and Ma, L. (2013). Monoclonal antibody against the ectodomain of E-cadherin (DECMA-1) suppresses breast carcinogenesis: Involvement of the HER/PI3K/Akt/mTOR and IAP pathways. *Clinical Cancer Research*, *19*(12), 3234–3246.

Brummelkamp, T. R., Bernards, R., and Agami, R. (2002). A System for Stable Expression of Short Interfering RNAs in Mammalian Cells. *Science (New York, NY)*, *296*(5567), 550–553.

Cairns, J. (1975). Mutation selection and the natural history of cancer. *Nature*, *255*, 197-200.

Cano, A., Pérez-Moreno, M. A., Rodrigo, I., Locascio, A., Blanco, M. J., del Barrio, M. G., Portillo, F., and Nieto, M. A. (2000). The transcription factor Snail controls epithelial–mesenchymal transitions by repressing E-cadherin expression. *Nature Cell Biology*, *2*(2), 76–83.

Carramusa, L., Ballestrem, C., Zilberman, Y., and Bershadsky, A. D. (2007). Mammalian diaphanous-related formin Dia1 controls the organization of E-cadherin-mediated cell-cell junctions. *Journal of Cell Science*, *120*(21), 3870–3882.

Cavey, M., Rauzi, M., Lenne, P., and Lecuit, T. (2008). A two-tiered mechanism for stabilization and immobilization of E-cadherin. *Nature*, *453*(7196), 751–756.

Chao, J. A., Patskovsky, Y., Patel, V., Levy, M., Almo, S. C., and Singer, R. H. (2010). ZBP1 recognition of β-actin zipcode induces RNA looping. *Genes and Development*, *24*(2), 148–158.

Chen, A., Beetham, H., Black, M. A., Priya, R., Telford, B. J., Guest, J., Wiggins, G. A. A., Godwin, T. D., Alpha, S. Y., and Guilford, P. J. (2014). E-cadherin loss alters cytoskeletal organization and adhesion in non-malignant breast cells but is insufficient to induce an epithelial-mesenchymal transition. *BMC Cancer*, *14*(1), 552.

Chen, C., and Chen, H. (2009). Functional suppression of E-cadherin by protein kinase Cδ. *Journal of Cell Science*, *122*, 513–523.

Collins, C., Denisin, A. K., Pruitt, B. L., and Nelson, W. J. (2017). Changes in E-cadherin rigidity sensing regulate cell adhesion. *PNAS*, *114*(29), E5835–E5844.

Condeelis, J., and Singer, R. H. (2005). How and why does beta-actin mRNA target? *Biology of the Cell, 97*(1), 97–110.

Costes, S. V, Daelemans, D., Cho, E. H., Dobbin, Z., Pavlakis, G., and Lockett, S. (2004). Automatic and quantitative measurement of protein-protein colocalization in live cells. *Biophysical Journal*, *86*(6), 3993–4003.

Cruz, L. A., Vedula, P., Gutierrez, N., Shah, N., Rodriguez, S., Ayee, B., Davis, J., and Rodriguez, A. J. (2015). Balancing Spatially Regulated β-actin Translation and Dynamin-Mediated Endocytosis is Required to Assemble Functional Epithelial Monolayers. *Cytoskeleton*, *72*(12), 597–608.

Curtis, M. W., Johnson, K. R., and Wheelock, M. J. (2008). E-Cadherin/Catenin Complexes Are Formed Cotranslationally in the Endoplasmic Reticulum/Golgi Compartments. *Cell Communication and Adhesion*, *15*(4), 365–78.

Davidson, E. H. (1971). Note on the control of gene expression during development. *J. Theor. Bio.l*, *32*(1), 123–130.

de Beco, S., Gueudry, C., Amblard, F., and Coscoy, S. (2009). Endocytosis is required for E-cadherin redistribution at mature adherens junctions. *PNAS*, *106*(17), 7010–7015.

Desai, R., Sarpal, R., Ishiyama, N., Pellikka, M., Ikura, M., and Tepass, U. (2013). Monomeric α-catenin links cadherin to the actin cytoskeleton. *Nature Cell*

Biology, *15*(3), 261–73.

Drees, F., Pokutta, S., Yamada, S., Nelson, W. J., and Weis, W. I. (2005). α-Catenin Is a Molecular Switch that Binds E-Cadherin-β-Catenin and Regulates Actin-Filament Assembly. *Cell*, *123*(5), 903–915.

Dugina, V., Zwaenepoel, I., Gabbiani, G., Clément, S., and Chaponnier, C. (2009). Beta and gamma-cytoplasmic actins display distinct distribution and functional diversity. *Journal of Cell Science*, *122*(Pt 16), 2980–2988.

Dukes, J. D., Whitley, P., and Chalmers, A. D. (2011). The MDCK variety pack: Choosing the right strain. *BMC Cell Biology*, *12*, 2–5.

Farina, K. L., Hüttelmaier, S., Musunuru, K., Darnell, R., and Singer, R. H. (2003). Two ZBP1 KH domains facilitate β-actin mRNA localization, granule formation, and cytoskeletal attachment. *Journal of Cell Biology*, *160*(1), 77–87.

Fingleton, B., Lynch, C. C., Vargo-Gogola, T., and Matrisian, L. M. (2010). Cleavage of E-cadherin by matrix Metalloproteinase-7 Promotes Cellular Proliferation in Nontransformed Cell Lines via Activation of RhoA. *Journal of Oncology*, *2010*, 1-11.

Gloushankova, N. A., Alieva, N. A., Krendel, M. F., Bonder, E. M., Feder, H. H., Vasiliev, J. M., and Gelfand, I. M. (1997). Cell-cell contact changes the dynamics of lamellar activity in nontransformed epitheliocytes but not in their ras-transformed descendants. *PNAS*, *94*(3), 879–83.

Gomez, G. A., McLachlan, R. W., Wu, S. K., Caldwell, B. J., Moussa, E., Verma, S., Bastiani, M., Priya, R., Parton, R. G., Gaus, K., Sap, J and Yap, A. S.

(2015). An RPTPα/Src Family Kinase /Rap1 signaling module recruits Myosin IIB to support contractile tension at apical E-cadherin junctions. *Molecular Biology of the Cell*, *26*, 1249-1262

Gooding, J. M., Yap, K. L., and Ikura, M. (2004). The cadherin-catenin complex as a focal point of cell adhesion and signalling: New insights from three-dimensional structures. *BioEssays*, *26*(5), 497–511.

Grieve, A. G., and Rabouille, C. (2014). Extracellular cleavage of E-cadherin promotes epithelial cell extrusion. *Journal of Cell Science*, *127*, 3331–3346.

Gu, W., Katz, Z., Wu, B., Park, H. Y., Li, D., Lin, S., Wells, A. L., and Singer, R. H. (2012). Regulation of local expression of cell adhesion and motility-related mRNAs in breast cancer cells by IMP1/ZBP1. *Journal of Cell Science*, *125*(1), 81–91.

Gutierrez, N., Eromobor, I., Petrie, R. J., Vedula, P., Cruz, L., and Rodriguez, A. J. (2014). The β-actin mRNA zipcode regulates epithelial adherens junction assembly but not maintenance. *RNA*, *20*(5), 689–701.

Halbleib, J. M., and Nelson, W. J. (2006). Cadherins in development: Cell adhesion, sorting, and tissue morphogenesis. *Genes and Development*, *20*(23), 3199–3214.

Hamilton, K. E., Chatterji, P., Lundsmith, E. T., Andres, S. F., Giroux, V., Hicks, P. D., Noubissi, F. K., Spiegelman, V. S., and Rustgi, A. K. (2015). Loss of Stromal Imp1 Promotes a Tumorigenic Microenvironment in the Colon. *Molecular Cancer Research*, *13*(November), 1478–1487.

Hansen, T. V. O., Hammer, N. A., Nielsen, J., Madsen, M., Dalbaeck, C., Wewer, U. M., Christiansen, J., and Nielsen, F. C. (2004). Dwarfism and Impaired Gut Development in Insulin-Like Growth Factor II mRNA-Binding Protein 1-Deficient Mice. *Molecular and Cellular Biology*, *24*(10), 4448–4464.

Harris, A. R., Daeden, A., and Charras, G. T. (2014). Formation of adherens junctions leads to the emergence of a tissue-level tension in epithelial monolayers. *Journal of Cell Science*, 2507–2517.

Harris, T. J., and Tepass, U. (2010). Adherens junctions: from molecules to morphogenesis. *Nat. Rev. Mol. Cell Biol.*, *11*(7), 502–514.

Hong, S., Troyanovsky, R. B., and Troyanovsky, S. M. (2010). Spontaneous assembly and active disassembly balance adherens junction homeostasis. *PNAS*, *107*(8), 3528–33.

Hong, S., Troyanovsky, R. B., and Troyanovsky, S. M. (2013). Binding to F-actin guides cadherin cluster assembly, stability, and movement. *Journal of Cell Biology*, *201*(1), 131–143.

Hu, Y., Lu, S., Szeto, K. W., Sun, J., Wang, Y., Lasheras, J. C., and Chien, S. (2014). FAK and paxillin dynamics at focal adhesions in the protrusions of migrating cells. *Scientific Reports*, *4*, 6024.

Hüttelmaier, S., Zenklusen, D., Lederer, M., Dictenberg, J., Lorenz, M., Meng, X., Bassell, G. J., Condeelis, J., and Singer, R. H. (2005). Spatial regulation of β-actin translation by Src-dependent phosphorylation of ZBP1. *Nature*, *438*(November), 512–515.

Izumi, G., Sakisaka, T., Baba, T., Tanaka, S., Morimoto, K., and Takai, Y. (2004). Endocytosis of E-cadherin regulated by Rac and Cdc42 small G proteins through IQGAP1 and actin filaments. *Journal of Cell Biology*, *166*(2), 237–248.

Jeffery, W. R., Tomlinson, C. R., and Brodeur, R. D. (1983). Localization of actin messenger RNA during early ascidian development. *Developmental Biology*, *99*(2), 408–417.

Kametani, Y., and Takeichi, M. (2007). Basal-to-apical cadherin flow at cell junctions. *Nature Cell Biology*, *9*(1), 92–8.

Kislauskis, E. H., Zhu, X., and Singer, R. H. (1994). Sequences Responsible for Intracellular Localization of β-Actin Messenger RNA Also Affect Cell Phenotype. *The Journal of Cell Biology*, *127*(2), 441–51.

Kobielak, A., Pasolli, H. A., and Fuchs, E. (2004). Mammalian formin-1 participates in adherens junctions and polymerization of linear actin cables. *Nature Cell Biology*, *6*(1), 21–30.

Koch, A. W., Farooq, A., Shan, W., Zeng, L., Colman, D. R., and Zhou, M. M. (2004). Structure of the neural (N-) cadherin prodomain reveals a cadherin extracellular domain-like fold without adhesive characteristics. *Structure*, *12*(5), 793–805.

Korpal, M., Lee, E. S., Hu, G., and Kang, Y. (2008). The miR-200 family inhibits epithelial-mesenchymal transition and cancer cell migration by direct targeting of E-cadherin transcriptional repressors ZEB1 and ZEB2. *Journal of Biological Chemistry*, *283*(22), 14910–14914.

Kovacs, E. M., Ali, R. G., McCormack, A. J., and Yap, A. S. (2002). E-cadherin homophilic ligation directly signals through Rac and phosphatidylinositol 3-kinase to regulate adhesive contacts. *Journal of Biological Chemistry*, *277*(8), 6708–6718.

Kovacs, E. M., Goodwin, M., Ali, R. G., Paterson, A. D., and Yap, A. S. (2002). Cadherin-directed actin assembly: E-cadherin physically associates with the Arp2/3 complex to direct actin assembly in nascent adhesive contacts. *Current Biology*, *12*(5), 379–382.

Krendel, M. F., and Bonder, E. M. (1999). Analysis of actin filament bundle dynamics during contact formation in live epithelial cells. *Cell Motility and the Cytoskeleton*, *43*(4), 296–309.

Ladoux, B., Anon, E., Lambert, M., Rabodzey, A., Hersen, P., Buguin, A., Silberzan, P., and Mège, R. M. (2010). Strength Dependence of Cadherin-Mediated Adhesions. *Biophysical Journal*, *98*(4), 534–542.

Latham, V. M., Yu, E. H. S., Tullio, A. N., Adelstein, R. S., and Singer, R. H. (2001). A Rho-dependent signaling pathway operating through myosin localizes β-actin mRNA in fibroblasts. *Current Biology*, *11*(13), 1010–1016.

Lawrence, J. B., and Singer, R. H. (1986). Intracellular localization of messenger RNAs for cytoskeletal proteins. *Cell*, *45*(3), 407–15.

Le, T. L., Yap, A. S., and Stow, J. L. (1999). Recycling of E-cadherin: A potential mechanism for regulating cadherin dynamics. *Journal of Cell Biology*, *146*(1), 219–232.

Le Duc, Q., Shi, Q., Blonk, I., Sonnenberg, A., Wang, N., Leckband, D., and De Rooij, J. (2010). Vinculin potentiates E-cadherin mechanosensing and is recruited to actin-anchored sites within adherens junctions in a myosin II-dependent manner. *Journal of Cell Biology*, *189*(7), 1107–1115.

Leckband, D. E., and de Rooij, J. (2014). Cadherin Adhesion and Mechanotransduction. *Annual Review of Cell and Developmental Biology*, *30*(1), 291–315.

Liu, Z., Tan, J. L., Cohen, D. M., Yang, M. T., Sniadecki, N. J., Ruiz, S. A., Nelson, C. M., and Chen, C. S. (2010). Mechanical tugging force regulates the size of cell-cell junctions. *PNAS*, *107*(22), 9944–9949.

Lombaerts, M., van Wezel, T., Philippo, K., Dierssen, J. W. F., Zimmerman, R. M. E., Oosting, J., van Eijk, R., Eilers, P. H., van de Water, B., Cornelisse, C. J., and Cleton-Jansen, A-M. (2006). E-cadherin transcriptional downregulation by promoter methylation but not mutation is related to epithelial-to-mesenchymal transition in breast cancer cell lines. *British Journal of Cancer*, *94*, 661–671.

Lyubimova, A., Bershadsky, A. D., and Ben-Zeev, A. (1999). Autoregulation of Actin Synthesis Requires the 3’-UTR of Actin mRNA and Protects Cells from Actin Overproduction. *Journal of Cellular Biochemistry*, *76*, 1–12.

Macia, E., Ehrlich, M., Massol, R., Boucrot, E., Brunner, C., and Kirchhausen, T. (2006). Dynasore, a Cell-Permeable Inhibitor of Dynamin. *Developmental Cell*, *10*(6), 839–850.

Madani, F., Lind, J., Damberg, P., Adams, S. R., Tsien, R. Y., and Gra, A. O.

(2009). Hairpin Structure of a Biarsenical - Tetracysteine Motif Determined by NMR Spectroscopy. *J. AM. CHEM. SOC, 131,* 4613–4615.

Maretzky, T., Reiss, K., Ludwig, A., Buchholz, J., Scholz, F., Proksch, E., de Strooper, B., Hartmann, D., and Saftig, P. (2005). ADAM10 mediates E-cadherin shedding and regulates epithelial cell-cell adhesion, migration, and beta-catenin translocation. *PNAS*, *102*(26), 9182–9187.

Marjoram, R. J., Lessey, E. C., and Burridge, K. (2014). Regulation of RhoA Activity by Adhesion Molecules and Mechanotransduction. *Current Molecular Medicine*, *14*(2), 199–208.

Mccluskey, A., Daniel, J. A., Hadzic, G., Chau, N., Clayton, E. L., Mariana, A., Whiting, A., Gorgani, N. N., Lloyd, J., Quan, A., Moshkanbaryans, L., Krishnan, S., Perera, S., Chircop, M., von Kleist, L., Mcgeachie, A. B., Howes, M. T., Parton, R. G., Campbell, M., Sakoff, J. A., Wang, X., Sun, J. Y., Robertson, M J., Deane, F. M., Nguyen, T. H., Meunier, F. A., Cousin, M. A., Robinson, P. J. (2013). Building a better dynasore: The dyngo compounds potently inhibit dynamin and endocytosis. *Traffic*, *14*, 1272–1289.

McLachlan, R. W., Kraemer, A., Helwani, F. M., Kovacs, E. M., and Yap, A. S. (2007). E-cadherin Adhesion Activates c-Src Signaling at Cell-Cell contacts. *Molecular Biology of the Cell*, 18, 3214-3223.

McLachlan, R. W., and Yap, A. S. (2007). Not so simple: The complexity of phosphotyrosine signaling at cadherin adhesive contacts. *Journal of Molecular Medicine*, *85*(6), 545–554.

McLachlan, R. W., and Yap, A. S. (2011). Protein tyrosine phosphatase activity is necessary for E-cadherin-activated Src signaling. *Cytoskeleton*, *68*(1), 32–43.

Nagafuchi, A. (2001). Molecular architecture of adherens junctions. *Current Opinion in Cell Biology*, *13*(5), 600–603.

Nichols, S. A., Roberts, B. W., Richter, D. J., Fairclough, S. R., and King, N. (2012). Origin of metazoan cadherin diversity and the antiquity of the classical cadherin/β-catenin complex. *PNAS*, *109*(32), 13046–51.

Niessen, C. M., Leckband, D., and Yap, A. S. (2011). Tissue organization by cadherin adhesion molecules: dynamic molecular and cellular mechanisms of morphogenetic regulation. *Physiological Reviews*, *91*(2), 691–731.

Nwokafor, C. U., Sellers, R. S., and Singer, R. H. (2016). IMP1 , an mRNA binding protein that reduces the metastatic potential of breast cancer in a mouse model, *7*(45), 1–10.

Oleynikov, Y., and Singer, R. H. (2003). Real-time visualization of ZBP1 association with β-actin mRNA during transcription and localization. *Current Biology*, *13*(3), 199–207.

Ozawa, M. (2002). Lateral dimerization of the E-cadherin extracellular domain is necessary but not sufficient for adhesive activity. *Journal of Biological Chemistry*, *277*(22), 19600–19608.

Ozawa, M., Ringwald, M., and Kemler, R. (1990). Uvomorulin-catenin complex formation is regulated by a specific domain in the cytoplasmic region of the cell adhesion molecule. *PNAS*, *87*(11), 4246–50.

Papusheva, E., and Heisenberg, C.-P. (2010). Spatial organization of adhesion: force-dependent regulation and function in tissue morphogenesis. *The EMBO Journal*, *29*(16), 2753–68.

Pinho, S. S., Seruca, R., Gärtner, F., Yamaguchi, Y., Gu, J., Taniguchi, N., and Reis, C. A. (2011). Modulation of E-cadherin function and dysfunction by N-glycosylation. *Cellular and Molecular Life Sciences*, *68*(6), 1011–1020.

Priya, R., Gomez, G. A., Budnar, S., Verma, S., Cox, H. L., Hamilton, N. A., and Yap, A. S. (2015). Feedback regulation through myosin II confers robustness on RhoA signalling at E-cadherin junctions. *Nature Cell Biology*, *17*(10), 1282–1293.

Rodriguez, A. J., Czaplinski, K., Condeelis, J. S., and Singer, R. H. (2008). Mechanisms and cellular roles of local protein synthesis in mammalian cells. *Journal Of Cell Biology*, *20*(2), 144–149.

Rodriguez, A. J., Shenoy, S. M., Singer, R. H., and Condeelis, J. (2006). Visualization of mRNA translation in living cells. *Journal of Cell Biology*, *175*(1), 67–76.

Roskoski, R. (2004). Src protein-tyrosine kinase structure and regulation. *Biochemical and Biophysical Research Communications*, *324*(4), 1155–1164.

Roskoski, R. (2015). Src protein-tyrosine kinase structure, mechanism, and small molecule inhibitors. *Pharmacological Research*, *94*, 9–25.

Ross, A. F., Oleynikov, Y., Kislauskis, E. H., Taneja, K. L., and Singer, R. H. (1997). Characterization of a β-Actin mRNA Zipcode-Binding Protein, *17*(4),

2158–2165.

Saleh, T., Jankowski, W., Sriram, G., Rossi, P., Shah, S., Lee, K., Cruz L. A., Rodriguez, A. J., Birge, R. B., and Kalodimos, C. G. (2015). Cyclophilin A promotes cell migration via the Abl-Crk signaling pathway. *Nature Chemical Biology*, 12(December), 117–123.

Schneider, M. R., Dahlhoff, M., Horst, D., Hirschi, B., Trülzsch, K., Müller-Höcker, J., Vogelmann, R., Allgäuer, M., Gerhard, M., Steininger, S., Wolf, E., and Kolligs, F. T. (2010). A key role for E-cadherin in intestinal homeostasis and paneth cell maturation. *PLoS ONE*, *5*(12), e14325.

Shestakova, E. A., Singer, R. H., and Condeelis, J. (2001). The physiological significance of β-actin mRNA localization in determining cell polarity and directional motility. *PNAS*, *98*(13), 7045–50.

Shestakova, E. a, Wyckoff, J., Jones, J., Singer, R. H., and Condeelis, J. (1999). Correlation of β-actin Messenger RNA Localization with Metastatic Potential in Rat Adenocarcinoma Cell Lines. *Cancer Research*, *59*(6), 1202–1205.

Shewan, A. M., Maddugoda, M., Kraemer, A., Stehbens, S, J., Verma, S., Kovacs, E, M., and Yap, A, S. (2005). Myosin 2 Is a Key Rho Kinase Target Necessary for the Local Concentration of E-cadherin at Cell-Cell Contacts. *Molecular Biology of the Cell*, *16*, 4531–4542.

Smutny, M., Cox, H. L., Leerberg, J. M., Kovacs, E. M., Conti, M. A., Ferguson, C., Hamilton, N. A., Parton, R. G., Adelstein, R. S., and Yap, A. S. (2010). Myosin II isoforms identify distinct functional modules that support integrity of the

epithelial zonula adherens. *Nature Cell Biology*, *12*(7), 696–702.

Sundell, C. L., and Singer, R. H. (1991). Requirement of Microfilaments in Sorting of Acting Messenger RNA. *Science*, *253*(5025), 1275–1277.

Takeichi, M. (2014). Dynamic contacts: rearranging adherens junctions to drive epithelial remodelling. *Nature Reviews Molecular Cell Biology*, *15*(6), 397–410.

Thiery, J. P. (2003). Epithelial-Mesenchymal Transitions in Development and Pathologies. *Curr Opin Cell Biol*, *15*(5), 740–746.

Truffi, M., Dubreuil, V., Liang, X., Vacaresse, N., Nigon, F., Han, S. P., Yap, A. S., Gomez, G. A., and Sap, J. (2014). RPTP controls epithelial adherens junctions, linking E-cadherin engagement to c-Src-mediated phosphorylation of cortactin. *Journal of Cell Science*, *127*(11), 2420–2432.

Umbas, R., Schalken, J. a, Aalders, T. W., Carter, B. S., Karthaus, H. F. M., Schaafsma, H. E., Debruyne, F. M. J., and Isaacs, W. B. (1992). Expression of the Cellular Adhesion Molecular E-cadherin Is Reduced or Absent in High-Grade Prostate Cancer. *Cancer Research*, *52*, 5104–5109.

Van Roy, F., and Berx, G. (2008). The cell-cell adhesion molecule E-cadherin. *Cellular and Molecular Life Sciences*, *65*(23), 3756–3788.

Vedula, P., Cruz, L. A., Gutierrez, N., Davis, J., Ayee, B., Abramczyk, R., and Rodriguez, A. J. (2016). Quantifying cadherin mechanotransduction machinery assembly/disassembly dynamics using fluorescence covariance analysis. *Scientific Reports*, *6*(October 2015), 28822.

Vestweber, D., and Kemler, R. (1985). Identification of a putative cell adhesion domain of uvomorulin. *The EMBO Journal*, *4*(13A), 3393–3398.

Volberg, T., Geiger, B., Kartenbeck, J., and Franke, W. W. (1986). Changes in membranes-microfilament interaction in intercellular adherens junctions upon removal of extracelular ca++ ions. *J. Cell Biol.*, *102*(May), 1832–1842.

Wang, G., Huang, Z., Liu, X., Huang, W., Chen, S., Zhou, Y., Li, D., Singer, R. H., and Gu, W. (2016). IMP1 suppresses breast tumor growth and metastasis through the regulation of its target mRNAs. *Oncotarget*, *7*(13), 15690-15702.

Watanabe, N., Kato, T., Fujita, A., Ishizaki, T., and Narumiya, S. (1999). Cooperation between mDia1 and ROCK in Rho-induced actin reorganization. *Nature Cell Biology*, *1*(3), 136–143.

Waterman-Storer, C. M., Desai, A., Bulinski, J. C., and Salmon, E. D. (1998). Fluorescent speckle microscopy, a method to visualize the dynamics of protein assemblies in living cells. *Current Biology, 8*(22), 1227–1230.

Weber, G. F., Bjerke, M. A., and DeSimone, D. W. (2011). Integrins and cadherins join forces to form adhesive networks. *Journal of Cell Science*, *124*(8), 1183–1193.

Wu, Y., Kanchanawong, P., and Zaidel-Bar, R. (2015). Actin-Delimited Adhesion-Independent Clustering of E-Cadherin Forms the Nanoscale Building Blocks of Adherens Junctions. *Developmental Cell*, *32*(2), 139–154.

Xu, W., Harrison, S. C., and Eck, M. J. (1997). Three-dimensional structure of the tyrosine kinase c-Src. *Nature*, *385*(February), 595–602.

Yamada, S., and Nelson, W. J. (2007). Localized zones of Rho and Rac activities drive initiation and expansion of epithelial cell-cell adhesion. *Journal of Cell Biology*, *178*(3), 517–527.

Yamada, S., Pokutta, S., Drees, F., Weis, W. I., and Nelson, W. J. (2005). Deconstructing the cadherin-catenin-actin complex. *Cell*, *123*(5), 889–901.

Yonemura, S., Wada, Y., Watanabe, T., Nagafuchi, A., and Shibata, M. (2010). alpha-Catenin as a tension transducer that induces adherens junction development. *Nature Cell Biology*, *12*(6), 533–42.

Zhang, J., Betson, M., Erasmus, J., Zeikos, K., Bailly, M., Cramer, L. P., and Braga, V. M. M. (2005). Actin at cell-cell junctions is composed of two dynamic and functional populations. *Journal of Cell Science*, *118*, 5549–5562.

Zinchuk, V., Wu, Y., and Grossenbacher-Zinchuk, O. (2013). Bridging the gap between qualitative and quantitative colocalization results in fluorescence microscopy studies. *Scientific Reports*, *3*, 1365.

Appendix 1: Difference in # of β-actin monomer synthesis sites between cell pairs 3 hours post-contact when E-cadherin is knockdown

	CONTROL		~70% Remaining E-cadherin protein expression		~50% Remaining E-cadherin protein expression		~30% Remaining E-cadherin protein expression	
Cell pair#	Cell 1	Cell 2	Cell 1	Cell 2	Cell 1	Cell 2	Cell 1	Cell 2
1	62	3	166	40	0	0	38	0
2	26	20	147	42	34	8	54	21
3	22	1	0	0	0	0	7	2
4	72	8	7	0	3	0	5	0
5	76	5	4	0	0	0	27	21
6	82	26	6	0	0	0	5	0
7	41	6	0	0	12	2	10	0
8	31	1	6	0	13	0	0	0
9	40	34	3	0	52	0	0	0
10	3	0	36	22	21	6	18	0

	Difference in # of β-actin monomer synthesis sites between cell pairs			
Cell pair#	CONTROL	~70% Remaining E-cadherin protein expression	~50% Remaining E-cadherin protein expression	~30% Remaining E-cadherin protein expression
1	59	126	0	38
2	6	105	26	33
3	21	0	0	5
4	64	7	3	5
5	71	4	0	6
6	56	6	0	5
7	35	0	10	10
8	30	6	13	0
9	6	3	52	0
10	3	14	15	18
AVERAGE	**35**	**27**	**12**	**12**

Appendix 2: Difference in # of β-actin monomer synthesis sites between cell pairs 3 hours post-contact in the presence of E-cadherin function blocking antibodies (DECMA-1)

	CONTROL		DECMA-1 (50 ug/ml)		DECMA-1 (100 ug/ml)		DECMA-1 (200 ug/ml)	
Cell pair#	Cell 1	Cell 2	Cell 1	Cell 2	Cell 1	Cell 2	Cell 1	Cell 2
1	16	0	12	0	0	0	18	16
2	61	24	19	9	22	0	15	4
3	24	7	39	15	0	0	10	0
4	20	4	38	27	0	0	5	2
5	13	0	48	47	0	0	10	0
6	0	0	0	0	0	0	12	4
7	3	2	38	13	6	0	8	2
8	24	0	40	26	17	3	12	2
9	11	0	1	0	0	0	7	2
10	5	2	0	0	0	0	15	15
11	27	17	0	0	0	0	0	0
12	57	8	0	0	0	0	3	0
13	11	8	5	1	142	80	28	14
14	3	0	18	0	21	0	1	0
15	0	0	4	0	1	0	16	2
16	0	0	0	0	13	0	12	1
17	9	0	0	0	1	0	1	0
18	3	0	0	0	0	0	6	0
19	15	0	18	13	0	0	4	0
20	14	0	133	25	0	0	0	0
21	17	0	0	0	3	0	0	0
22	17	16	0	0	1	0	10	0
23	32	0	0	0	1	0	14	3
24	16	11	0	0	84	3	5	0
25	55	2	0	0	0	0	5	2
26	4	4	0	0	32	0	0	0
27	42	9	0	0	42	13	18	0
28	57	30	0	0	37	0	30	5
29	119	47	36	0	26	0	0	0
30	47	11	25	0	22	0	68	21
31	49	0	3	0	84	48	0	0
32	15	0	46	0	0	0	0	0
33	6	4	4	3	12	6	0	0
34	14	0	70	23	0	0	0	0
35	9	0	14	0	35	23	0	0
36	9	0	39	29	17	0	5	0
37	15	3	29	0	0	0	14	0
38	0	0	0	0	0	0	0	0
39	7	1	0	0	0	0	0	0
40	23	12	16	0	0	0	0	0
41	16	12	0	0	0	0	0	0
42	34	1	64	4	0	0	17	0
43	8	0	42	3	20	17	0	0
44	7	6	0	0	0	0	5	0
45	43	0	79	32	0	0	0	0
46	4	4	73	52	32	0	0	0
47	42	9	28	15	42	13	18	0
48	57	30	0	0	37	0	30	5
49	119	47	0	0	26	0	0	0
50	47	11	36	0	22	0	68	21
51	49	0	0	0	16	3	0	0
52	15	0	0	0	3	0	0	0
53	6	4	0	0	12	6	0	0
54	14	0	48	16	0	0	0	0
55	9	0	0	0	35	23	0	0
56	9	0	8	0	17	0	5	0
57	15	3	0	0	0	0	14	0
58	0	0	0	0	103	76	0	0
59	7	1	0	0	0	0	0	0
60	23	12	163	119	0	0	0	0
61	16	12	0	0	0	0	0	0
62	34	1	0	0	0	0	17	0
63	8	0	0	0	20	17	0	0
64	7	6	35	0	0	0	5	0
65	43	0	0	0	0	0	0	0

	Difference in # of β-actin monomer synthesis sites between cell pairs			
Cell pair#	CONTROL	DECMA-1 (50 µg/ml)	DECMA-1 (100 µg/ml)	DECMA-1 (200 µg/ml)
1	16	12	0	2
2	37	10	22	11
3	17	24	0	10
4	16	11	0	3
5	13	1	0	10
6	0	0	0	8
7	1	25	6	6
8	24	14	14	10
9	11	1	0	5
10	3	0	0	0
11	10	0	0	0
12	49	0	0	3
13	3	4	62	14
14	3	18	21	1
15	0	4	1	14
16	0	0	13	11
17	9	0	1	1
18	3	0	0	6
19	15	5	0	4
20	14	108	0	0
21	17	0	3	0
22	1	0	1	10
23	32	0	1	11
24	5	0	81	5
25	53	0	0	3
26	0	0	32	0
27	33	0	29	18
28	27	0	37	25
29	72	36	26	0
30	36	25	22	47
31	49	3	36	0
32	15	46	0	0
33	2	1	6	0
34	14	47	0	0
35	9	14	12	0
36	9	10	17	5
37	12	29	0	14
38	0	0	0	0
39	6	0	0	0
40	11	16	0	0
41	4	0	0	0
42	33	60	0	17
43	8	39	3	0
44	1	0	0	5
45	43	47	0	0
46	0	21	32	0
47	33	13	29	18
48	27	0	37	25
49	72	0	26	0
50	36	36	22	47
51	49	0	13	0
52	15	0	3	0
53	2	0	6	0
54	14	32	0	0
55	9	0	12	0
56	9	8	17	5
57	12	0	0	14
58	0	0	27	0
59	6	0	0	0
60	11	44	0	0
61	4	0	0	0
62	33	0	0	17
63	8	0	3	0
64	1	35	0	5
65	43	0	0	0
AVERAGE	**17**	**12**	**10**	**6**

Appendix 3:

Active Src (pY416) and total Src antibodies both detect a molecular weight band of ~60 kDa.

(A) MDCK cell lysates at steady state probed for active Src (pY418-Src), lanes 1 to 6; and total Src (yellow box), lanes 7 to 12.

(B) Table showing different primary antibody dilutions (1°Ab) and different secondary antibody dilutions (2°Ab) used to detect active Src (pY416-Src). The respective immunoblot is shown in **A**.

(C) Table showing different total Src antibody dilutions (1°Ab) and different secondary antibody dilutions (2°Ab) to detect total Src used for immunoblot in **A**.

A

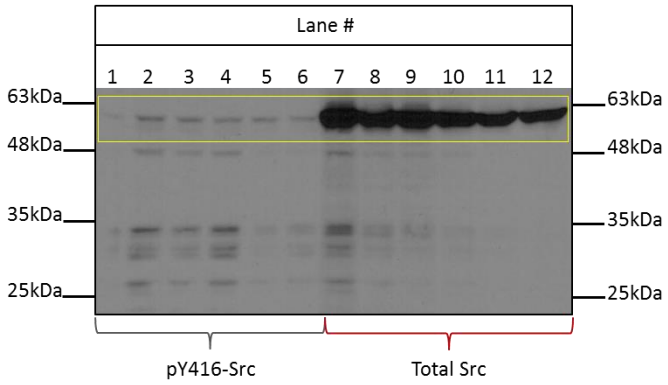

B

Lane #	1°Ab pY416-Src	2° Ab
1	1 : 1,000	1 : 3,000
2	1 : 1,500	
3	1 : 1,000	1 : 4,000
4	1 : 1,500	
5	1 : 1,000	1 : 5,000
6	1 : 1,500	

C

Lane #	1°Ab Total Src	2° Ab
7	1: 2,000	1 : 5,000
8	1: 4,000	
9	1: 8,000	
10	1: 2,000	1 : 10,000
11	1: 4,000	
12	1: 8,000	

Appendix 4:

Custom Scripts for FCI analysis

I would like to acknowledge Dr. Pavan Vedula in writing these scripts and teaching me how to use them. The scripts shown are modified to extract values from my data sets; the scripts are taken from “Spatially regulated β-actin translation in epithelia: analysis of adherens junction assembly, membrane cytoskeletal dynamics and tissue function” by Pavan Vedula. Ph.D. Thesis. Rutgers University. Newark, 2016.

Make a folder containing the .csv files to be analyzed by MATLab and the two custom scripts.

Open the **first script** in MATLab:

```
% Reads .csv files and stores the measurement values in an array.
function [mystruct1] = readData(filename)

% Input the number of columns present in the .csv files to be
read. The number of columns in all .csv files should be the same
for the script to run properly. If the .csv files in a group of a
dataset have different number of columns, make another folder
containing .csv files with the same number of columns.

    NumCols = 27;
    fid = fopen(filename,'r');
    InputText=textscan(fid,'%s',NumCols,'delimiter',',');


% Reads and inputs header line into a new array called InputText.
Searches header lines for the following expressions: '[-
/\s()."µm³]', ''), and deletes them. These characters are not
compatible with the script.

    HeaderLines=InputText{1};
    HeaderLines = regexprep(HeaderLines, '[-/\s()."µm³]', '');
    FormatString=repmat('%s', 1, NumCols);

%Creates format string based on parameter
    InputText=textscan(fid,FormatString, ...
                            'delimiter',',');
    for i = 1:27

%Inputs the right number of columns present in the .csv files.
        InputText{i} = str2double(regexprep(InputText{i}, '["]',
''));
    end
```

```
% All values enclosed with quotation marks in the original data
are removed to convert strings to floating point numbers.

    Data=cell2mat(InputText);

% Converts to numerical array from cell
     mystruct1 = struct(HeaderLines{1, 1}, Data(:, 1)');


% The loop below writes all the values from the .csv files into an
array with the headerlines taken from the first row.
     for j = 2:NumCols
         name = HeaderLines{j, 1};
         newName = regexprep(name,'[-/\s().]','');
         mystruct1.(newName) = Data(:, j)';
     end

     fclose(fid);
end
```

Open **second script** in MATLab:

```
% Reading values stored in an array using the first script above.

Computes FCI values or returns PPC values for a specified data set

in a folder.

function [myExps, out1, out2, out3] = combineExps()
 fileList = dir('*.csv');
 myExps = [];

%The following loop reads all .csv files and writes them into
%arrays by running the readData (first script) function.
 for i = 1: length(fileList)
  myData = readData(fileList(i).name);
  myExps = [myExps myData];
 end

%The loop below sets a lower threshold on all PCC values (PCC
%values below 0.1 will be reassigned to 0.1 values).
 for k = 1:1:length(fileList)
   a = myExps(k).PearsonsCorrelation; %Storing all PCs in a
                                      %matrix.

    for j = 1:1:length(a) %Defining the number of cells
                          %("length(a)") to be checked for PC
                          %values.

     if 0 > a(j);        %Checking for any negative PC.

         a(j) = 0.1;     %Input Least Possible PC to set for
```

```
                        %all PCC(s) that are negative.

     elseif a(j) < 0.1; %Checking for all PC that are positive
                        %and below the Least Possible PC.


          a(j) = 0.1;   %Input Least Possible PCC to set for
                        %all PC(s) positive and below the
                        %Least Possible PC


     end %End the checking loop for a single cell.


    myExps(k).PearsonsCorrelation = a; %Store all the %corrected
PC(s) in the original array.

    end %End the checking loop for one file.
 end



%The following loop runs a user defined value of k for j times.
The k value is set to the number of the first .csv file which is
part of the same time point and/or condition (e.g. 1 hour
recovery). The value of j depends on how many fields of view were
acquired with the microscope and quantified for a particular time
point and/or treatment. Check the proper increments in k and how
many fields of view were acquired for a specific time point within
a particular data set.


 Rec_1hr = [];
  k = 1;
  for j = 1: 4
   out1 =
myExps(k+3).PearsonsCorrelation./myExps(k).PearsonsCorrelation;
   out2 =
myExps(k+4).PearsonsCorrelation./myExps(k+1).PearsonsCorrelation;
   out3 =
myExps(k+5).PearsonsCorrelation./myExps(k+2).PearsonsCorrelation;

   Rec_1hr = [Rec_1hr; out1' out2' out3'];
   k = k+6;
  end


 Rec_2hr = [];
  k = 25;
  for j = 1: 4
   out1 =
myExps(k+3).PearsonsCorrelation./myExps(k).PearsonsCorrelation;
```

```
   out2 =
myExps(k+4).PearsonsCorrelation./myExps(k+1).PearsonsCorrelation;
   out3 =
myExps(k+5).PearsonsCorrelation./myExps(k+2).PearsonsCorrelation;
   Rec_2hr = [Rec_2hr; out1' out2' out3'];
   k = k+6;
  end


 LC = [];
  k = 49;
  for j = 1: 4
   out1 =
myExps(k+3).PearsonsCorrelation./myExps(k).PearsonsCorrelation;
   out2 =
myExps(k+4).PearsonsCorrelation./myExps(k+1).PearsonsCorrelation;
   out3 =
myExps(k+5).PearsonsCorrelation./myExps(k+2).PearsonsCorrelation;
   LC = [LC; out1' out2' out3'];
   k = k+6;
  end


 SS = [];
  k = 73;
  for j = 1: 4
   out1 =
myExps(k+3).PearsonsCorrelation./myExps(k).PearsonsCorrelation;
   out2 =
myExps(k+4).PearsonsCorrelation./myExps(k+1).PearsonsCorrelation;
   out3 =
myExps(k+5).PearsonsCorrelation./myExps(k+2).PearsonsCorrelation;
   SS = [SS; out1' out2' out3'];
   k = k+6;
  end


%Log transforms the data obtained.
  Rec_1hrL = log10 (Rec_1hr);
  Rec_2hrL = log10 (Rec_2hr);
  Rec_LCL = log10 (LC);
  Rec_SSL = log10 (SS);


%Write the log transformed values into a text file.
 dlmwrite('ctrlFORdecma_FCI.txt', SSL)
 dlmwrite('ctrlFORdecma_FCI.txt', LCL, '-append', 'coffset', 1)
 dlmwrite('ctrlFORdecma_FCI.txt', Rec_1hrL, '-append', 'coffset',
 2)
 dlmwrite('ctrlFORdecma_FCI.txt', Rec_2hrL, '-append', 'coffset',
 3)
```

```
%Creates a bar graph in MATLab for a specified data set.

 Mean = [mean(SS);mean(LC);mean(Rec_1hr);mean(Rec_2hr)];

 bar(Mean)

end

%Execute the second script by going to the editor window in MATLab
and click on the Run bottom (F5).
```